R-08-133

Real Time Grouting Control Method

Development and application using Äspö HRL data

Shinji Kobayashi
Shimizu Corporation/Kungliga Tekniska Högskolan

Håkan Stille, Kungliga Tekniska Högskolan

Gunnar Gustafson, Chalmers Tekniska Högskola

Björn Stille, Skanska Teknik

October 2008

Svensk Kärnbränslehantering AB
Swedish Nuclear Fuel
and Waste Management Co

Box 250, SE-101 24 Stockholm
Phone +46 8 459 84 00

ISSN 1402-3091
SKB Rapport R-08-133

Real Time Grouting Control Method

Development and application using Äspö HRL data

Shinji Kobayashi
Shimizu Corporation/Kungliga Tekniska Högskolan

Håkan Stille, Kungliga Tekniska Högskolan

Gunnar Gustafson, Chalmers Tekniska Högskola

Björn Stille, Skanska Teknik

October 2008

Preface

In 2007 the report entitled “Design for rock grouting based on analysis of grout penetration – Verification using Äspö HRL data and parameter analysis” was published (SKB R-07-13). The report examines the time – penetration length relationship, as presented by Gustafson and Claesson, by evaluating the theory against recorded data from the TASQ tunnel at the SKB Äspö Hard Rock Laboratory. In this report “Real Time Grouting Control Method”, the theory is developed further and the concept of the “Real Time Grouting Control Method” method is established. The concept is to allow an active control of grouting by analysing the pump curves in order to assess the flow dimensionality and thus the penetration length.

The concept has been developed from the need to acquire a theoretically supported method for the design and execution of grouting operations. In the case of sealing the rock mass by means of grouting for a KBS-3 repository, the concept is of particular relevance as it focuses on acquiring the desired penetration length, but no more, which means that material use can be minimized.

For application of the method in production, the support from automatic logging and real time evaluation is needed. The intention is to fit the theory into a computerized logging tool, in order to be able to establish “Real Time Grouting Control Method” not only as a concept, but also as a practicable method for ensuring efficient production and confidence in the sealing result.

Calculations, evaluation and reporting were carried out mainly by Shinji Kobayashi, Shimizu Corporation, Japan. The overall concept was developed in cooperation between Shinji Kobayashi, Professor Håkan Stille at the Royal Institute of Technology, Professor Gunnar Gustafson at Chalmers University of Technology and Björn Stille Skanska/Chalmers. The work was reviewed by PhD Lars Hässler, Psicon.

Stockholm, October 2008

Ann Emmelin

Summary

The spread of grout is governed by a number of complex relations. The desired results, such as grout penetration and sealing of fractures, cannot be directly measured during the grouting process. This means that the issue of how or when the injection of grout should be stopped cannot be answered by simple rules of thumb. This is also the background to the great variety of empirical rules used in the grouting sector worldwide. The research during recent years has given a better understanding of the water-bearing structures of the rock mass as well as analytical solutions. In this report the methodology has been further studied and a method for design and control of rock grouting has been proposed. The concept of what we call the "Real Time Grouting Control Method" is to calculate the grout penetration and control grouting in real time by applying the development of the theories for grout spread. Our intention is to combine our method with a computerized logging tool to acquire an active tool in order to be able to govern the grout spread in real time during the grouting operation.

The objectives of this report are:

- to further develop the theory concerning the relationship between grout penetration and grouting time to describe the real course of grouting,
- to establish the concept of "Real Time Grouting Control Method" for design and control for rock grouting based on the developed theory, and
- to verify the concept by using the field data from the grouting experiment at the 450 m level in the Äspö HRL.

In this report, the approximations and analysis of dimensionality have been checked and further developments of the theory with respect to varying grouting pressure, time-dependent grout properties, changing grout mixes, and changing the flow dimension of the fracture have been carried out.

The concept of "Real Time Grouting Control Method" has been described in order to calculate the grout penetration and to control grouting in real time by applying developed theories for grout spread. The stop criterion can with this method be related to achieved grout spread such as the fact that grouting is completed when the grout penetration for the smallest fracture that has to be sealed is above a certain minimum value (target value) or before the grout penetration for the largest fracture aperture reaches a certain maximum value (limiting value). Based on the calculated penetration length it might be possible to add certain other options to the method, such as estimation of joint aperture, prediction of grout flow and grout penetration, calculation of the risk of uplift, and prediction of water leakage to the tunnel.

In order to verify the "Real Time Grouting Control Method", the field data from the grouting field experiment at the 450 m level in the Äspö HRL has been used. The calculated flow dimensionality, the calculated fracture apertures and the calculated grout flows were quite close to those measured. This indicates that the "Real Time Grouting Control Method" may be applicable to real grouting design and control.

Sammanfattning

Brukets spridning i berget styrs av komplexa samband. Spridningen och i vilken omfattning bergets sprickor har tätats kan inte direkt mätas under injekteringsprocessen. Det betyder att direkta stoppkriterier för avslutande av injekteringen av ett borrhål inte kan upprättas. Detta bekräftas av det faktum att det idag förekommer flera olika stoppkriterier. Forskning utförd under de senaste åren har givit en bättre förståelse över bergets vattenvägar och analytiskt grundade lösningar för brukets spridning. I denna rapport har problemet studerats ytterligare och en metod för kontroll och styrning av injekteringsprocessen föreslås. Vi har kallat konceptet för "Real Time Grouting Control Method". Den innebär att vi i takt med den pågående injekteringen, d v s i realtid, analyserar förloppet för att på så sätt få underlag för att styra processen. Vårt mål är att kombinera vårt koncept med datoriserad insamling av data under injekteringsförloppet för att på så sätt erhålla ett aktivt redskap för styrning av bruksinträngningen.

Syftet med rapporten är följande:

- Att ytterligare utveckla de teorier som styr förloppet.
- Att koppla ihop dessa teorier till ett praktiskt verktyg för att dimensionera och kontrollera injekteringsprocessen som vi kallat "Real Time Grouting Control Method".
- Att verifiera verktyget genom att applicera det på data från injekteringsexperimentet på 450 m nivån i Äspö HRL.

Teorierna för spridning och dimensionalitet har kontrollerats och utvecklats för att kunna beakta varierande tryck, tidsberoende bruksegenskaper, ändring av brukblandning och dimensionalitet av flödet.

Tillämpning av konceptet "Real Time Grouting Control Method" beskrivs i detalj med koppling till teorierna. Kriterier för att avsluta injekteringen har relaterats till förväntad inträngning och krav på min respektive max tillåten spridning. Det är även möjligt att med erhållen tryck/flödeskurva ge underlag för att uppskatta sprickvidden, predicera flödet och inträngningen samt risken för hydraulisk lyftning.

För att verifiera metoden har data från ett injekteringsexperiment i Äspö på 450 m nivån använts. Beräknad dimensionalitet, sprickvidd och prognostiserat flöde stämde väl överens med uppmätta värden. Detta indikerar att konceptet "Real Time Grouting Control Method" kan vara tillämpbart för att dimensionera och kontrollera injekteringsprocesser i framtiden.

Contents

1 Introduction 9
1.1 Background 9
1.2 Objectives 9

2 Development of the theory of grout spread 11
2.1 Overview 11
2.2 Grout penetration of a Bingham fluid at constant pressure 11
2.2.1 Basic equations 11
2.2.2 Analytical solutions for grout penetration 12
2.2.3 Injected volume and grout flow 14
2.2.4 Analysis of dimensionality 14
2.2.5 Approximations for analytical grout penetration 15
2.2.6 Examples of theoretical grout penetration 18
2.2.7 Capacity of the grouting equipment 20
2.3 Varying grouting pressure 22
2.3.1 Corrected time 22
2.3.2 Examples of theoretical grout penetration 24
2.4 Time-dependent grout properties 25
2.4.1 Hardening of the grout 25
2.4.2 Corrected time 26
2.4.3 Examples of theoretical grout penetration 27
2.4.4 Varying grouting pressure and time-dependent properties 28
2.4.5 Examples of theoretical grout penetration 29
2.5 Changing grout mixes 30
2.5.1 Upper and lower boundaries 30
2.5.2 Examples of theoretical grout penetration using upper and lower boundaries 31
2.5.3 Middle method 33
2.5.4 Examples of theoretical grout penetration using the middle method 34
2.6 Dimensionality of flow in the fracture 36
2.6.1 Indexes for analysis of dimensionality 36
2.6.2 $Q \cdot t/V$ 37
2.6.3 $Q/V \cdot t_0$ 39
2.6.4 $Q/V \cdot t_0 \cdot I_D \cdot (dI_D/dt_D)^{-1}$ 40
2.7 Changing the flow dimension of the fracture 41
2.7.1 2D to 1D case 41
2.7.2 1D to 2D case 45

3 Grouting control with “Real Time Grouting Control Method” 49
3.1 Grouting control and Stop criteria 49
3.2 Grouting control using “Real Time Grouting Control Method” 49
3.2.1 Procedure for grouting control 49
3.2.2 Required data 49
3.2.3 Determination of dimensionality 52
3.2.4 Calculation of penetration length 53
3.2.5 Estimation of fracture apertures and related theoretical grout flow 54
3.2.6 Correction of penetration length 56
3.2.7 Stop Criteria 57

3.3 Other options of the "Real Time Grouting Control Method" 58
3.3.1 Possible other options 58
3.3.2 Prediction of grout flow and grout penetration 59
3.3.3 Calculation of the risk of uplift 61
3.3.4 Prediction of water leakage 64

4 Application using Äspö HRL data 67
4.1 Field experiment at Äspö HRL 67
4.1.1 Overview 67
4.1.2 Grouting design in the field experiment 67
4.1.3 Grouting results measured in previous field experiment 68
4.2 Verification of "Real Time Grouting Control Method" 69
4.2.1 Input data 69
4.2.2 Calculation 70
4.3 Comparison of calculated and measured results 70
4.3.1 Dimensionality 70
4.3.2 Fracture aperture 73
4.3.3 Grout flow 78
4.3.4 Penetration length 79
4.4 Conclusions regarding verification 83

5 Conclusions and proposals 85
5.1 Conclusions 85
5.2 Proposals 85

References 87

Appendix A Inflow during drilling and estimated hydraulic apertures 89
Appendix B Inflow during drilling and estimated hydraulic apertures 91
Appendix C Inflow during drilling and estimated hydraulic apertures 93
Appendix D Inflow during drilling and estimated hydraulic apertures 95
Appendix E Inflow during drilling and estimated hydraulic apertures 97
Appendix F Inflow during drilling and estimated hydraulic apertures 125

1 Introduction

1.1 Background

The spread of grout is governed by a number of complex relations. The desired results such as grout penetration and sealing of fractures cannot be directly measured during the grouting process. This means that the issue of how or when the injection of grout should be stopped cannot be answered by simple rules of thumb. This is also the reason for the great variety of empirical rules used in the grouting sector worldwide. During recent decades, there has been a substantial increase in the understanding of the mechanism behind the spreading of grout. Up to 1990, the understanding was more or less based on empirical knowledge as described in /Houlsby 1990/. A deeper theoretical understanding of the mechanism as manifested in /Lombardi 1985/, /Hässler et al. 1987/, /Gustafson and Stille 1996/ and /Eriksson et al. 2000/ has had an impact on the development of both a new stop criterion and new grouting materials.

The limitation so far has been the lack of analytical solutions of the grout spread. The research during recent years has given us a better understanding of the water-bearing structures of the rock mass as well as analytical solutions /Gustafson and Claesson 2005/. This has implied that tools for analyzing grout spread in real time can be developed. The principle was first described in /Gustafson and Stille 2005/ and was later further developed in /Kobayashi and Stille 2007/. In /Hässler 1991/ the concept of analysis of grout spread in real time was discussed for the first time but was at then based on numerical calculations.

In this report, the methodology has been further studied and a method for the design and control of rock grouting has been proposed. The concept of what we call the "Real Time Grouting Control Method" is to calculate the grout penetration and control grouting in real time by applying the development of the theories for grout spread. The theories and the analytical solutions are first given in Chapter 2 of this report as a background. The "Real Time Grouting Control Method" is then described in detail in Chapter 3. The application of the method is demonstrated in Chapter 4 for a well described case history of grouting carried out at Äspö Hard Rock Laboratory in Sweden. Nowadays, a computerized logging tool, which records grouting parameters such as grouting time, grouting pressure, grout flow and grouted volume, is often used in grouting projects. Our intention is to combine our method with this type of computerized logging tool to acquire an active tool in order to be able to govern the grout spread in real time during the grouting operation.

1.2 Objectives

The objectives of this report are:

- to further develop the theory concerning the relationship between grout penetration and grouting time to describe the real course of grouting,
- to establish the concept of "Real Time Grouting Control Method" for design and control for rock grouting based on the developed theory, and
- to verify the concept by using the field data from the grouting experiment at the 450 m level in the Äspö HRL.

2 Development of the theory of grout spread

2.1 Overview

The relationship between relative grout penetration and relative grouting time was derived in /Gustafson and Claesson 2005/ and it means that the relative grout penetration, which is defined as the ratio between the actual penetration and the maximum penetration, is the same in all fractures. Based on this study, theoretically derived stop criteria for rock grouting by using approximations of the relationship between relative grout penetration and relative grouting time were examined in /Gustafson and Stille 2005/. These are based on a Bingham fluid model in parallel planar fractures with constant aperture at constant grouting pressure. /Gustafson and Stille 2005/ also provided the rule to determine the flow dimensionality of the fracture. In /Kobayashi and Stille 2007/, the theory was developed in order to apply to real grouting procedures, including increasing the grouting pressure, changing the grout mix and the capacity of the grouting equipment. In this report, the approximations and the analysis of dimensionality are checked and further developments of the theory with respect to varying grouting pressure, time-dependent grout properties, changing grout mixes, and changing the flow dimension of the fracture are carried out.

2.2 Grout penetration of a Bingham fluid at constant pressure

2.2.1 Basic equations

Cement grouts can be described as Bingham fluids characterized by a yield strength τ_0 and a plastic viscosity μ_g. Figure 2-1 illustrates the grout penetration of a Bingham fluid into a parallel planar fracture with constant aperture b at constant grouting pressure $\Delta p\ (=p_g-p_w)$.

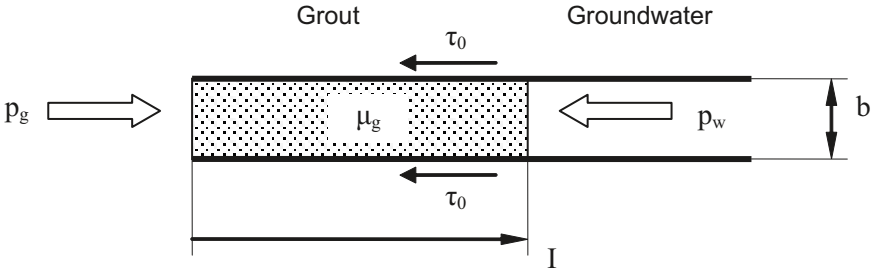

Figure 2-1. *Grout penetration of a Bingham fluid. P_g is the injection pressure produced by the grout pump and P_w is the groundwater pressure.*

According to /Hässler 1991/, the flow (or velocity) of grout, *dI/dt*, can be calculated from the Navier-Stokes equation as:

$$\frac{dI}{dt} = -\frac{dp}{dx} \cdot \frac{b^2}{12\mu_g} \left[1 - 3 \cdot \frac{Z}{b} + 4 \cdot \left(\frac{Z}{b} \right)^3 \right] \tag{2-1}$$

where

$$Z = \tau_0 \cdot \left| \frac{dp}{dx} \right|^{-1}, \quad Z < \frac{b}{2} \tag{2-2}$$

The maximum penetration can be calculated see for example /Hässler 1991/ based on a simple force balance when grouting has come to stop as:

$$I_{\max} = \left(\frac{\Delta p}{2\tau_0} \right) \cdot b \tag{2-3}$$

2.2.2 Analytical solutions for grout penetration

In order to obtain analytical solutions for grout penetration, the characteristic grouting time t_0, the relative grouting time t_D, and the relative grout penetration I_D are defined according to /Gustafson and Stille 2005/ as:

$$t_0 = \frac{6\Delta p \cdot \mu_g}{\tau_0^2} \tag{2-4}$$

$$t_D = \frac{t}{t_0} \tag{2-5}$$

$$I_D = \frac{I}{I_{\max}} \tag{2-6}$$

Using the equations (2-1) to (2-6), the relative penetration I_D as a functions of the relative grouting time t_D for both the one-dimensional (1D) and the two-dimensional (2D) cases is calculated in /Gustafson and Stille 2005/ as shown in Figure 2-2 and Figure 2-3.

The relative borehole radius expressed by the ratio between the maximum penetration and the radius of the injection borehole r_b ($\gamma = I_{max}/r_b$) will also to some degree influence the relative penetration for the 2D-case. Normal range of the ratio will be in the order of 300 to 1,000.

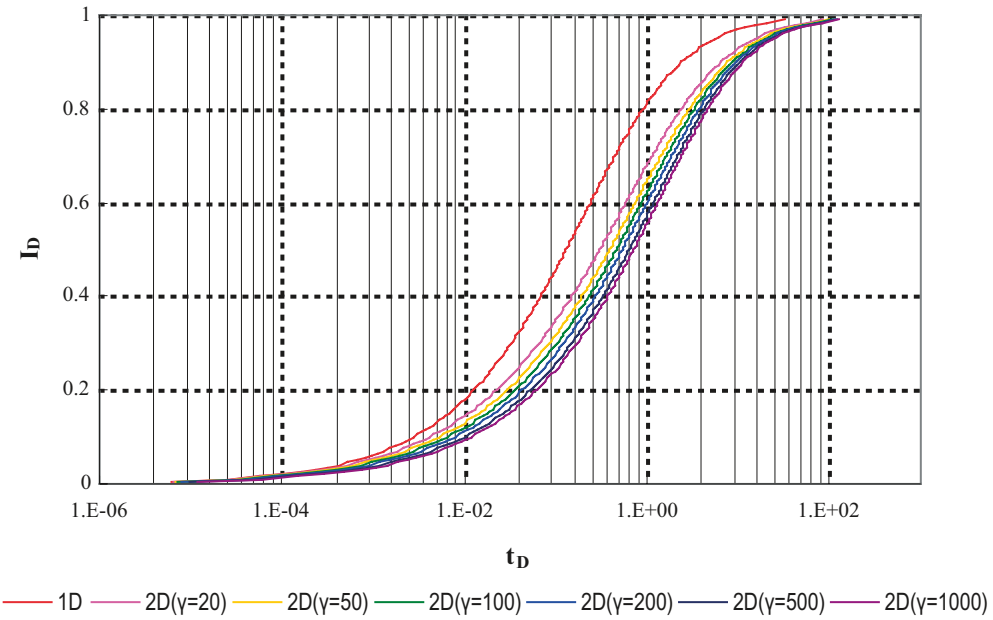

Figure 2-2. *The relative penetration as a function of the relative grouting time in the logarithmic X axis. ($\gamma=I_{max}/r_b$, r_b : the radius of the injection borehole).*

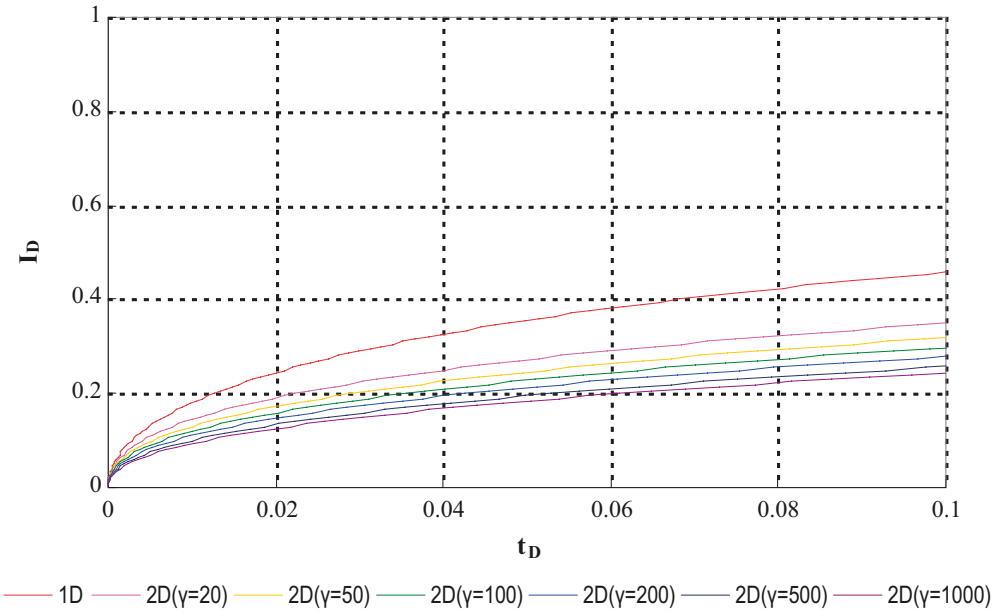

Figure 2-3. *The relative penetration as a function of the relative grouting time in the normal X axis.*

2.2.3 Injected volume and grout flow

The injected volume and grout flow for both 1D and 2D cases are also derived by /Gustafson and Stille 2005/ according to the following equations.

For the 1D case, the volume injected into the channel at width w and aperture b is calculated as:

$$V = I \cdot w \cdot b = I_D \cdot I_{\max} \cdot w \cdot b = I_D \cdot \left(\frac{\Delta p}{2\tau_0} \right) \cdot w \cdot b^2 \quad (2\text{-}7)$$

This is calculated for several fractures as:

$$V_{tot} = I_D \cdot \left(\frac{\Delta p}{2\tau_0} \right) \cdot \sum wb^2 = I_D \cdot V_{\max,1D} \quad (2\text{-}8)$$

The grout flow can be calculated as:

$$Q = \frac{dV_{tot}}{dt} = \frac{dI_D}{dt_D} \cdot \frac{1}{t_0} \cdot \left(\frac{\Delta p}{2\tau_0} \right) \cdot \sum wb^2 = \frac{dI_D}{dt_D} \cdot \frac{V_{\max,1D}}{t_0} \quad (2\text{-}9)$$

For the 2D case, the volume injected into the circular fracture with aperture b is calculated as:

$$V = \pi \cdot I^2 \cdot b = \pi \cdot \left(I_D \cdot I_{\max} \right)^2 \cdot b = \pi \cdot {I_D}^2 \cdot \left(\frac{\Delta p}{2\tau_0} \right)^2 \cdot b^3 \quad (2\text{-}10)$$

This is calculated for several fractures as:

$$V_{tot} = \pi \cdot {I_D}^2 \cdot \left(\frac{\Delta p}{2\tau_0} \right)^2 \cdot \sum b^3 = {I_D}^2 \cdot V_{\max,2D} \quad (2\text{-}11)$$

The grout flow can be calculated as:

$$Q = \frac{dV_{tot}}{dt} = 2\pi \cdot I_D \cdot \frac{dI_D}{dt_D} \cdot \frac{1}{t_0} \cdot \left(\frac{\Delta p}{2\tau_0} \right)^2 \cdot \sum b^3 = I_D \cdot \frac{dI_D}{dt_D} \cdot \frac{V_{\max,2D}}{t_0} \quad (2\text{-}12)$$

2.2.4 Analysis of dimensionality

In order to analyze the flow dimensionality of the fracture, $Q \cdot t/V$ is pointed out as an index in /Gustafson and Stille 2005/. Figure 2-4 shows the plots of $Q \cdot t/V$ as a function of t_D. A significant and characteristic difference can be seen between 1D and 2D cases.

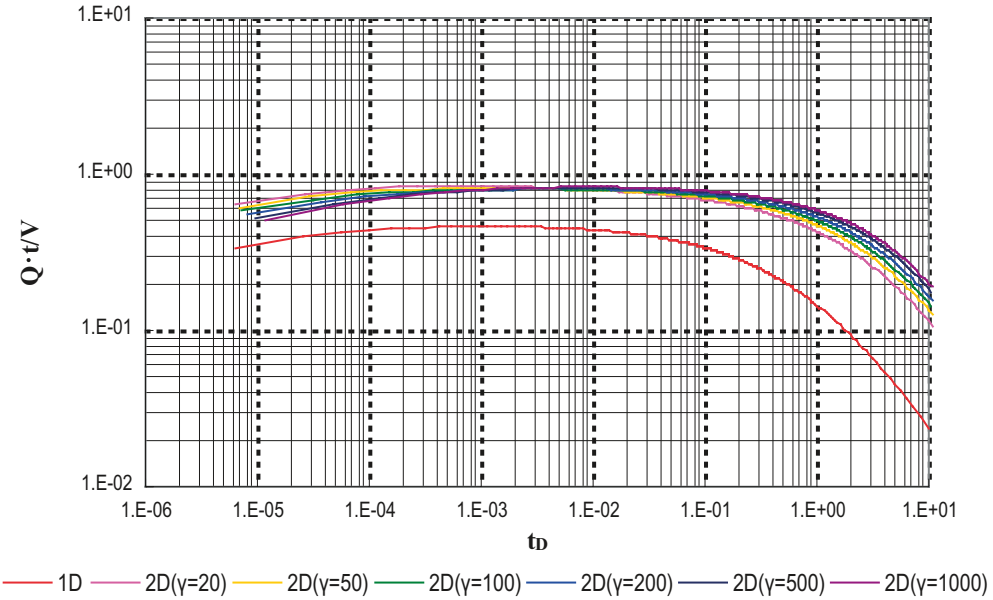

Figure 2-4. *The index for analyzing the dimensionality, Q·t/V for 1D and 2D cases.*

2.2.5 Approximations for analytical grout penetration

The relationships between the relative penetration and the relative time for both 1D and 2D cases have to be approximated in order to develop a handy solution. First attempt was by /Eriksson and Stille 2005/. Later /Gustafson and Stille 2005/ developed the relationships by proposing the following:

$$I_D = \sqrt{\theta^2 + 4\theta} - \theta \tag{2-13}$$

$$\theta_{1D} = \frac{t_D}{2(0.6 + t_D)} \tag{2-14}$$

$$\theta_{2D} = \frac{t_D}{2(3 + t_D)} \tag{2-15}$$

The problem in connection with these approximations is that a poor accuracy is found for the 2D case when t_D is very small. This is of special interest for obtaining quick information on the response of an increase in grouting pressure. An example of a better approximation for the 2D case can be written as:

$$I_D = 0.7032 \cdot \exp\left(0.9072 \cdot \log(t_D)\right) \qquad t_D < 0.2413 \tag{2-16a}$$

$$I_D = 0.3643 \cdot \log(t_D) + 0.6266 \qquad 0.2413 < t_D < 2.7546 \tag{2-16b}$$

$$I_D = 1 - 0.4522 \cdot \exp\left(-1.7098 \cdot \log(t_D)\right) \qquad t_D > 2.7546 \tag{2-16c}$$

As shown in Figure 2-5 to Figure 2-8, the approximation obtained when using equation (2-16c) appears to be better than that acquired when using equations (2-13) and (2-15). Therefore it is used to analyze 2D cases in the following chapters of the report.

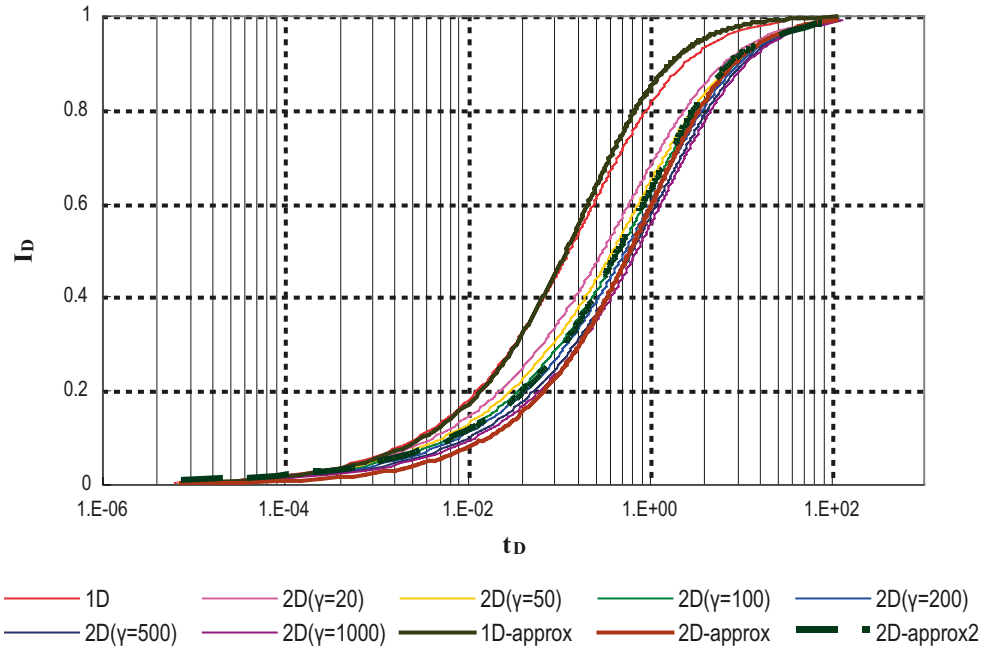

Figure 2-5. *Approximations of relative penetration as a function of relative time in the logarithmic X axis.1D-approx: 1D approximation using equation (2-13) and (2-14), 2D-approx: 2D approximation using equation (2-13) and (2-15), 2D-approx2: 2D approximation using equation (2-16c).*

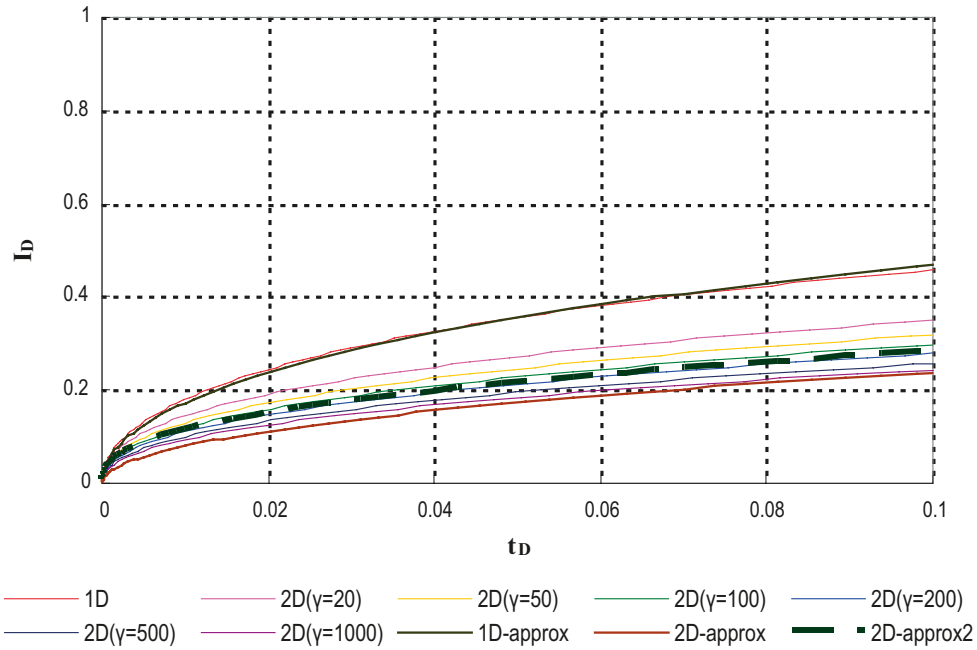

Figure 2-6. *Approximations of relative penetration as a function of relative time in the normal X axis.*

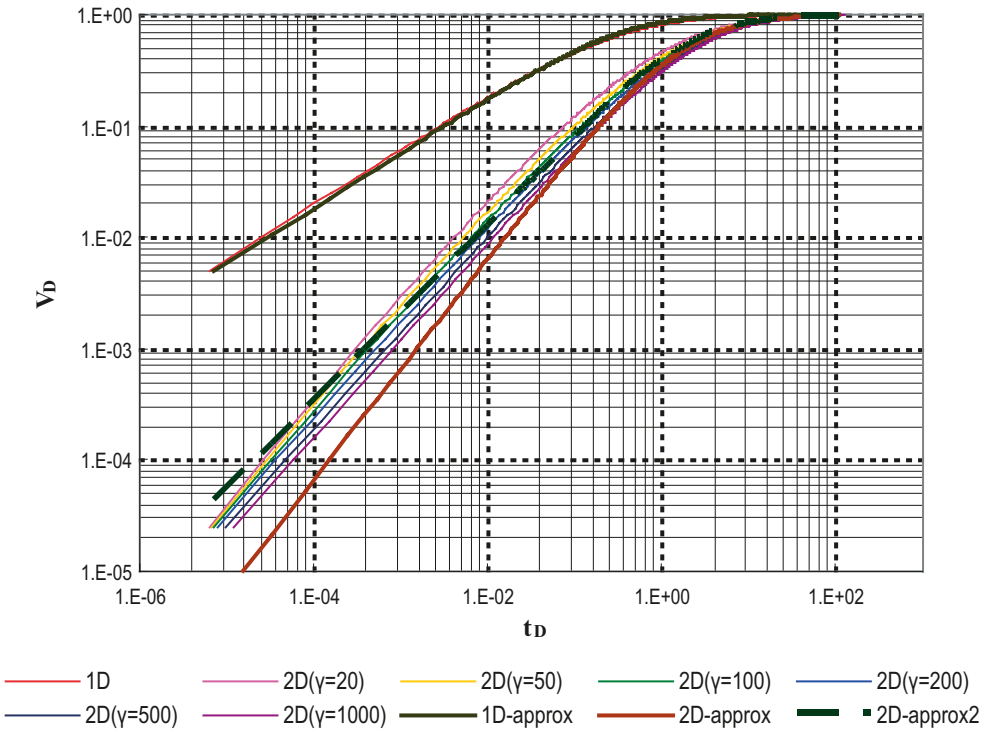

Figure 2-7. *Approximations of relative injected volume V_D (=V/V_{max}) as a function of relative time.*

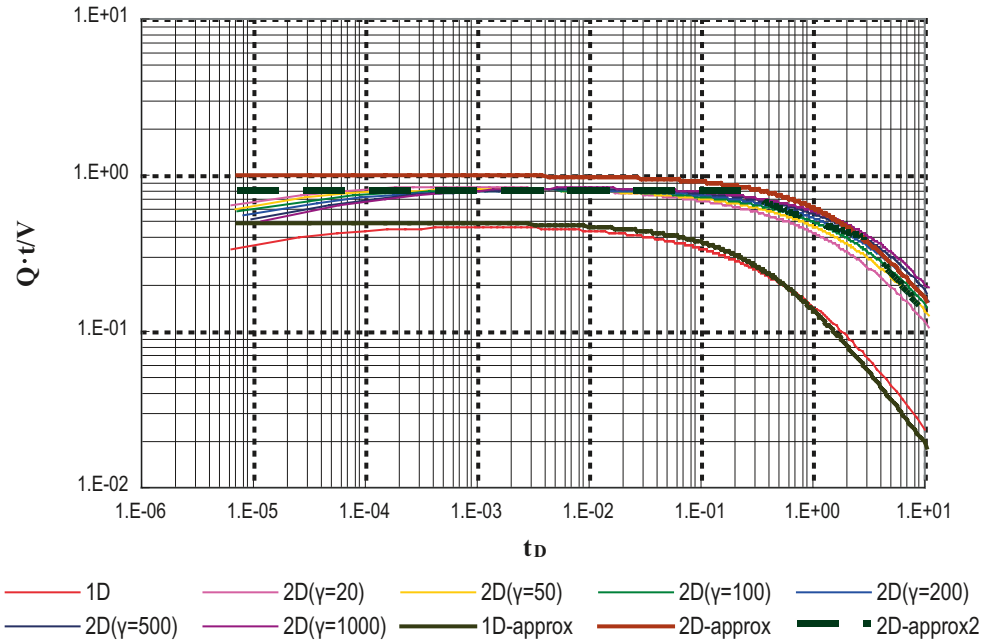

Figure 2-8. *Approximations of Q·t/V as a function of relative time.*

2.2.6 Examples of theoretical grout penetration

Figure 2-9 to Figure 2-12 show examples of theoretical grout penetration of a Bingham fluid into a fracture at constant grouting pressure. The grouting parameters are shown below:

- Grouting pressure (Δp): 3 MPa.
- Grout properties Yield value (τ_0): 0.296 Pa, Viscosity (μ_g): 0.0056 Pas.
- Fracture Number of fractures: 1, Aperture (b): 0.15 mm, Width for 1D case (w): 10 m.

The values specified above correspond to a very thin grout given a characteristic grouting time of 1.15 10^{-6} s. The examples clearly demonstrate the possibility of the theories and analytical solutions to calculate the grout flow, grouted volume and penetration of the grout in the joints. The dimensionality of the flow can also be evaluated by calculating the ratio between flow, volume and time (Qt/V) as described above.

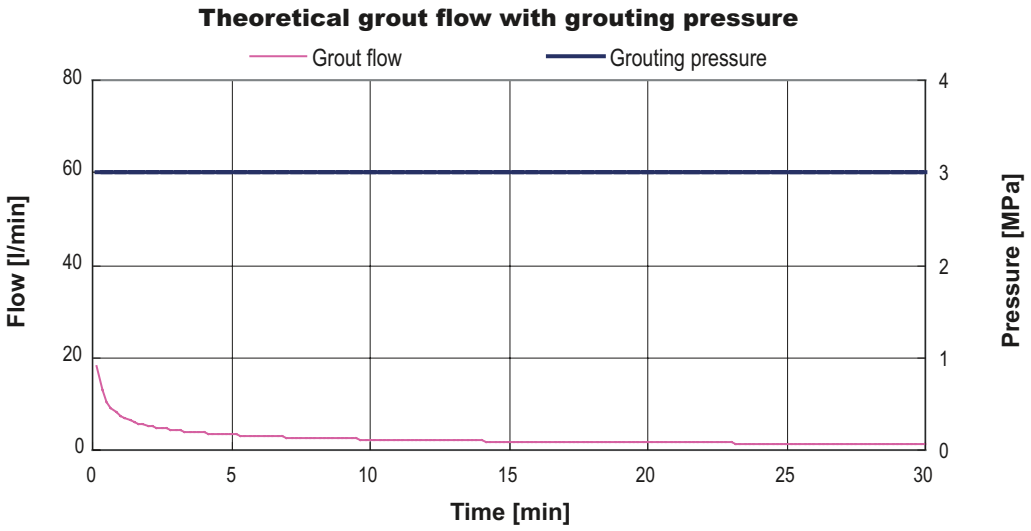

Figure 2-9. *Theoretical grout flow of a Bingham fluid at constant pressure for 1D case.*

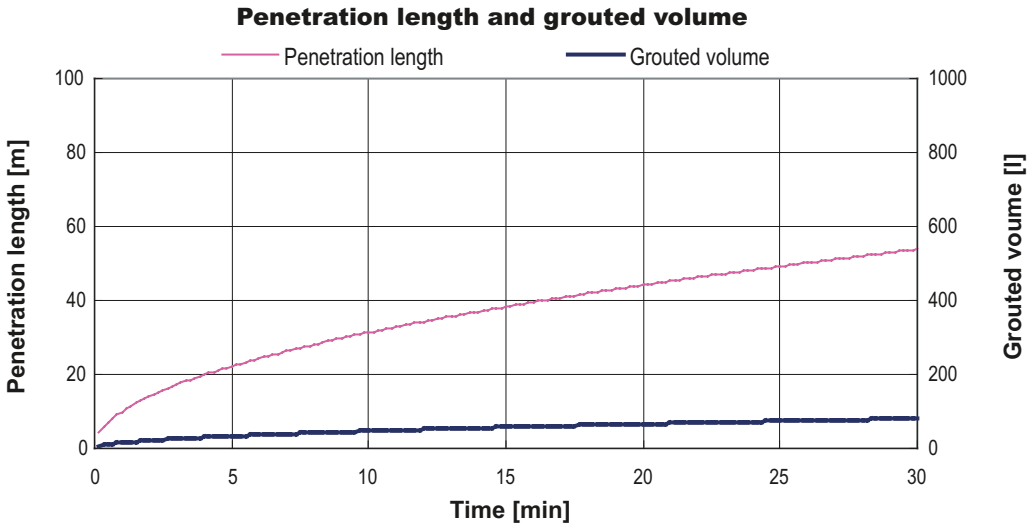

Figure 2-10. *Theoretical penetration length and grouted volume of a Bingham fluid at constant pressure for 1D case.*

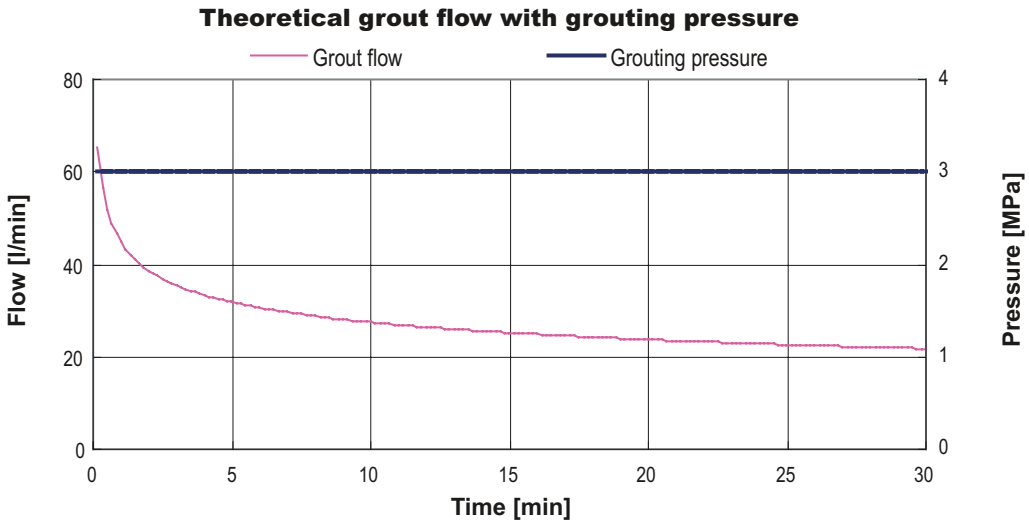

Figure 2-11. *Theoretical grout flow of a Bingham fluid at constant pressure for 2D case.*

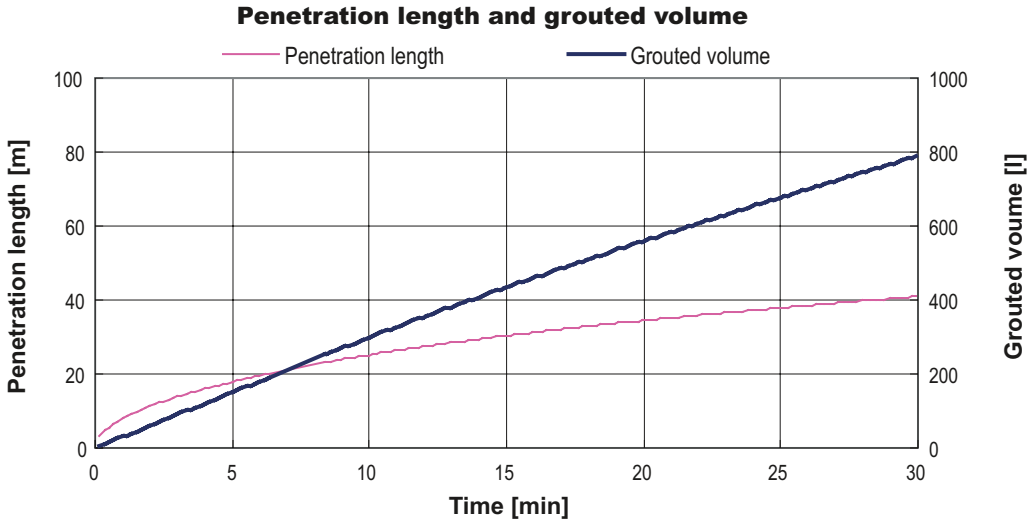

Figure 2-12. *Theoretical penetration length and grouted volume of a Bingham fluid at constant pressure for 2D case.*

2.2.7 Capacity of the grouting equipment

In reality, the capacity of the grouting equipment such as the grout pump and the grout mixer is restricted to a certain maximum flow, see /Kobayashi and Stille 2007/. Figure 2-13 shows how the grout flow and grout penetration change according to the capacity of the grouting equipment. In this figure, the following equations are derived:

$$V = Q_{\max} \cdot t \qquad t < t_2 \tag{2-17a}$$

$$V = Q_{\max} \cdot t_2 + \int_{t_1}^{t-(t_2-t_1)} q\,dt \qquad t > t_2 \tag{2-17b}$$

$$I(t_1) = I(t_2) \tag{2-18a}$$

$$I = f(V) \tag{2-18b}$$

The equations are based on the assumption that the flow, after the pressure has reached its defined value, will follow the flow curve for constant pressure and from the time when the same penetration should be achieved. Penetration will depend on volume, geometry of the joint and dimension of the flow. The shape of theoretical grouting pressure curve until time t_2 of the grouting including the grouting equipment capacity is described as straight because it does not have much effect on the grouting result.

Figure 2-14 and Figure 2-15 show theoretical grout penetration using the same parameters as Figure 2-11 and adding the grouting equipment capacity as:

- Grouting equipment capacity Maximum grout flow (Q_{max}): 30 litres/min.

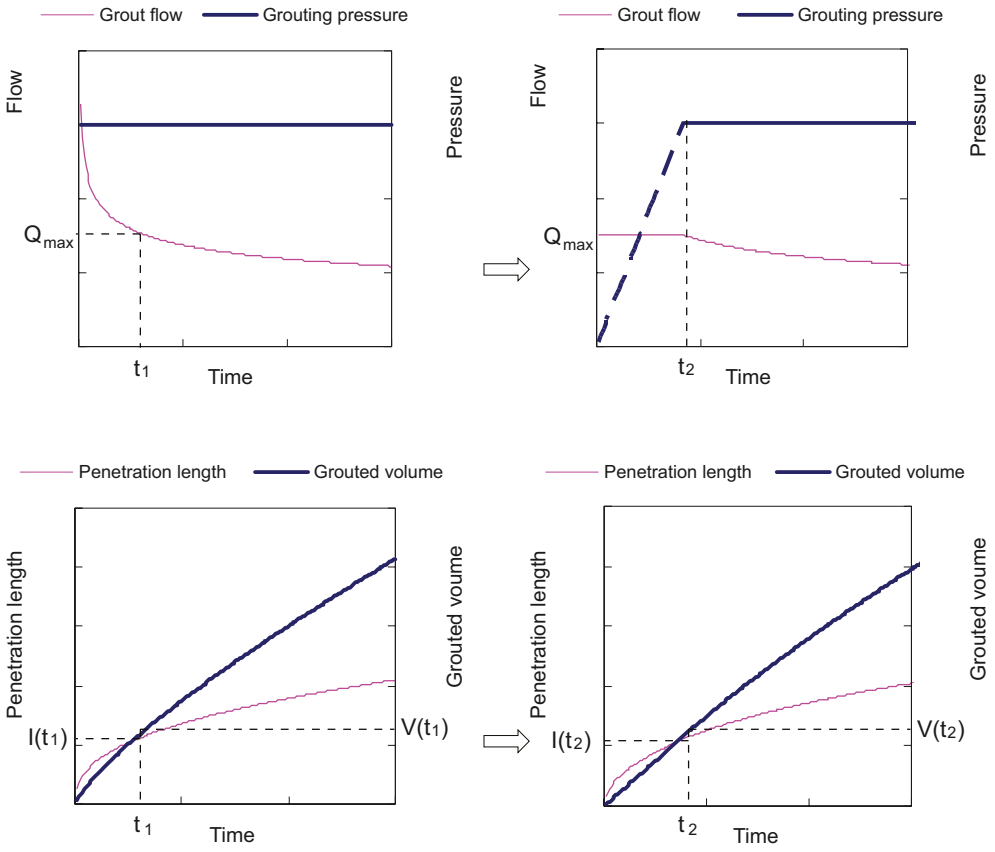

Figure 2-13. *Influence of the grouting equipment capacity. The graph on the top left shows the theoretical grout flow. The graph on the top right shows the theoretical grout flow including the grouting equipment capacity. The graph on the bottom left show the penetration length and grouted volume. The graph on the bottom right shows the penetration length and grouted volume including the grouting equipment capacity.*

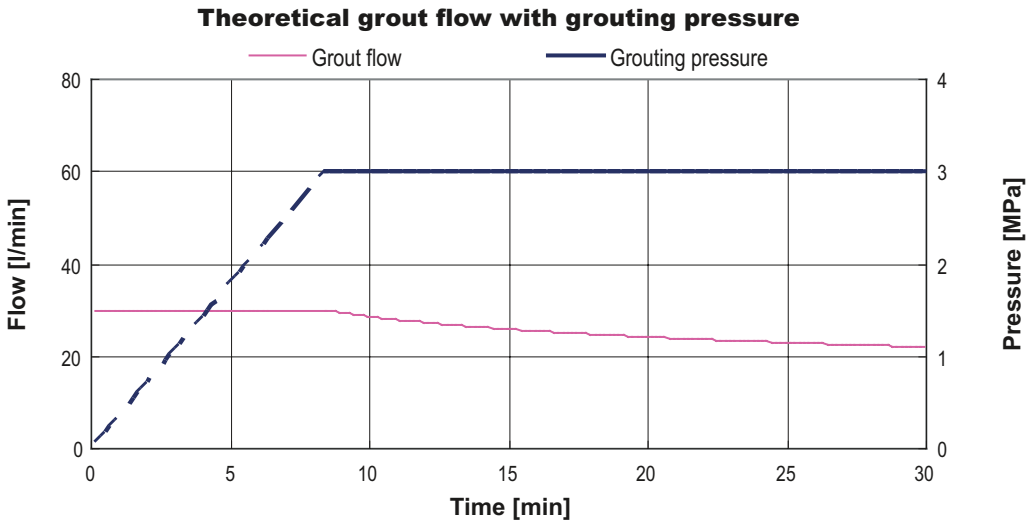

Figure 2-14. *Theoretical grout flow of a Bingham fluid for 2D case including the grouting equipment capacity.*

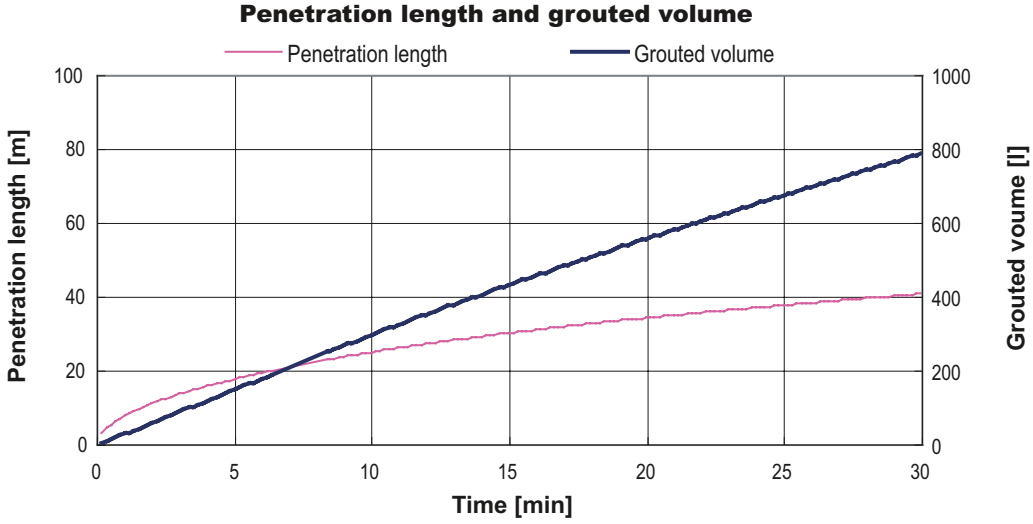

Figure 2-15. *Theoretical penetration length and grouted volume of a Bingham fluid for 2D case including the grouting equipment capacity.*

2.3 Varying grouting pressure

2.3.1 Corrected time

In reality, the grouting pressure is not constant because grouting normally starts at a low grouting pressure which is then increased to the maximum. In a simple case description, the grouting pressure increases from p_a to p_b at time t_1, see Figure 2-16. According to /Kobayashi and Stille 2007/, the relationship between grouting time and grout penetration length can be calculated as:

$$I = I_{Pa}(t), \qquad t < t_1 \tag{2-19a}$$

$$I = I_{Pb}(t - (t_1 - t_{c1})), \qquad t > t_1 \tag{2-19b}$$

$$I_{Pb}(t_{c1}) = I_{Pa}(t_1) = I_1 \tag{2-19c}$$

where $I_{Pa}(t)$ is the relationship between time and penetration under the constant pressure p_a and $I_{Pb}(t)$ is the relationship between time and penetration under the constant pressure p_b.

t_{c1} can be defined as a corrected time of t_1 and will be calculated as follows.

$$I = I_D \cdot I_{\max} = I_D \cdot \frac{\Delta p \cdot b}{2\tau_0} \tag{2-20}$$

is derived from the equations (2-3) and (2-6). Using the equation (2-19c) and (2-20), the relationship between $I_{D,\,Pa}$ (relative penetration under the pressure p_a) and $I_{D,\,Pb}$ (relative penetration under the pressure p_b) is calculated as:

$$I_{D,Pb} = I_{D,Pa} \cdot \frac{p_a}{p_b} \tag{2-21}$$

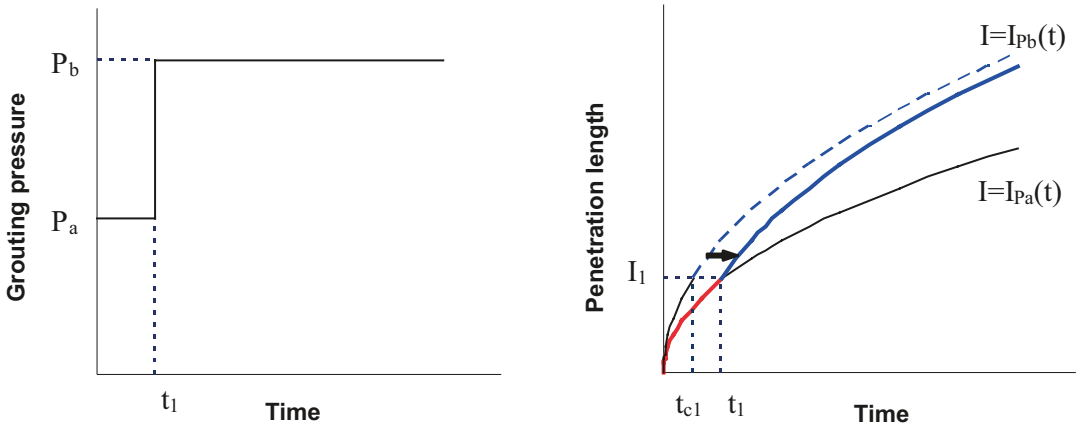

Figure 2-16. *Relationship between time and penetration when the grouting pressure increases from P_a to P_b. The graph on the left shows the relationship between grouting time and grouting pressure. The graph on the right shows how penetration changes as the grouting pressure increases.*

The equations (2-13) to (2-16c)) are reformulated as:

$$\theta = \frac{I_D{}^2}{4 - 2I_D} \tag{2-22}$$

$$t_{1D} = \frac{1.2\theta_D}{1 - 2\theta_D} \tag{2-23}$$

$$t_{2D} = \frac{6\theta_D}{1 - 2\theta_D} \tag{2-24}$$

$$\begin{aligned} t_D &= 10^{\ln(I_D / 0.7032)/0.9072} && I_D < 0.4016 \\ t_D &= 10^{(I_D - 0.6266)/0.3643} && 0.4016 < I_D < 0.7869 \\ t_D &= 10^{\ln((1-I_D)/0.4522)/(-1.7098)} && I_D > 0.7869 \end{aligned} \tag{2-25}$$

For both 1D and 2D cases, from the equations (2-21) to (2-24), $t_{D,\,Pb}$ (relative time under the pressure p_b) will be calculated as a function of $I_{D,\,Pa}$ which is derived from $t_{D,\,Pa}$ (relative time under the pressure P_a). With a combination of the equations (2-4) and (2-5), the corrected time t_{c1} (t_{Pb}) will be calculated as:

$$t_{c1} = t_{Pb} = t_{D,Pb} \cdot \frac{6P_b \cdot \mu_g}{\tau_0^2} \tag{2-26}$$

,see Figure 2-17.

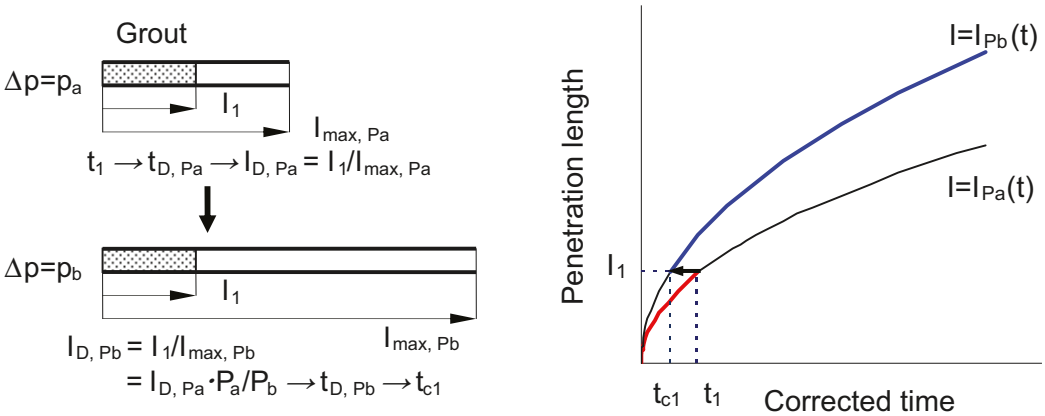

Figure 2-17. *Relationship between real time t_1 and corrected time t_{c1}. The figure on the left illustrates how the grouting time is corrected as the grouting pressure increase. The graph on the right shows the relationship between corrected time and grout penetration.*

2.3.2 Examples of theoretical grout penetration

Figure 2-18 to Figure 2-21 show the examples of theoretical grout penetration of a Bingham fluid into a fracture at varying pressure. The grouting parameters are shown below:

- Grouting pressure (Δp): 1 MPa (10 min.), 2 MPa (10 min.), 3 MPa (10 min.)
- Grout properties Yield value (τ_0): 0.296 Pa, Viscosity (μ_g): 0.0056 Pas.
- Fracture Aperture (b): 0.15 mm, Width for 1D case (w): 10 m.

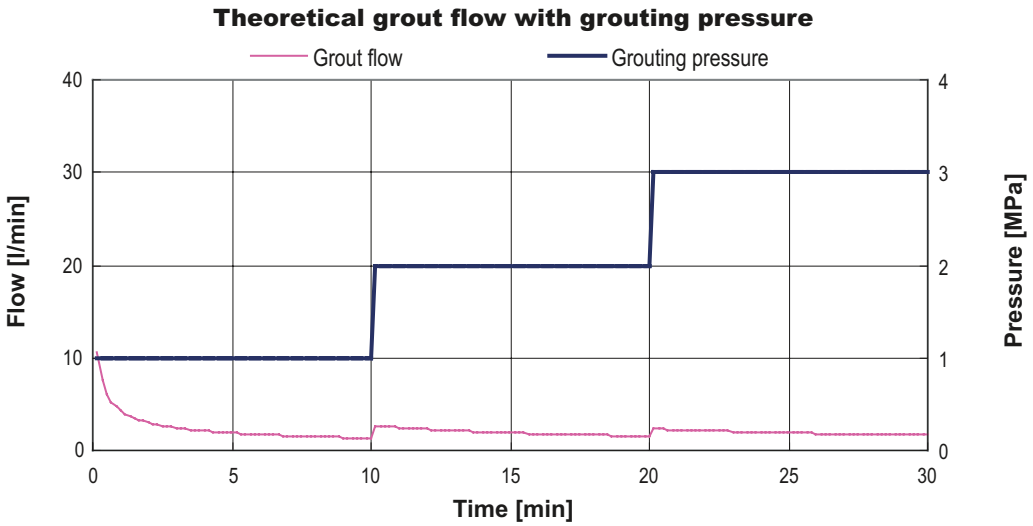

Figure 2-18. *Theoretical grout flow of a Bingham fluid at varying pressure for 1D case.*

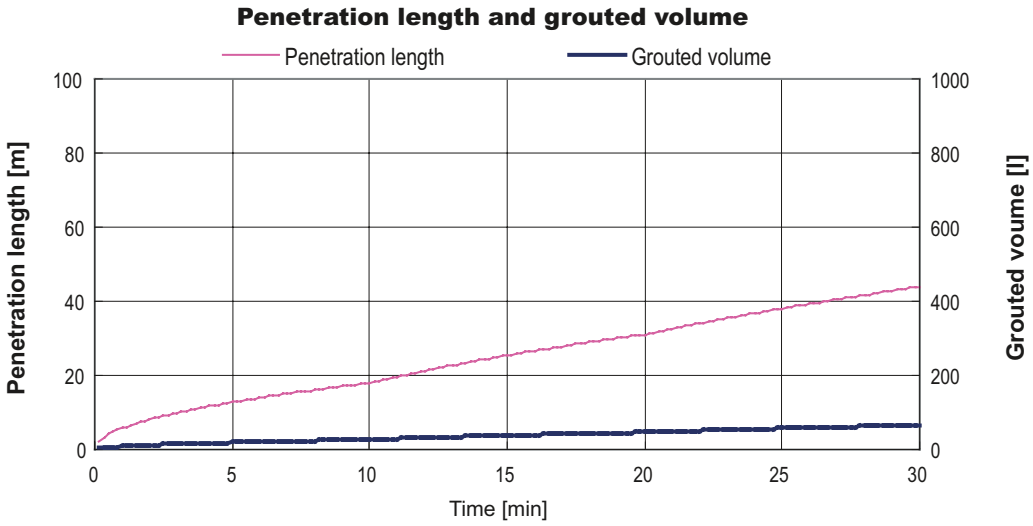

Figure 2-19. *Theoretical penetration length and grouted volume of a Bingham fluid at varying pressure for 1D case.*

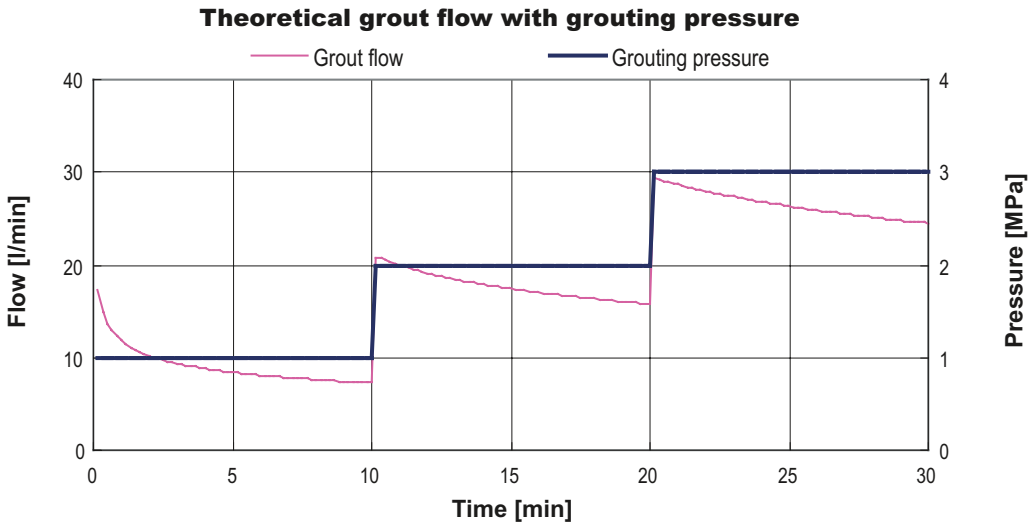

Figure 2-20. *Theoretical grout flow of a Bingham fluid at varying pressure for 2D case.*

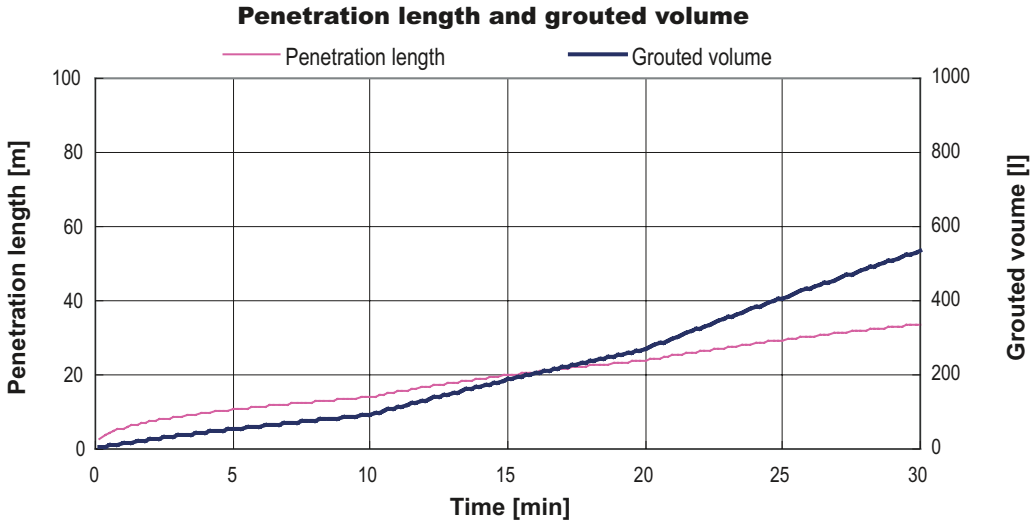

Figure 2-21. *Theoretical penetration length and grouted volume of a Bingham fluid at varying pressure for 2D case.*

2.4 Time-dependent grout properties

2.4.1 Hardening of the grout

The grout is characterized in terms of rheology such as yield strength and plastic viscosity. There are two methods of using the properties for the calculation. One is to use constants, which are shown above. The other is to use the method in which the properties are described as time-dependent, which was the alternative used in the experiment at the Äspö HRL by /Emmelin et al. 2004/, (see Table 2-1 and Figure 2-22).

Table 2-1. Grout properties valid for t < 3,600sec.

Property		Grout A UF 16, w/c 2.0 0.9% HPM	B UF 16, w/c 1.0 0.9% HPM	C UF 16, w/c 0.8 0.9% HPM
Rheology	Yield value [Pa]	$0.296 \cdot e^{0.0004t}$	$1.5 \cdot e^{0.0004t}$	–
	Viscosity [Pas]	$0.0056 \cdot e^{0.0004t}$	$0.017 \cdot e^{0.0004t}$	–

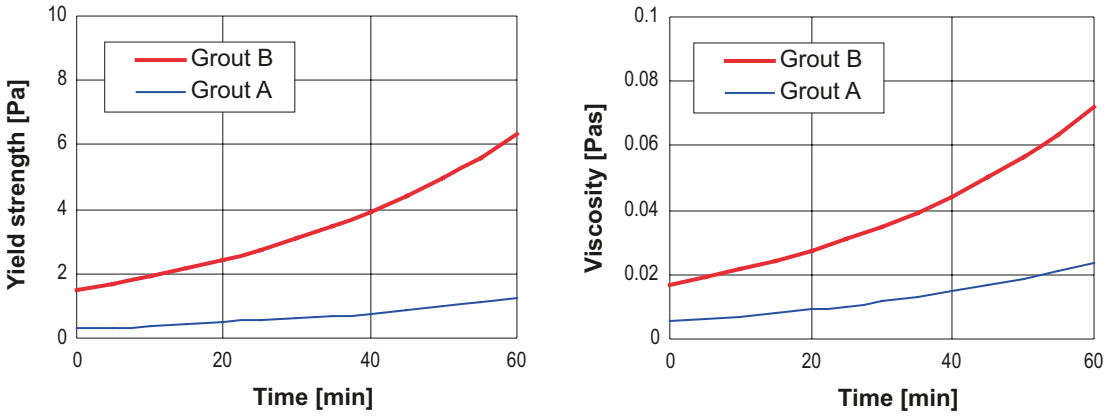

Figure 2-22. *Hardening of the grouts. The graph on the left shows the relationship between time and yield strength. The graph on the right shows the relationship between time and viscosity.*

2.4.2 Corrected time

In order to take time-dependent grout properties into account, the simple case is described in which the yield strength and the viscosity increase from τ_{0a}, μ_{ga} to τ_{0b}, μ_{gb} at time t_1, see Figure 2-16. In the same way as in Section 2.3, the relationship between grouting time and grout penetration length can be calculated as:

$$I = I_a(t), \qquad t < t_1 \tag{2-27}$$

$$I = I_b(t - (t_1 - t_{c1})), \qquad t > t_1 \tag{2-28}$$

$$I_b(t_{c1}) = I_a(t_1) = I_1 \tag{2-29}$$

where $I_a(t)$ is the relationship between time and penetration of the grout with the yield strength τ_{0a} and the viscosity μ_{ga}, and $I_b(t)$ is the relationship between time and penetration of the grout with the yield strength τ_{0b} and the viscosity μ_{gb}.

Using the equation (2-20) and (2-29), the relationship between I_{Da} (relative penetration of the grout with the yield strength τ_{0a} and the viscosity μ_{ga}) and I_{Db} (relative penetration of the grout with the yield strength τ_{0b} and the viscosity μ_{gb}) is calculated as:

$$I_{Db} = I_{Da} \cdot \frac{\tau_{0b}}{\tau_{0a}} \tag{2-30}$$

For both 1D and 2D cases, t_{Db} (relative time of the grout with the yield strength τ_{0b} and the viscosity μ_{gb}) will be calculated as a function of I_{Db} and the corrected time t_{c1} will be calculated as:

$$t_{c1} = t_{Db} \cdot \frac{6\Delta p \cdot \mu_{gb}}{\tau_{0b}^{\,2}} \tag{2-31}$$

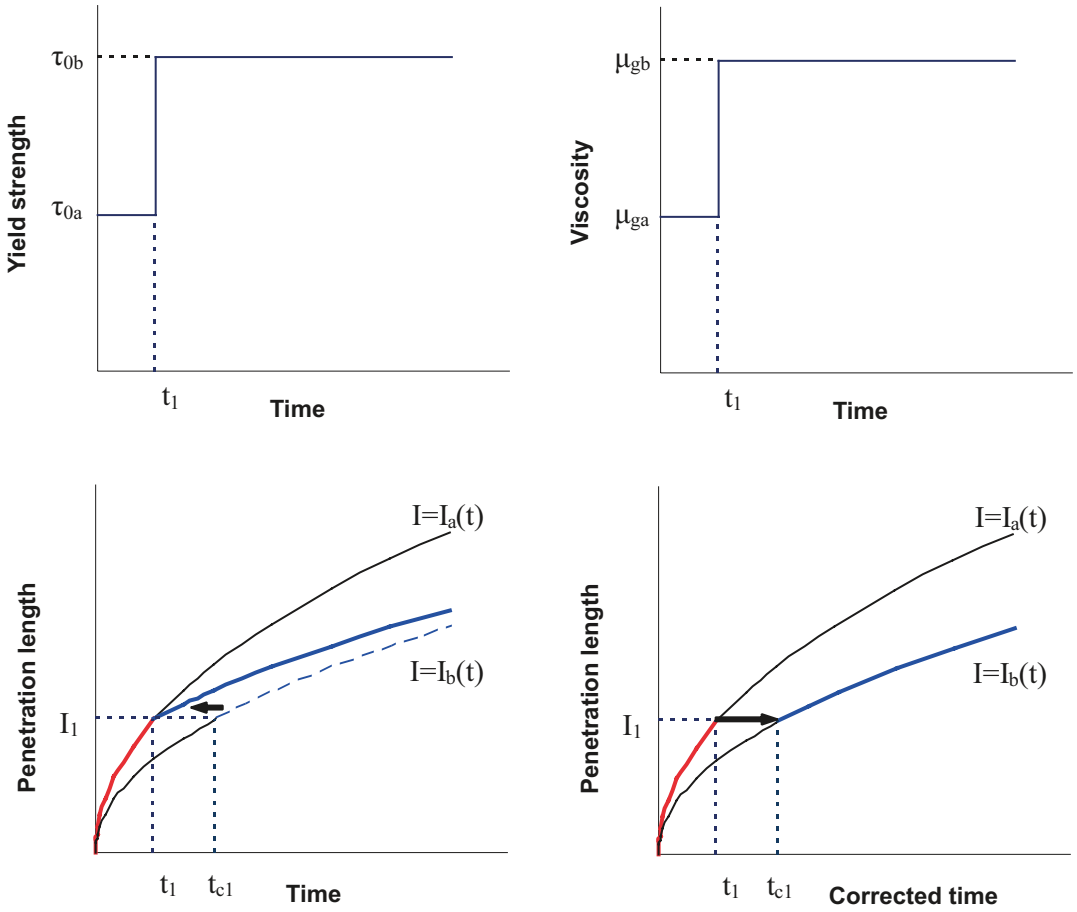

Figure 2-23. *Relationship between time and penetration when the yield strength and the viscosity increase from τ_{0a}, μ_{ga} to τ_{0b}, μ_{gb}. The graphs on the top show the relationship between grouting time and grout properties. The graph on the bottom left shows how penetration changes as the grout properties change. The graph on the bottom right shows the relationship between corrected time and grout penetration.*

2.4.3 Examples of theoretical grout penetration

Figure 2-24 and Figure 2-25 show the examples of theoretical grout penetration of a Bingham fluid with time-dependent grout properties into a fracture at constant pressure. The grouting parameters are shown below:

- Grouting pressure (Δp): 3 MPa.
- Grout properties Yield value (τ_0): $0.296 \cdot e^{0.0004t}$ Pa, Viscosity (μ_g): $0.0056 \cdot e^{0.0004t}$ Pas (same as Grout A in Table 2-1, t: time [sec]).
- Fracture Aperture (b): 0.15 mm, Width for 1D case (w): 10 m.

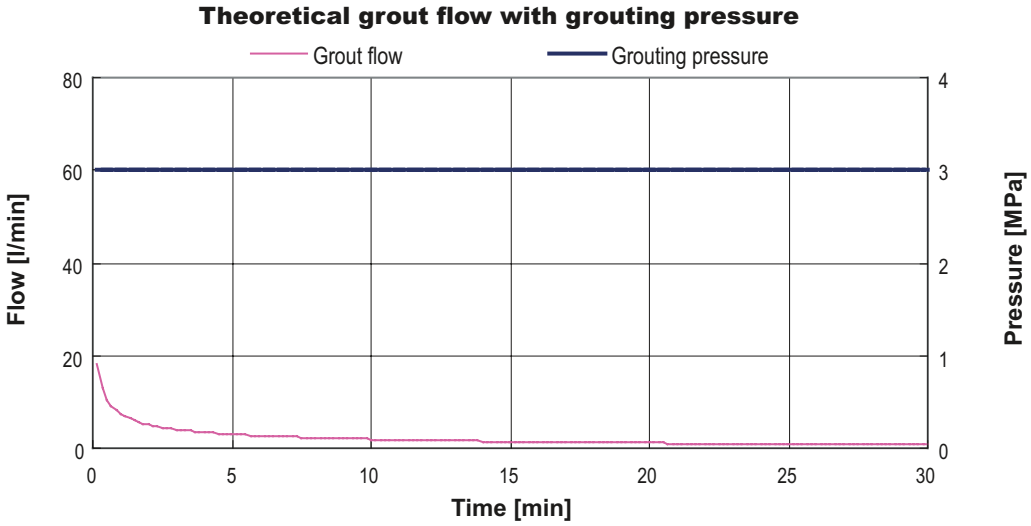

Figure 2-24. *Theoretical grout flow of a Bingham fluid with time-dependent grout properties at constant pressure for 1D case.*

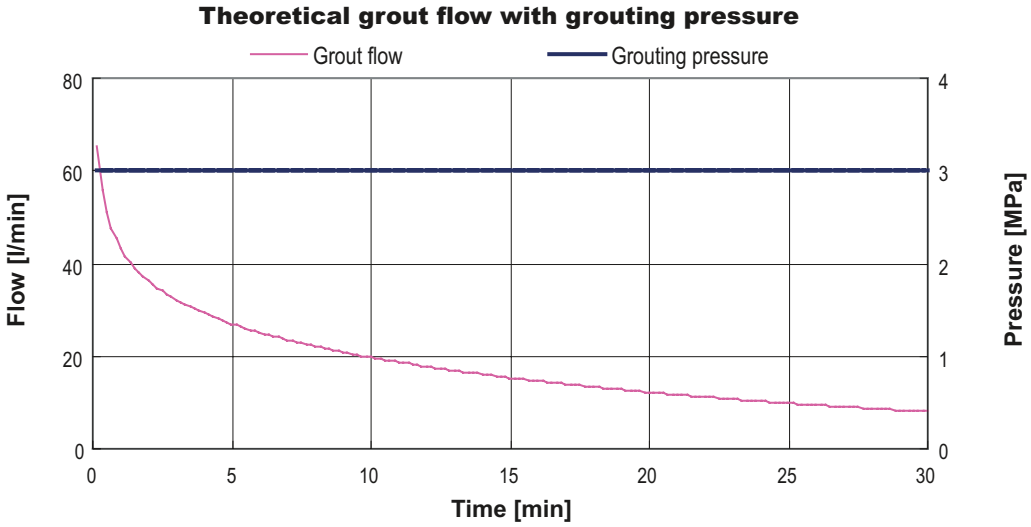

Figure 2-25. *Theoretical grout flow of a Bingham fluid with time-dependent grout properties at constant pressure for 2D case.*

2.4.4 Varying grouting pressure and time-dependent properties

With a combination of theories concerning varying grouting pressure and time-dependent properties, the relationship between $I_{Da,\,Pa}$ (relative penetration of the grout with the yield strength τ_{0a} and the viscosity μ_{ga} under the pressure p_a) and $I_{Db,\,Pb}$ (relative penetration of the grout with the yield strength τ_{0b} and the viscosity μ_{gb} under the pressure p_b) is calculated as:

$$I_{Db,Pb} = I_{Da,Pa} \cdot \frac{p_a}{p_b} \cdot \frac{\tau_{0b}}{\tau_{0a}} \tag{2-32}$$

For both 1D and 2D cases, $t_{Db,\,Pb}$ (relative time of the grout with the yield strength τ_{0b} and the viscosity μ_{gb} under the pressure p_b) will be calculated as a function of $I_{Db,\,Pb}$ and the corrected time t_{c1} will be calculated as:

$$t_{c1} = t_{Db,Pb} \cdot \frac{6P_b \cdot \mu_{gb}}{\tau_{0b}^{\,2}} \tag{2-33}$$

2.4.5 Examples of theoretical grout penetration

Figure 2-26 and Figure 2-27 show the examples of theoretical grout penetration of a Bingham fluid with time-dependent grout properties into a fracture at varying pressure. The grouting parameters are shown below:

- Grouting pressure (Δp): 1 MPa (10 min.), 2 MPa (10 min.), 3 MPa (10 min.).
- Grout properties Yield value (τ_0): $0.296 \cdot e^{0.0004t}$ Pa, Viscosity (μ_g): $0.0056 \cdot e^{0.0004t}$ Pas.
- Fracture Aperture (b): 0.15 mm, width for 1D case (w): 10 m.

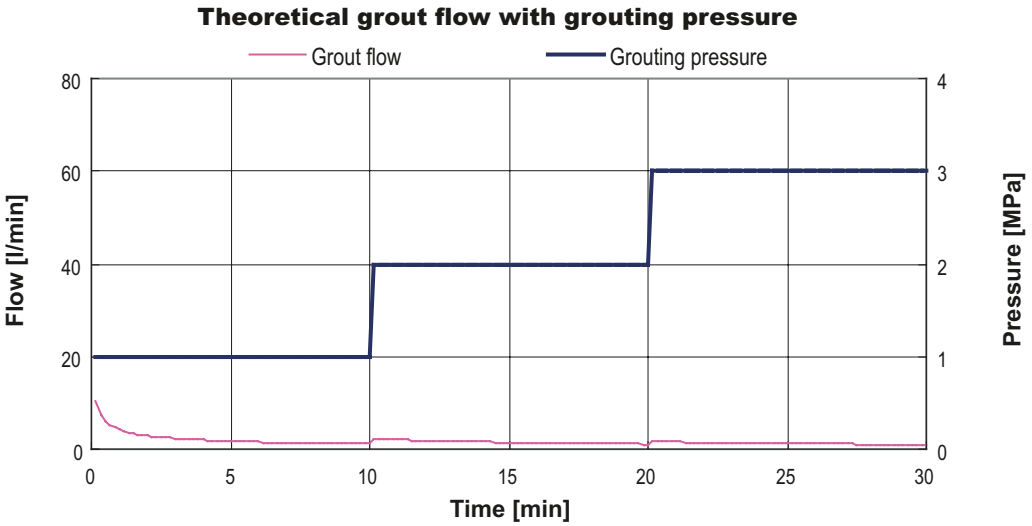

Figure 2-26. *Theoretical grout flow of a Bingham fluid with time-dependent grout properties at varying pressure for 1D case.*

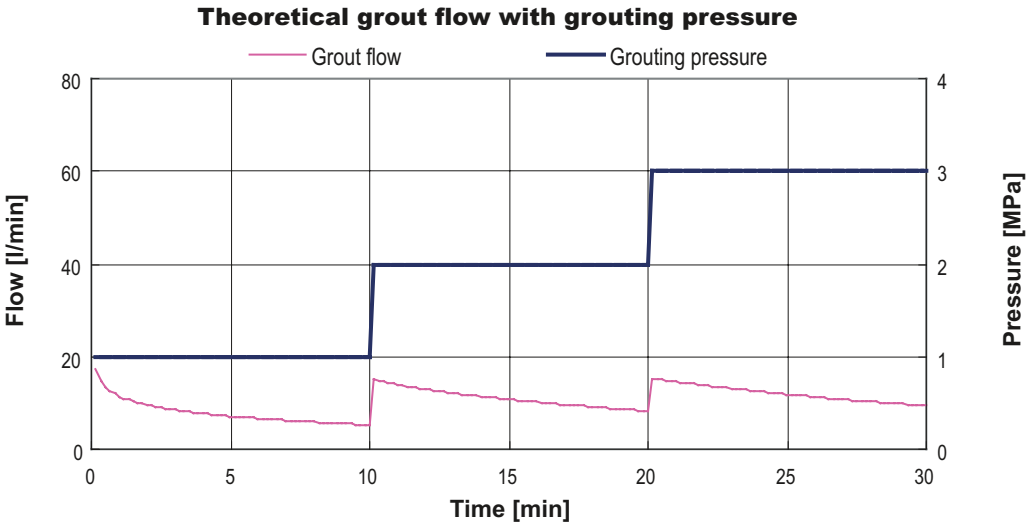

Figure 2-27. *Theoretical grout flow of a Bingham fluid with time-dependent grout properties at varying pressure for 2D case.*

2.5 Changing grout mixes

2.5.1 Upper and lower boundaries

In normal grouting work, it is quite common to change the recipe from thin grout to thick grout during grouting. However, since obtaining the theoretical solution for changing grout mixes is not a straightforward matter, the lower and upper boundaries for penetration length after the grout mix is changed from thin grout (Grout A) to thick grout (Grout B) were calculated in /Kobayashi and Stille 2007/.

The lower boundary is calculated on the assumption that the properties of the pre-injected grout (Grout A) are the same as those of new grout (Grout B), see Figure 2-28. Based on this assumption, grout penetration after time t_1 can be described by using the penetration curve for new grout (Grout B) from penetration I_1 as:

$$I = I_{Ga}(t), \qquad t < t_1 \tag{2-34}$$

$$I = I_{Gb}(t + t_{c1} - t_1), \qquad t > t_1 \tag{2-35}$$

$$I_{Gb}(t_{c1}) = I_{Ga}(t_1) = I_1 \tag{2-36}$$

where $I_{Ga}(t)$ is the relationship between time and penetration of Grout A and $I_{Gb}(t)$ is the relationship between time and penetration of Grout B.

The upper boundary is calculated on the assumption that the properties of the pre-injected grout (Grout A) are the same as those of the groundwater, see Figure 2-29. Based on this assumption, grout penetration after time t_1 can be described by using the penetration curve for new grout (Grout B) from penetration 0 as:

$$I = I_{Ga}(t), \qquad t < t_1 \tag{2-37}$$

$$I = I_{Ga}(t_1) + I_{Gb}(t - t_1), \qquad t > t_1 \tag{2-38}$$

$$I_{Ga}(t_1) = I_1 \tag{2-39}$$

Depending on flow properties of the grout and time to change grout mixes the upper boundary approach will give both an increase or a decrease of the grout flow. Figure 2-30 shows how penetration changes after the grout mix is changed.

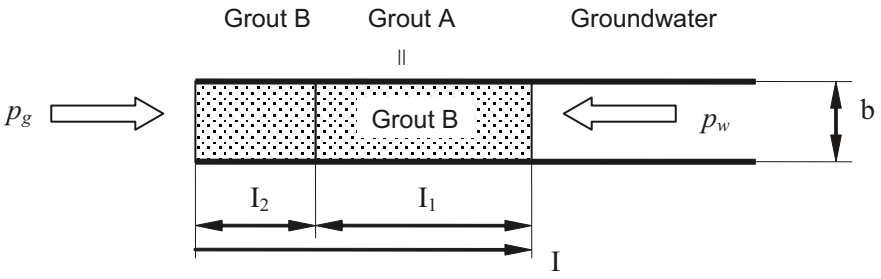

Figure 2-28. *Assumption for calculating the lower boundary.*

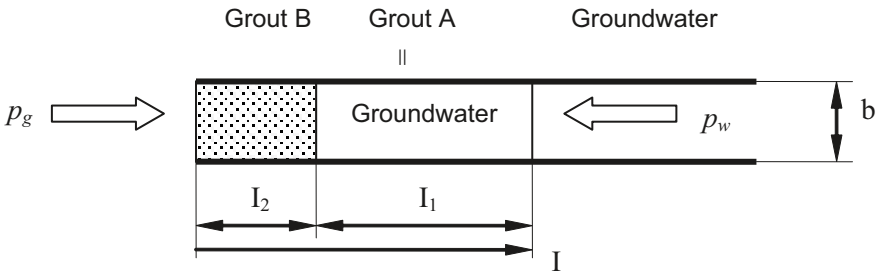

Figure 2-29. *Assumption for calculating the upper boundary.*

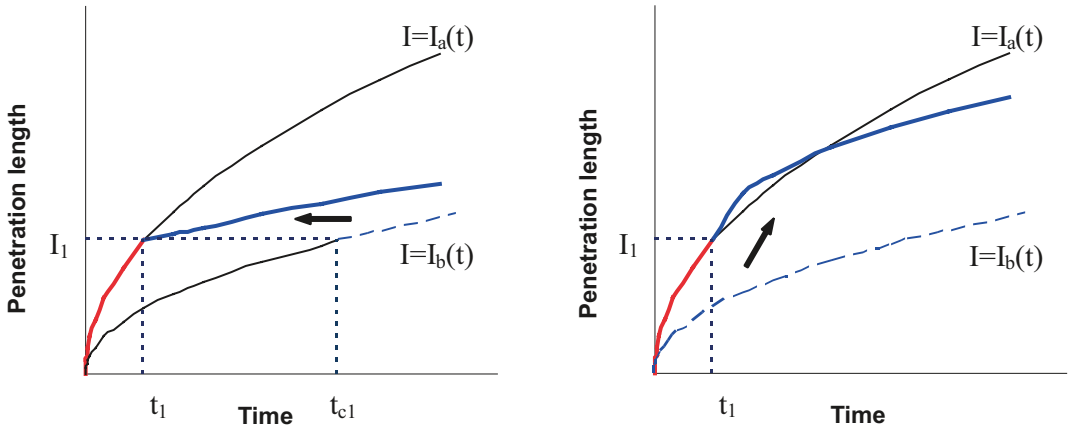

Figure 2-30. *Lower and upper boundaries of the relationship between time and penetration when the grout mix changes from Grout A to Grout B. The graph on the left shows the lower boundary and the graph on the right shows the upper boundary.*

2.5.2 Examples of theoretical grout penetration using upper and lower boundaries

Figure 2-32 to Figure 2-35 show the examples of theoretical grout penetration of Bingham fluids into a fracture at varying pressure. The grouting parameters are shown below:

- Grouting pressure Figure 2-31.
- Grout properties

  Grout A Yield value (τ_0): 0.296 Pa, viscosity (μ_g): 0.0056 Pas.

  Grout B Yield value (τ_0): 1.5 Pa, viscosity (μ_g): 0.017 Pas.
- Fracture Aperture (b): 0.15 mm, width for 1D case (w): 10 m.
- Grouting starts with Grout A and, after 40 minutes, the grout is changed to Grout B.

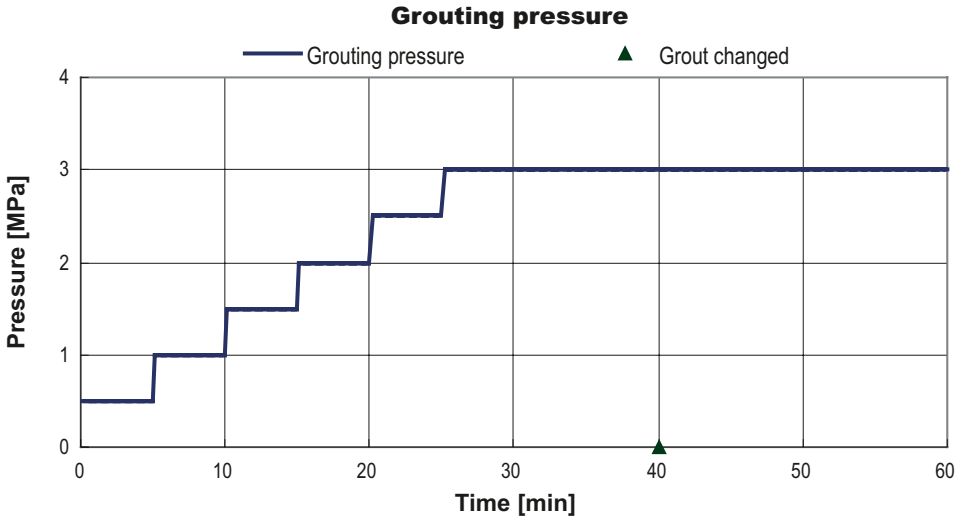

Figure 2-31. *Grouting pressure used for the calculation.*

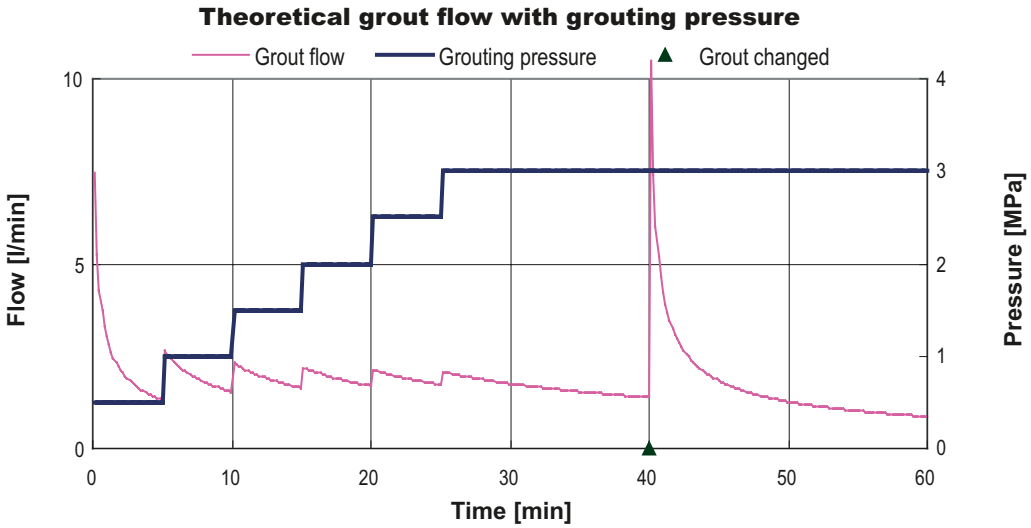

Figure 2-32. *Upper boundary of grout flow when the grout mix changes for 1D case.*

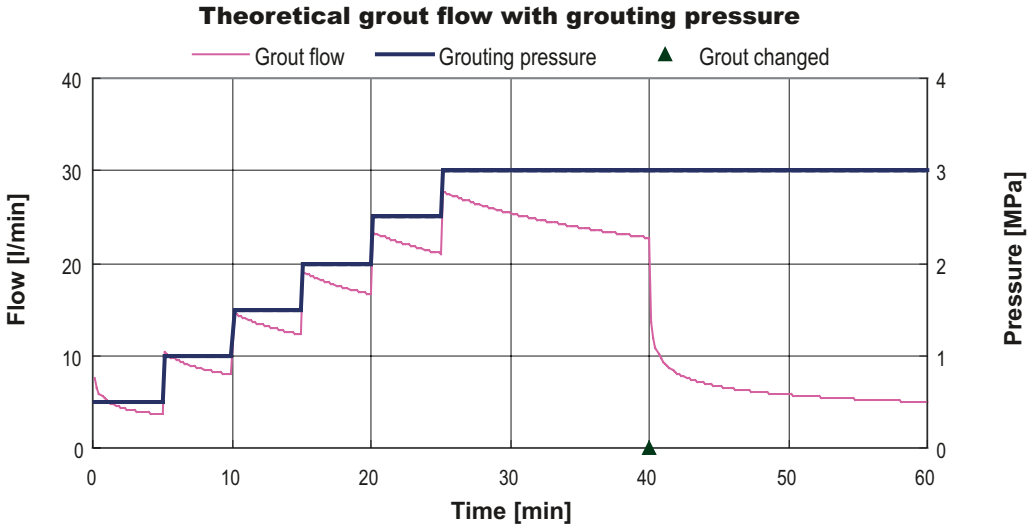

Figure 2-33. *Upper boundary of grout flow when the grout mix changes for 2D case.*

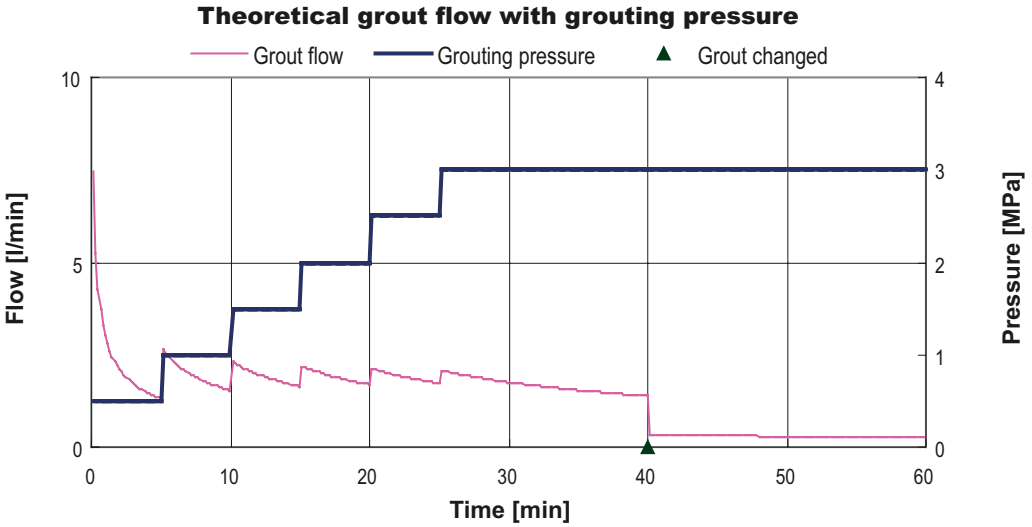

Figure 2-34. *Lower boundary of grout flow when the grout mix changes for 1D case.*

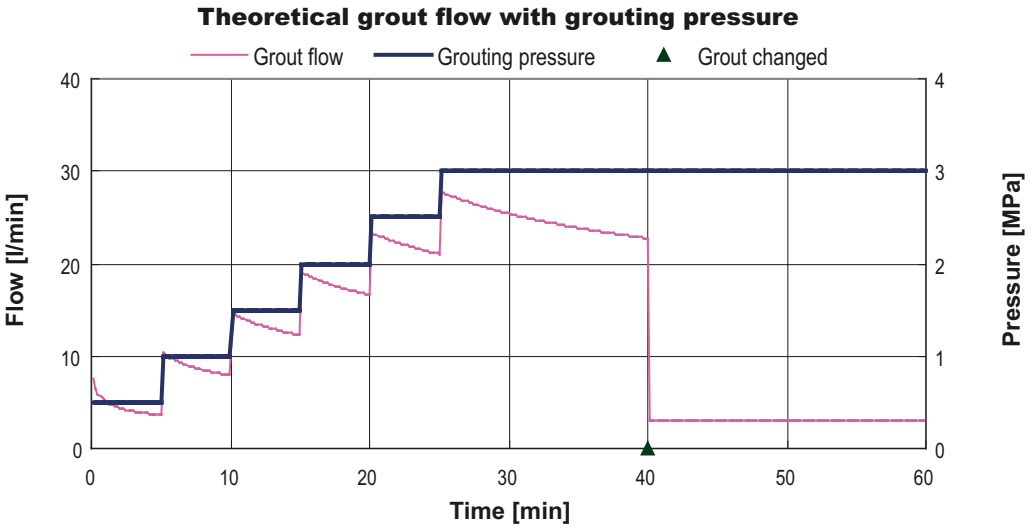

Figure 2-35. *Lower boundary of grout flow when the grout mix changes for 2D case.*

2.5.3 Middle method

As can be seen from Figure 2-32, the upper boundary of the grout flow when the grout mix changes for 1D case is too large and seems unrealistic. On the other hand, the lower boundaries of the grout flow when the grout mix changes for both 1D and 2D cases appear to be too small (see Figure 2-34 and Figure 2-35). Another method is to calculate the middle values of the upper and lower boundaries. These are calculated on the assumption that the properties of part of the pre-injected grout (Grout A) are the same as those of new grout (Grout B) and those of the other part are the same as those of the groundwater, see Figure 2-36. I_1' is the length of the part in which the properties are the same as those of Grout B and will be set as the length that is calculated from the same grouting time as Grout A. On this assumption, grout penetration after time t_1 can be described by using the penetration curve for new grout (Grout B) from penetration I_1' (time t_1) as:

$$I = I_{Ga}(t), \qquad t < t_1 \tag{2-40}$$

$$I = I_{Ga}(t_1) + I_{Gb}(t) - I_{Gb}(t_1), \quad t > t_1 \tag{2-41}$$

Figure 2-36 shows how penetration changes after the grout mix is changed.

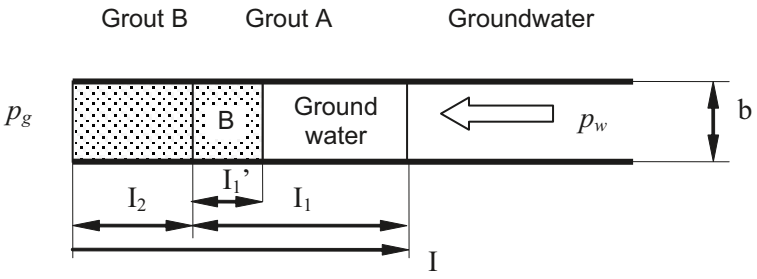

Figure 2-36. *Middle method assumptions.*

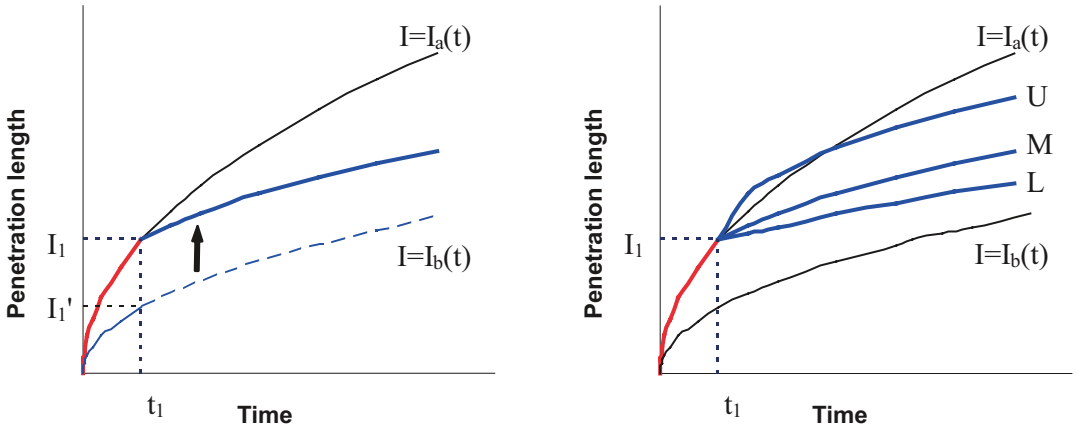

Figure 2-37. *Relationship between time and penetration when the grout mix changes from Grout A to Grout B. The graph on the left shows the penetration using the middle method. The graph on the right shows the upper boundary (U), the middle method (M) and the lower boundary (L).*

2.5.4 Examples of theoretical grout penetration using the middle method

Figure 2-38 to Figure 2-43 show the examples of theoretical grout penetration of Bingham fluids into a fracture at varying pressure using the middle method. The grouting parameters are the same as those shown in Section 2.5.2.

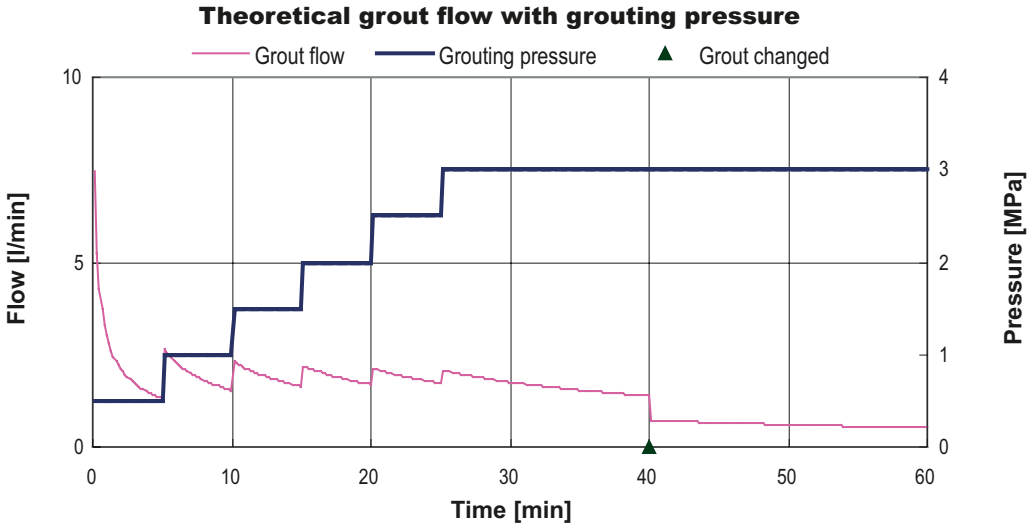

Figure 2-38. *Grout flow using the middle method when the grout mix changes for 1D case.*

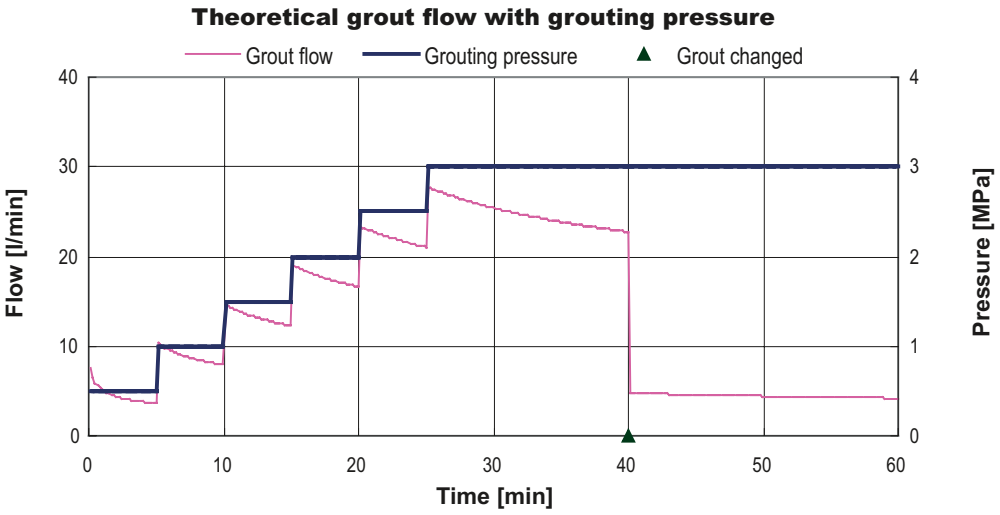

Figure 2-39. *Grout flow using the middle method when the grout mix changes for 2D case.*

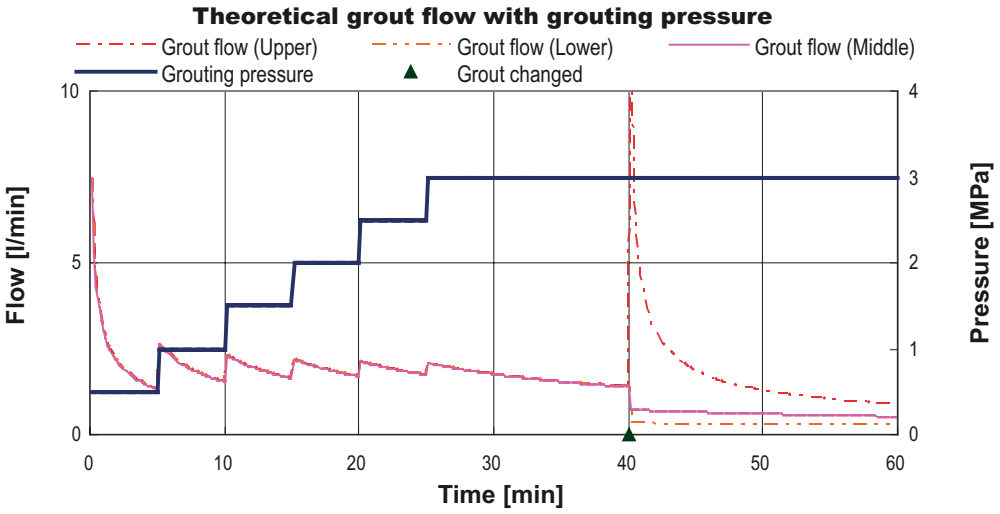

Figure 2-40. *Grout flow comparison between the upper boundary, the lower boundary and the middle method when the grout mix changes for 1D case.*

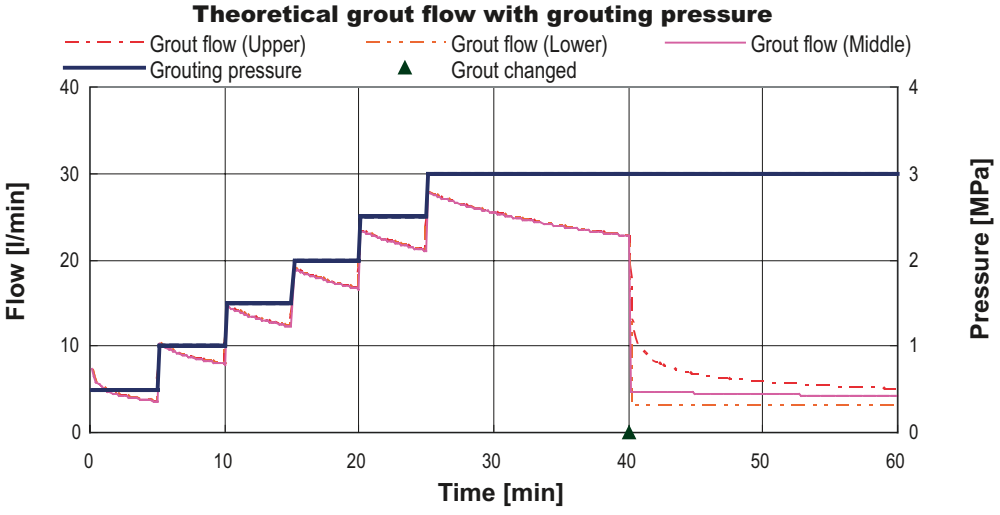

Figure 2-41. *Grout flow comparison between the upper boundary, the lower boundary and the middle method when the grout mix changes for 2D case.*

2.6 Dimensionality of flow in the fracture

2.6.1 Indexes for analysis of dimensionality

In addition to $Q \cdot t/V$, which is described in Section 2.2.4, two other indexes for analyzing the flow dimensionality of the fracture can be defined. The requirement of the index is that the dimensionality can also be distinguished for changes in pressure and that it is robust for variations in pressure and flow. There are three types of index:

- $Q \cdot t/V$.
- $Q/V \cdot t_0$.
- $Q/V \cdot t_0 \cdot I_D \cdot (dI_D/dt_D)^{-1}$.

The first index can be directly calculated from the grout take and the grouting time. The other two can only be calculated if the grout properties are known. The disadvantage of the first index is that erroneous results can be obtained if it is not corrected for changes in pressure and grout properties, which therefore also have to be known.

The indexes are compared by using the theoretical grout penetration of Bingham fluids with time-dependent grout properties into a fracture at varying pressure using the middle method when the grout mix changes. The grouting parameters are shown below:

- Grouting pressure Figure 2-31.
- Grout properties

  Grout A Yield value (τ_0): $0.296 \cdot e^{0.0004t}$ Pa, viscosity (μ_g): $0.0056 \cdot e^{0.0004t}$ Pas.

  Grout B Yield value (τ_0): $1.5 \cdot e^{0.0004t}$ Pa, viscosity (μ_g): $0.017 \cdot e^{0.0004t}$ Pas.
- Fracture Aperture (b): 0.15 mm, width for 1D case (w): 10 m.
- Grouting starts with Grout A which, after 40 minutes, is changed to Grout B.

Figure 2-42 and Figure 2-43 show the theoretical flow for both 1D and 2D cases.

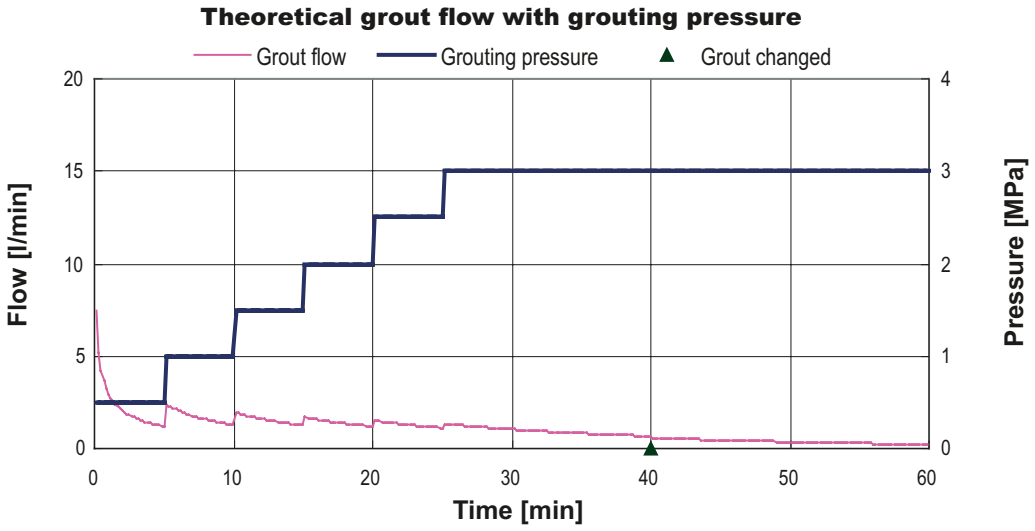

Figure 2-42. *Theoretical grout flow of Bingham fluids with time-dependent grout properties at varying pressure using the middle method when the grout mix changes for 1D case.*

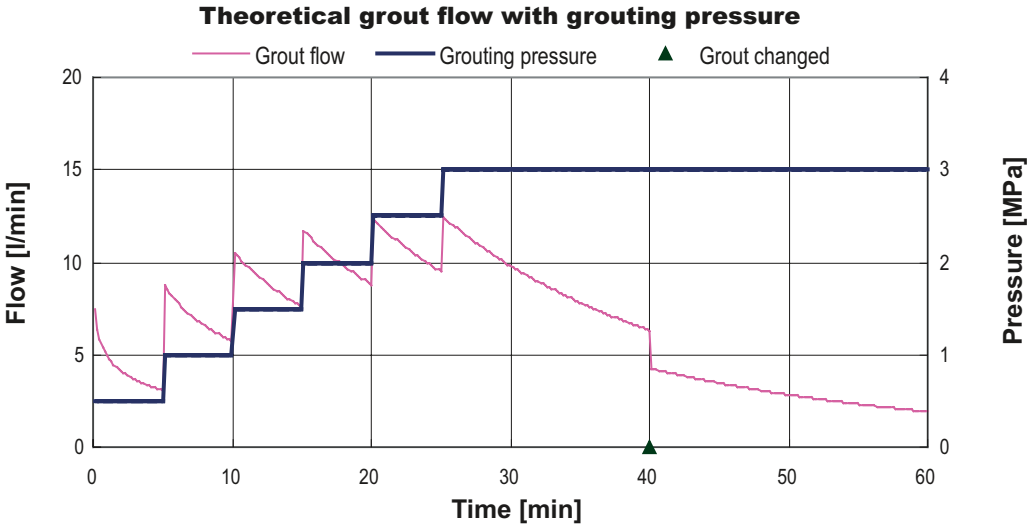

Figure 2-43. *Theoretical grout flow of Bingham fluids with time-dependent grout properties at varying pressure using the middle method when the grout mix changes for 2D case.*

2.6.2 Q·t/V

For the 1D case, $Q{\cdot}t/V$ is calculated from the equation (2-8) and (2-9) as:

$$\frac{Q \cdot t}{V} = \frac{t_D}{I_D} \cdot \frac{dI_D}{dt_D} \tag{2-42}$$

For the 2D case, it is also calculated from the equation (2-11) and (2-12) as:

$$\frac{Q \cdot t}{V} = 2 \cdot \frac{t_D}{I_D} \cdot \frac{dI_D}{dt_D} \tag{2-43}$$

In order to take varying grouting pressure, time-dependent grout properties and changing grout mixes into account, time must be corrected by using (2-32) and (2-33) Therefore, both 1D-correction and 2D-correction are necessary for analyzing the flow dimensionality of the fracture. Figure 2-44 shows the difference between 1D-correction and 2D-correction for the 1D case. 1D-corrected $Q{\cdot}t/V$ is the same as the 1D-theoretical. On the other hand, 2D-corrected $Q{\cdot}t/V$ is somewhat different from the 1D-theoritical. Since the difference is very little before changing grout, the dimensionality can be estimated to a satisfactory level of accuracy. The same applies for the 2D case as shown in Figure 2-45.

If time is not corrected, Q·t/V varies widely as shown in Figure 2-46 and Figure 2-47.

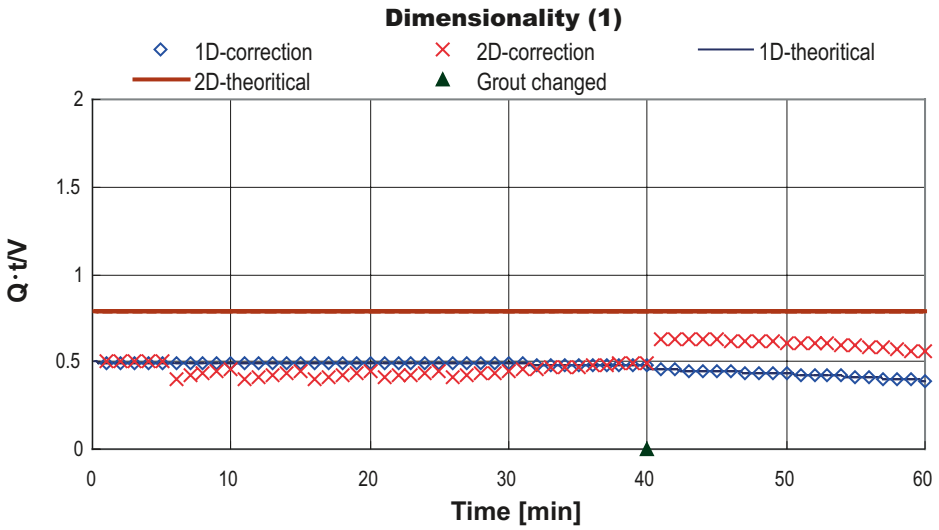

Figure 2-44. *Index for analyzing the dimensionality, $Q \cdot t_c/V$ for 1D case.*

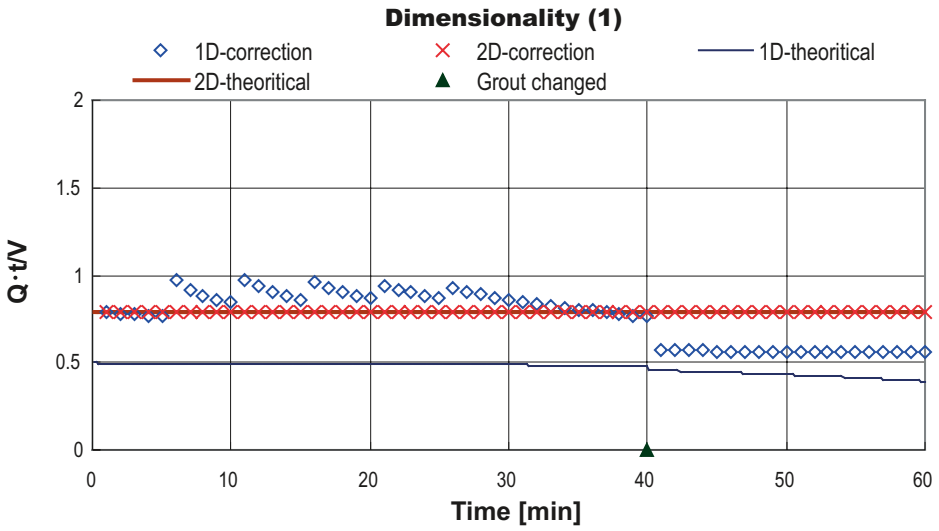

Figure 2-45. *Index for analyzing the dimensionality, $Q \cdot t_c/V$ for 2D case.*

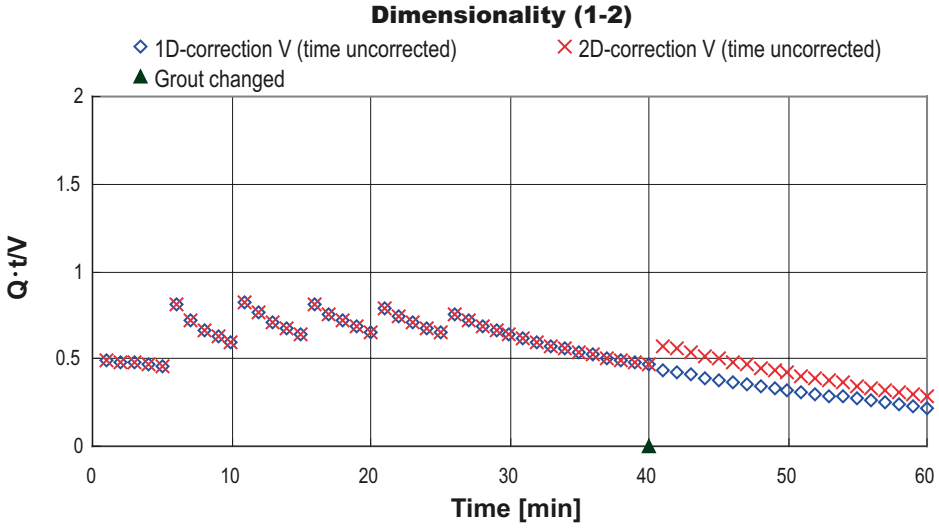

Figure 2-46. *Index for analyzing the dimensionality, $Q \cdot t/V$ for 1D case.*

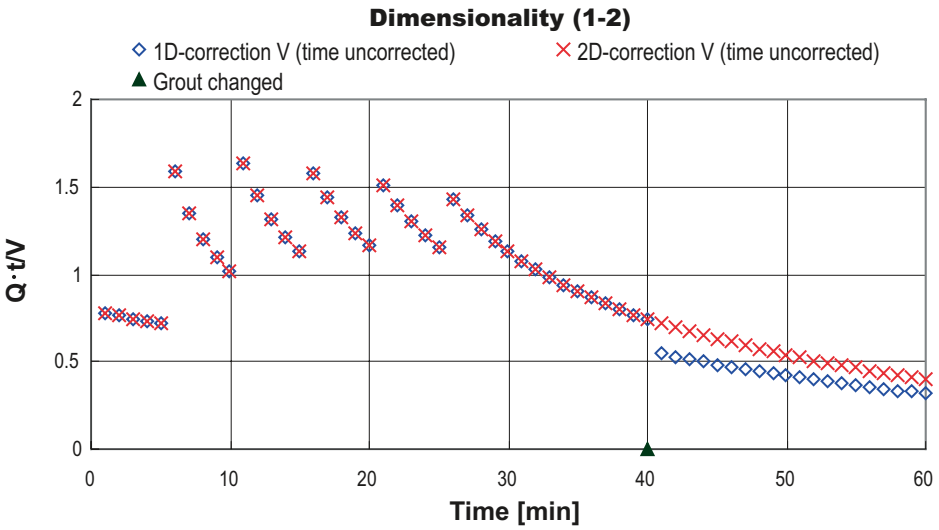

Figure 2-47. *Index for analyzing the dimensionality, Q·t/V for 2D case.*

2.6.3 Q/V·t_0

In order to avoid the complication of 1D and 2D correction, $Q/V \cdot t_0$ can be used. For the 1D case, Q/V is calculated from the equation (2-8) and (2-9) as:

$$\frac{Q}{V} = \frac{1}{t_o \cdot I_D} \cdot \frac{dI_D}{dt_D} \tag{2-44}$$

For the 2D case, it is also calculated from the equation (2-11) and (2-12) as:

$$\frac{Q}{V} = \frac{2}{t_o \cdot I_D} \cdot \frac{dI_D}{dt_D} \tag{2-45}$$

Figure 2-48 and Figure 2-49 show Q/V for both the 1D and 2D cases. Since the difference between the two curves is marginal, it may influence the possibility of interpreting the dimensionality from measured data.

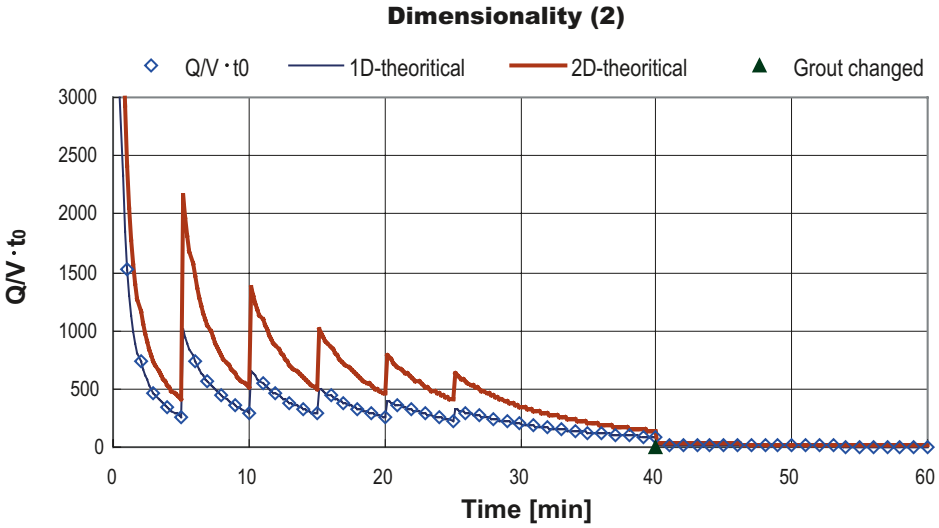

Figure 2-48. *Index for analyzing the dimensionality, , $Q/V \cdot t_0$ for the 1D case.*

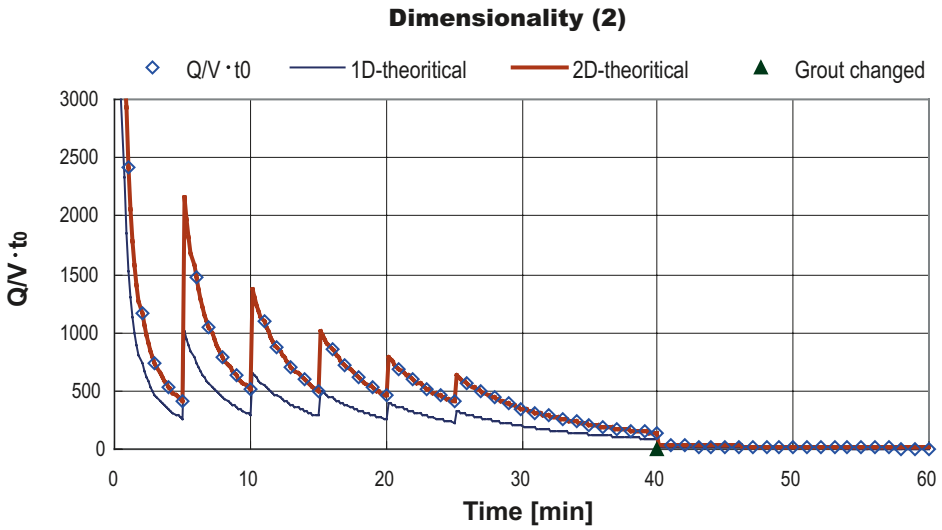

Figure 2-49. *Index for analyzing the dimensionality, $Q/V \cdot t_0$ for the 2D case.*

2.6.4 $Q/V \cdot t_0 \cdot I_D \cdot (dI_D/dt_D)^{-1}$

The other index is $Q/V \cdot t_0 \cdot I_D \cdot (dI_D/dt_D)^{-1}$ for analyzing the flow dimensionality of the fracture. Time must be corrected by using (2-32) and (2-33) for this index, but the difference in this index between the 1D and 2D cases is the most characteristic. For the 1D case, $Q/V \cdot t_0 \cdot I_D \cdot (dI_D/dt_D)^{-1}$ is calculated from the equation (2-8) and (2-9) as:

$$\frac{Q}{V} \cdot t_0 \cdot I_D \cdot \left(\frac{dI_D}{dt_D} \right)^{-1} = 1 \tag{2-46}$$

For the 2D case, it is also calculated from the equation (2-11) and (2-12) as:

$$\frac{Q}{V} \cdot t_0 \cdot I_D \cdot \left(\frac{dI_D}{dt_D} \right)^{-1} = 2 \tag{2-47}$$

Figure 2-50 and Figure 2-51 show $Q/V \cdot t_0 \cdot I_D \cdot (dI_D/dt_D)^{-1}$ for both the 1D and 2D cases.

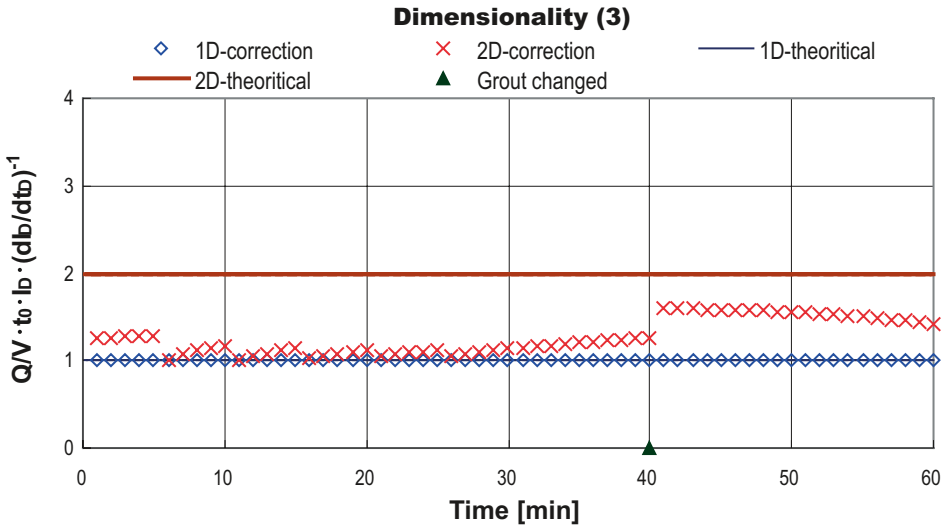

Figure 2-50. *Index for analyzing the dimensionality, $Q/V \cdot t_0 \cdot I_D \cdot (dI_D/dt_D)^{-1}$ for the 1D case.*

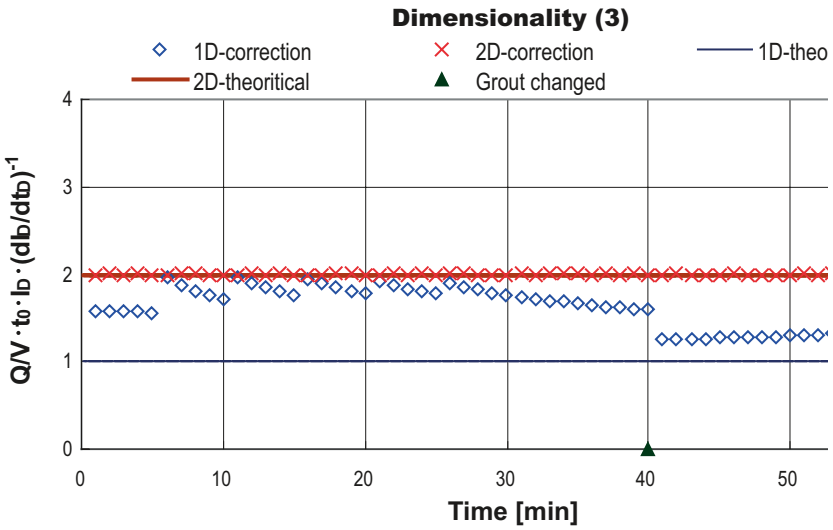

Figure 2-51. *Index for analyzing the dimensionality, $Q/V \cdot t_0 \cdot I_D \cdot (dI_D/dt_D)^{-1}$ for the 2D case.*

2.7 Changing the flow dimension of the fracture

2.7.1 2D to 1D case

It should be pointed out that the flow dimension of the fracture may change during the grouting. The assumption which describes the geometry for changing dimensionality is necessary. Figure 2-52 shows the image of changing the flow dimension of the fracture from 2D to 1D. On this assumption, grout penetration after time t_1 can be described by using the penetration curve for the 1D case from penetration I_1 as:

$$I = I_{2D}(t), \qquad t < t_1 \tag{2-48}$$

$$I = I_{1D}(t - (t_1 - t_2)), \quad t > t_1 \tag{2-49}$$

$$I_{1D}(t_2) = I_{2D}(t_1) = I_1 \tag{2-50}$$

where $I_{2D}(t)$ is the relationship between time and penetration for the2D case and $I_{1D}(t)$ is the relationship between time and penetration for the 1D case.

Grout flow after time t_1 can be described as:

$$Q = Q_{2D}(t), \qquad t < t_1 \tag{2-51}$$

$$Q = Q_{1D}(t - (t_1 - t_2)), \quad t > t_1 \tag{2-52}$$

$$Q_{2D}(t_1) = Q_1 \tag{2-53}$$

$$Q_{1D}(t_2) = Q_2 \tag{2-54}$$

$$Q_1 > Q_2 \tag{2-55}$$

where $Q_{2D}(t)$ is the relationship between time and grout flow for the 2D case and $Q_{1D}(t)$ is the relationship between time and grout flow for the 1D case, see Figure 2-53.

In the case of $Q_1 < Q_2$, the flow will remain as Q_1 for a certain period after changing the flow dimension. This case can not easily be analyzed and is not discussed further in this report.

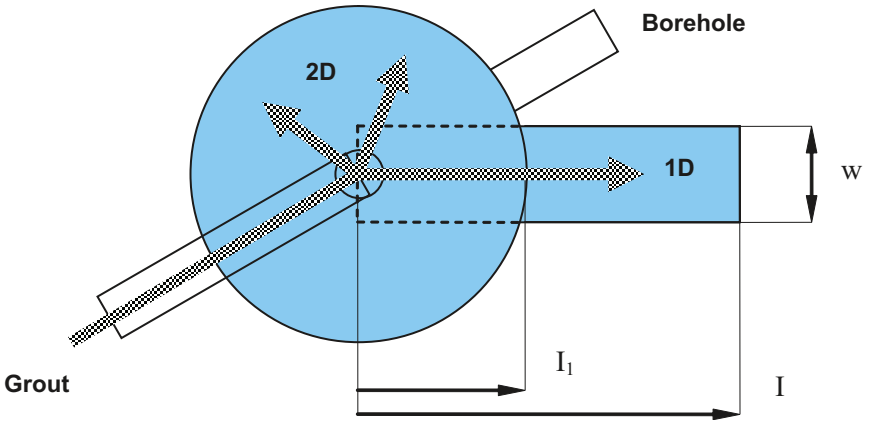

Figure 2-52. *Illustration of changing the flow dimension of the fracture from 2D to 1D.*

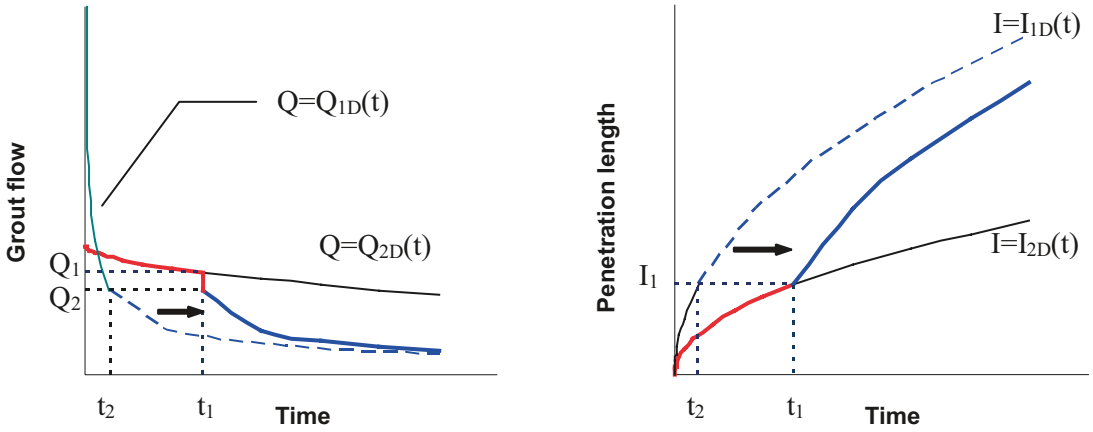

Figure 2-53. *Relationship between time and penetration when the flow dimension of the fracture changes from 2D to 1D. The graph on the left shows the relationship between grouting time and grout flow. The graph on the right shows how penetration changes as the flow dimension of the fracture changes from 2D to 1D.*

Figure 2-54 to Figure 2-58 show the examples of theoretical grout penetration of a Bingham fluid with time-dependent grout properties into a fracture at constant pressure. The grouting parameters are shown below:

- Grouting pressure (Δp): 3 MPa.
- Grout properties Yield value (τ_0): 0.296 Pa, viscosity (μ_g): 0.0056 Pas.
- Fracture Aperture (b): 0.1 mm, width for 1D case (w): 30 m.
- Flow dimension of the fracture changes from 2D to 1D after 15 minutes.

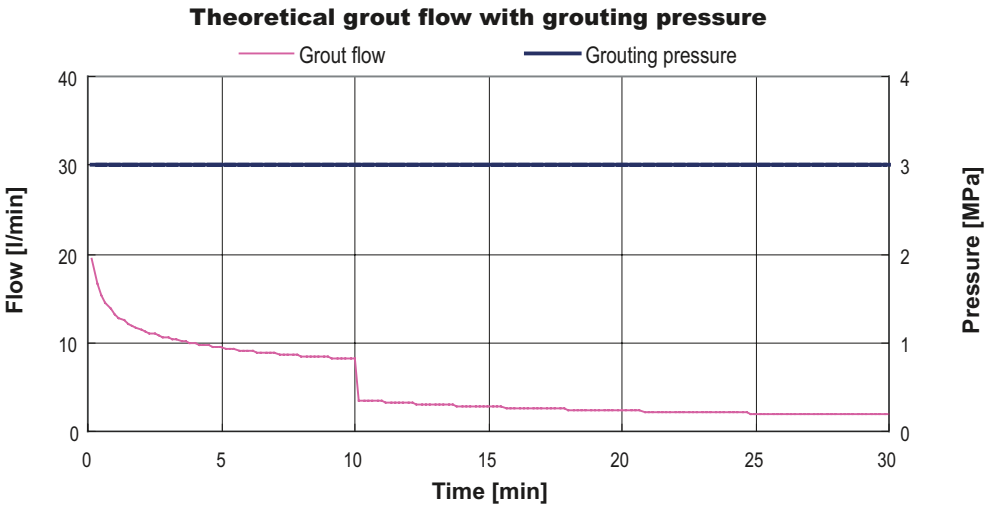

Figure 2-54. *Theoretical grout flow of a Bingham fluid at constant pressure with changing flow dimensionality of the fracture from 2D to 1D.*

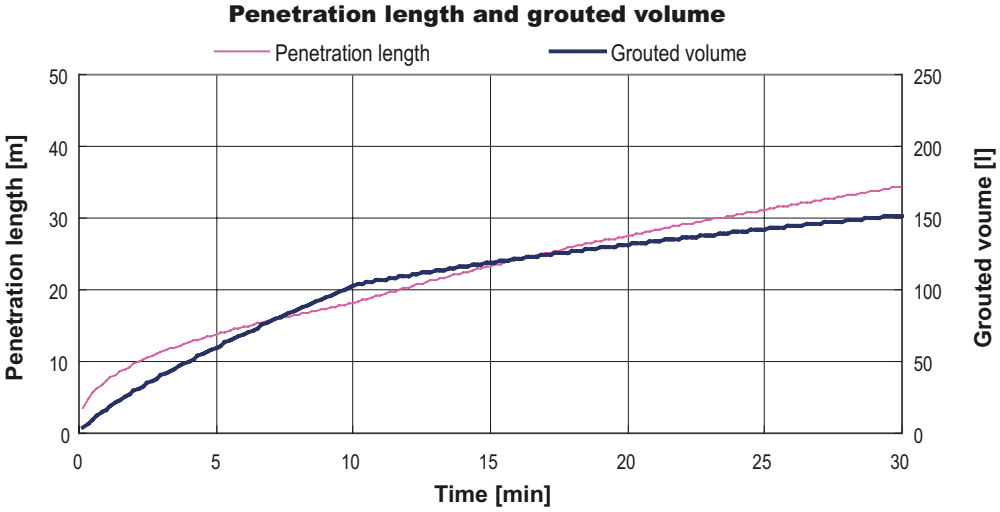

Figure 2-55. *Theoretical penetration length and grouted volume of a Bingham fluid at constant pressure with changing flow dimensionality of the fracture from 2D to 1D.*

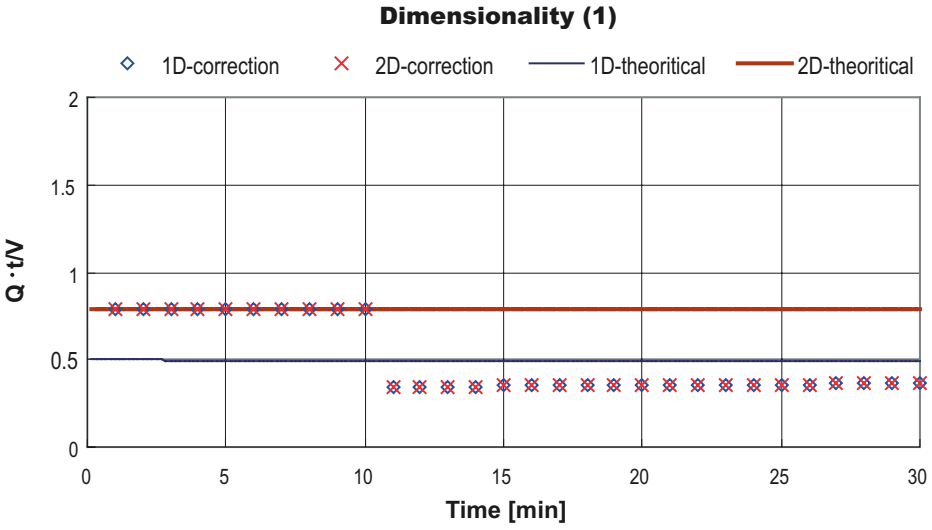

Figure 2-56. *Index for analyzing the dimensionality, Q·t/V from 2D to 1D.*

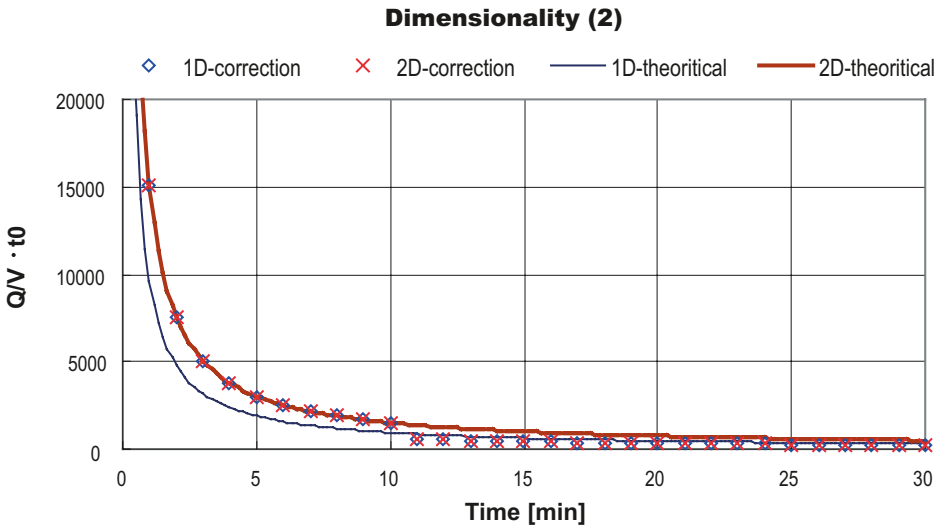

Figure 2-57. *Index for analyzing the dimensionality $Q/V \cdot t_0$ from 2D to 1D.*

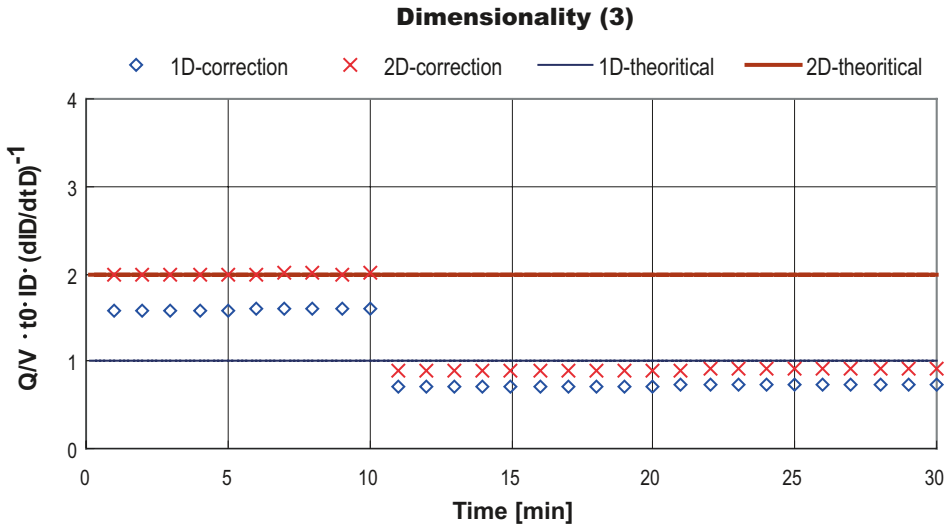

Figure 2-58. *Index for analyzing the dimensionality, $Q/V \cdot t_0 \cdot I_D \cdot (dI_D/dt_D)^{-1}$ from 2D to 1D.*

2.7.2 1D to 2D case

From the 1D to 2D case, it is not easy to make an assumption of geometrical model. One assumed image is shown in Figure 2-59. It is based on the case that the 2D structure is acting as a constriction of the flow or with other words that $Q_1 > Q_2$. On this assumption, grout penetration after time t_1 and grout flow can be described by considering the pressure drawdown as:

$$P_b = P_a - \frac{2\tau_0 \cdot I_1}{b} \tag{2-56}$$

$$I = I_{1D}(t), \qquad t < t_1 \tag{2-57}$$

$$I = I_{1D}(t_1) + I_{2D,Pb}(t - t_1), \qquad t > t_1 \tag{2-58}$$

$$I_{1D}(t_1) = I_1 \tag{2-59}$$

$$Q = Q_{1D}(t), \qquad t < t_1 \tag{2-60}$$

$$Q = Q_{2D,Pb}(t - t_1), \qquad t > t_1 \tag{2-61}$$

$$Q_{1D}(t_1) = Q_1 \tag{2-62}$$

$$Q_{2D,Pb}(t_1) = Q_2 \tag{2-63}$$

$$Q_1 > Q_2 \tag{2-64}$$

where p_a and p_b are the grouting pressure for the 1D and 2D fractures respectively. $I_{2D,Pa}(t)$ is the relationship between time and penetration for the 2D case under the pressure p_a and $I_{2D,Pb}(t)$ is that under the pressure p_b. $Q_{2D,Pa}(t)$ is the relationship between time and grout flow for the 2D case under the pressure p_a and $Q_{1D,Pb}(t)$ is the relationship between time and grout flow under the pressure p_b and $I_{2D,Pb}(t)$, see Figure 2-53. The problem has been simplified in respect of the change from 1D flow to 2D. Even if it is assumed that the grout will first flow in a 1D channel with a large width it will at the change to 2D flow occur in a single point.

In the case of $Q_1 < Q_2$, the flow to flow will remain as Q_1 for a certain period after changing the flow dimension as described in Section 2.2.7.

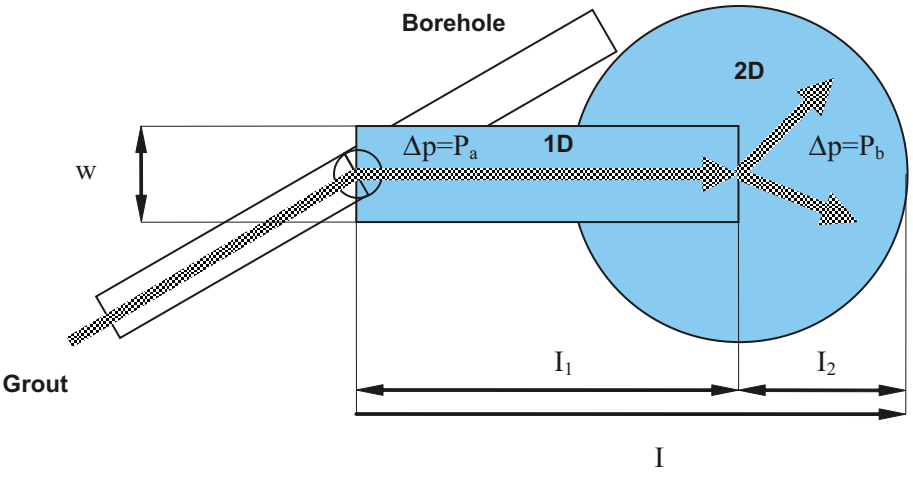

Figure 2-59. *Illustration of changing the flow dimension of the fracture from 1D to 2D.*

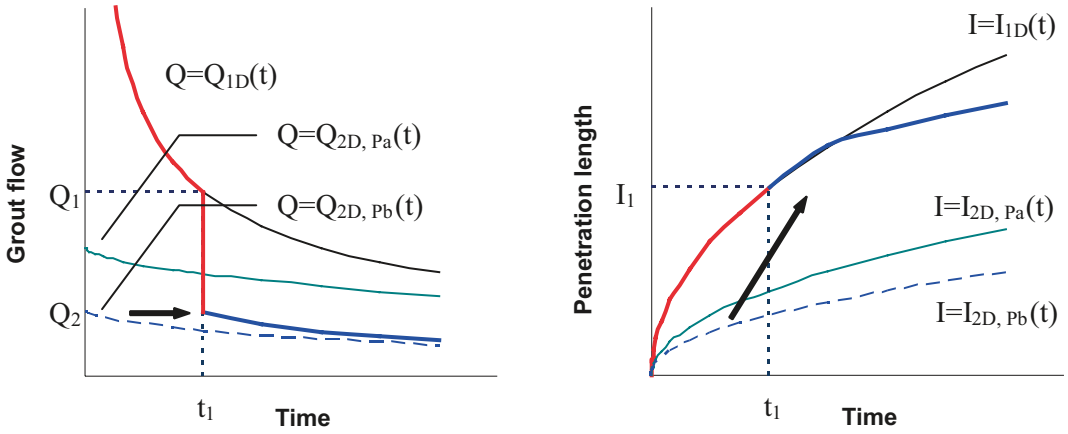

Figure 2-60. *Illustration of how the relationship between time and penetration may look like when the flow dimension of the fracture changes from 1D to 2D. The graph on the left shows the relationship between grouting time and grout flow. The graph on the right shows how penetration changes as the flow dimension of the fracture changes from 1D to 2D.*

The impact on the changes in dimensionality is illustrated in Figure 2-61 to 2-65. The example shows theoretical flow and grout penetration of a Bingham fluid with time-dependent grout properties into a fracture at constant pressure. The grouting parameters are shown below:

- Grouting pressure (Δp): 3 MPa.
- Grout properties Yield value (τ_0): 0.296 Pa, viscosity (μ_g): 0.0056 Pas.
- Fracture Aperture (b): 0.2 mm, width for 1D case (w): 20 m.
- Flow dimension of the fracture changes from 2D to 1D after 1 minute.

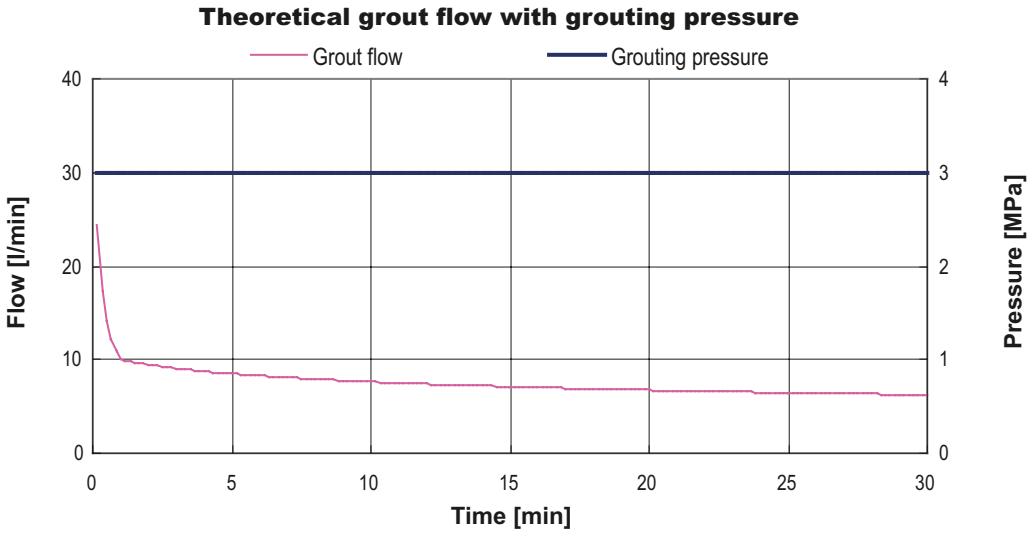

Figure 2-61. *Theoretical grout flow of a Bingham fluid at constant pressure with changing flow dimensionality of the fracture from 1D to 2D.*

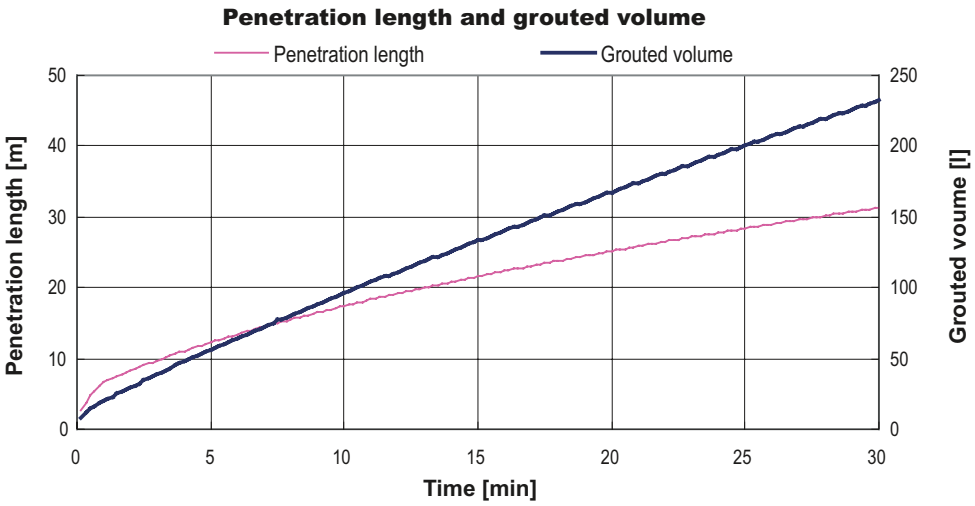

Figure 2-62. *Theoretical penetration length and grouted volume of a Bingham fluid at constant pressure with changing flow dimensionality of the fracture from 1D to 2D.*

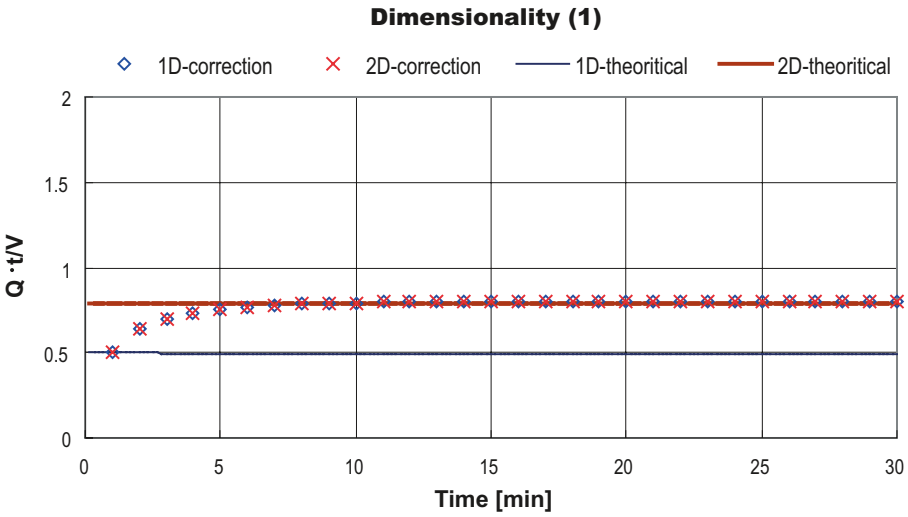

Figure 2-63. *Index for analyzing the dimensionality, Q·t/V from 1D to 2D.*

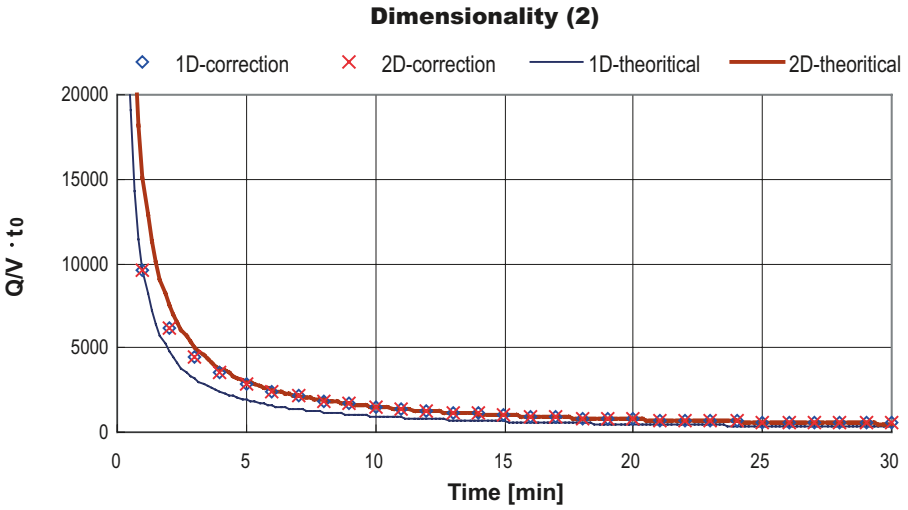

Figure 2-64. *Index for analyzing the dimensionality $Q/V \cdot t_0$ from 1D to 2D.*

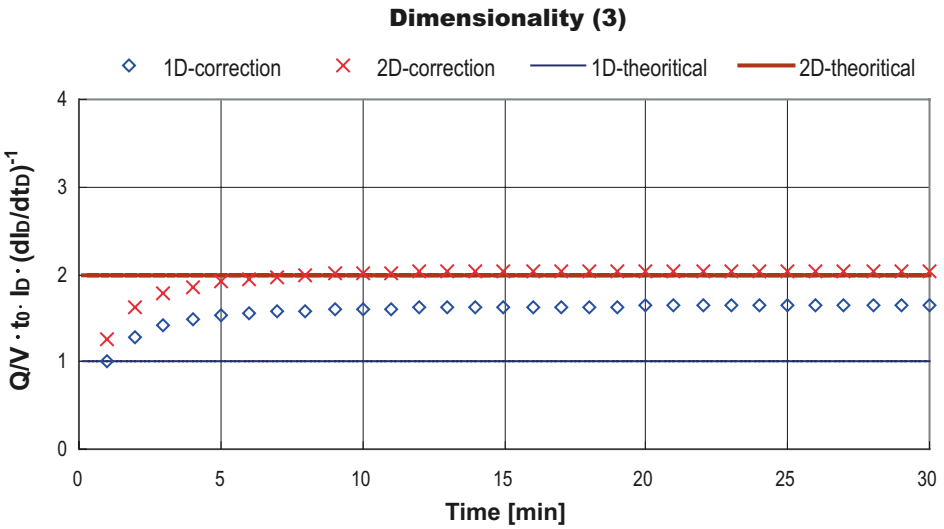

Figure 2-65. *Index for analyzing the dimensionality, $Q/V \cdot t_0 \cdot I_D \cdot (dI_D/dt_D)^{-1}$ from 1D to 2D.*

3 Grouting control with “Real Time Grouting Control Method”

3.1 Grouting control and Stop criteria

Stop criteria are one of the most important components in the grouting design and control. However, stop criteria have mainly been based on practical knowledge (e.g. /Houlsby 1990/), such as:

- Grouting is completed when the grout flow is less than a certain value at maximum pressure.
- Grouting is completed when the grout volume is above a certain value.
- Grouting is completed when the product of the grouting pressure and the grout take is above a certain value (GIN method /Lombardi and Deere 1993/).

Since these empirically based stop criteria are not directly related to grout penetration, the grouting result may be inadequate or uneconomical. On the other hand, by using the above developed grouting theory, stop criteria can be designed based directly on grout penetration, such as:

- Grouting is completed when the grout penetration of the smallest fracture, that has to be sealed, is above a certain minimum value (target value) or before the grout penetration for the largest fracture aperture reaches a certain maximum value (limiting value).

This has been the basic assumption in the development of the “Real Time Grouting Control Method” to control rock grouting. The other basic starting point has been that by following the flow and pressure during the grouting and applying the theories for grout spread, an active process can be achieved for directing grouting operations towards an optimal result.

3.2 Grouting control using “Real Time Grouting Control Method”

3.2.1 Procedure for grouting control

Nowadays, a computerized logging tool, which records grouting parameters such as grouting time, grouting pressure, grout flow and grouted volume, is often used in grouting projects. The concept of the “Real Time Grouting Control Method” is to calculate the grout penetration and control grouting in real time by applying the development of the theories for grout spread given in Chapter 2. The procedures for the “Real Time Grouting Control Method” system are shown in Figure 3-1.

3.2.2 Required data

In the “Real Time Grouting Control Method”, the grout penetration is used as stop criterion. Therefore, the minimum penetration length and/or maximum penetration length will be required as input data. Since the penetration length is proportional to the fracture aperture, the smallest aperture that has to be sealed as well as the aperture of the largest fracture will also be required. In order to calculate the penetration length, the grout material properties must be known /Eklund and Stille 2007/. In addition, other data such as groundwater pressure and hole filling volume are necessary. Table 3-1 shows the data required for the grouting control system.

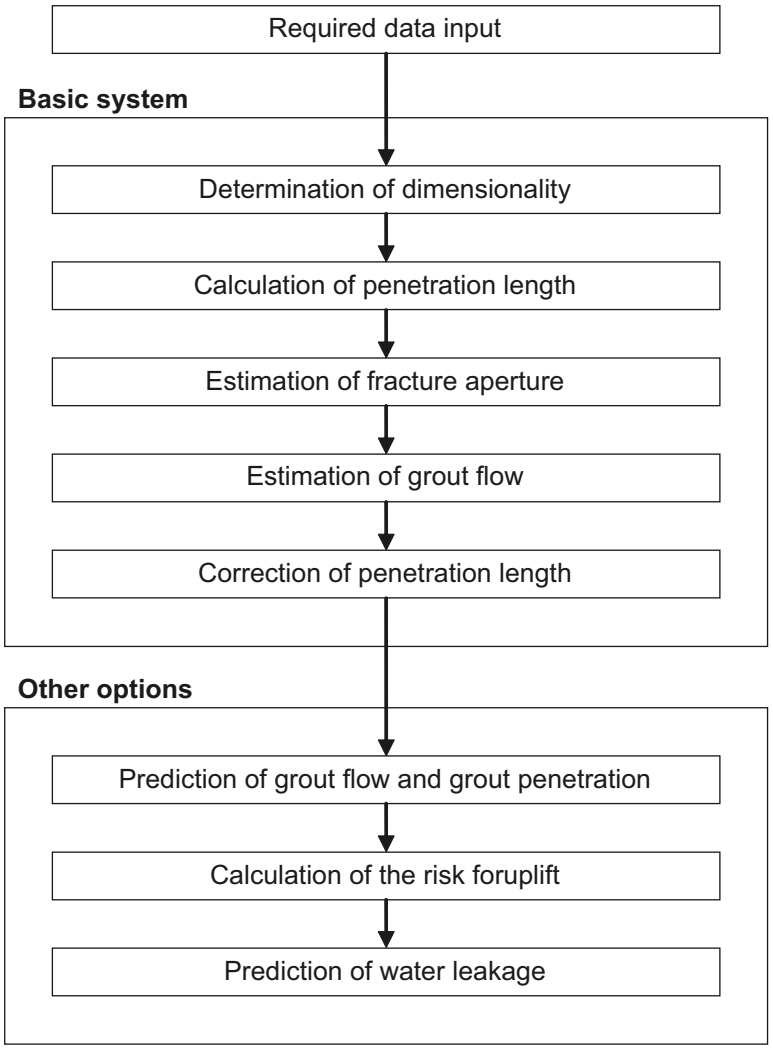

Figure 3-1. *Grouting control procedures using the "Real Time Grouting Control Method".*

Table 3-1. Required data for the "Real Time Grouting Control Method".

Requirements	Smallest aperture size that has to be sealed – Minimum penetration length
	Largest aperture size – Maximum penetration length
Grout material properties	Yield value
	Viscosity
	Grout mix penetrability (minimum aperture size)
Other data	Groundwater pressure
	Hole filling volume

In the following section, two actual grouting logs recorded from the grouting field experiment at the 450 m level in the Äspö HRL, and shown in Figure 3-2 and Figure 3-3, are used to explain the grouting control method. To complete the required data and make up an example, the following values are assumed:

- Requirements

  Smallest aperture size 0.1 mm – Minimum required penetration length 15 m.

  Largest aperture size 0.2 mm – Maximum required penetration length 40 m.
- Grout properties Yield value (τ_0): $0.296 \cdot e^{0.0004t}$ Pa, viscosity (μ_g): $0.0056 \cdot e^{0.0004t}$ Pas.
- Groudwater pressure 3.36 MPa.
- Hole filling volume 70 l.

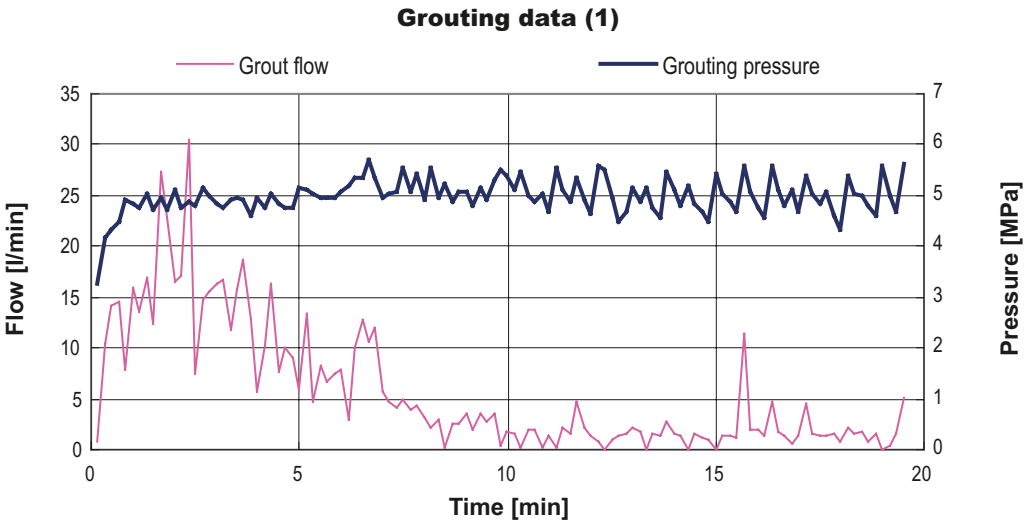

Figure 3-2. *Recorded grout flow and grouting pressure (No. 1).*

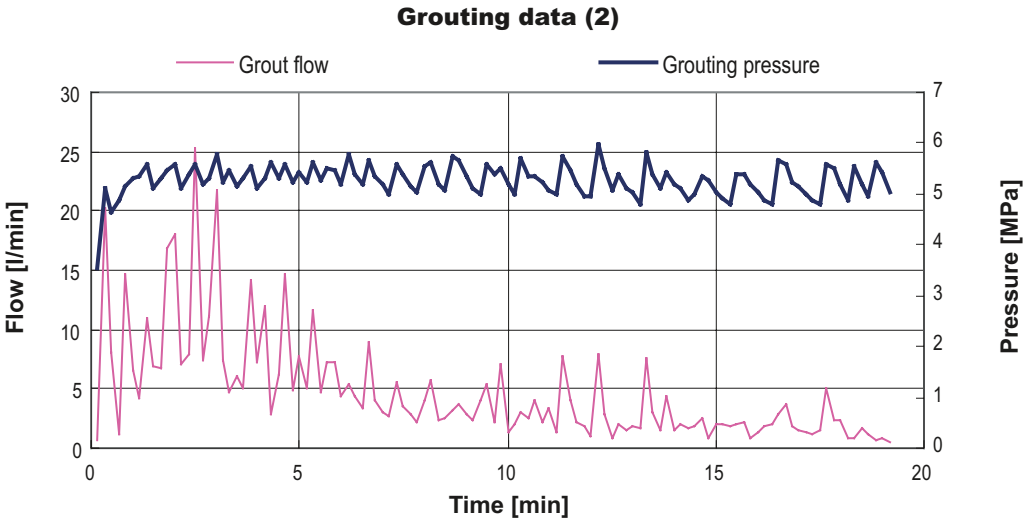

Figure 3-3. *Recorded grout flow and grouting pressure (No. 2).*

3.2.3 Determination of dimensionality

After the grout hole has been filled, corrected time can be calculated on the basis of the grouting pressure and the grout properties. By using the corrected time, the recorded grout flow and the grouted volume, the dimensionality of the flow in the fracture can be calculated during the grouting procedure. As examples, the indexes for determination of the dimensionality after 15 min. are shown in Figure 3-4 to Figure 3-7. Corrections as discussed in chapter 2.6 for both 1D and 2D had to be made and compared to the different theoretical values for both 1D and 2D flow in order to evaluate which one was the correct correction term. Although spread of the calculated values is found in both cases due to the fluctuation of the grouting pressure, it is likely that the flow dimension of Grouting No. 1 is 1D while that of Grouting No. 2 is 2D.

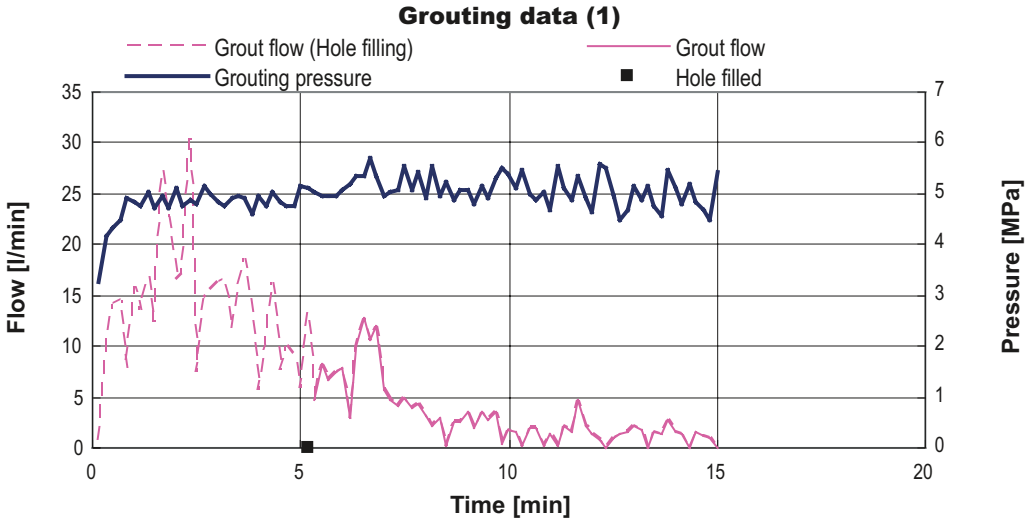

Figure 3-4. *Recorded grout flow and grouting pressure after 15 min. (No. 1).*

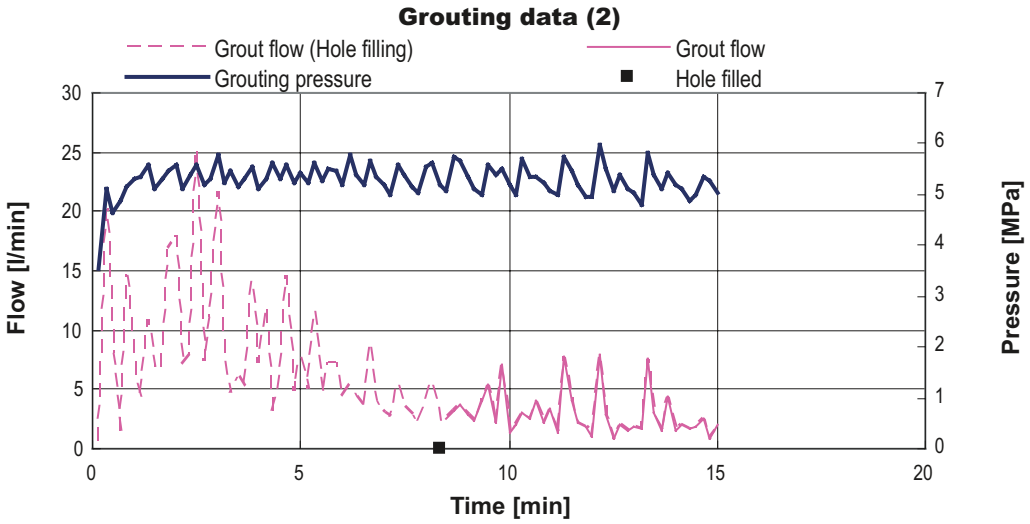

Figure 3-5. *Recorded grout flow and grouting pressure after 15 min. (No. 2).*

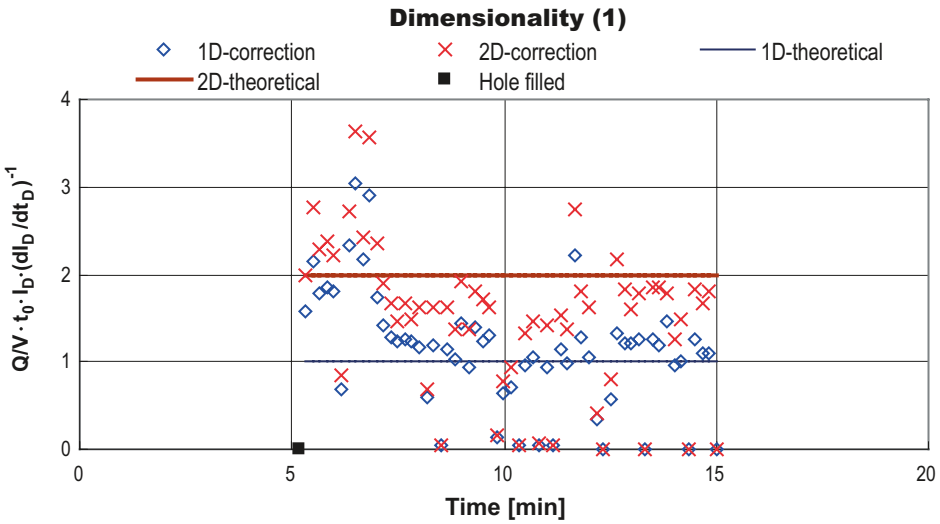

Figure 3-6. *Index for analyzing the dimensionality, $Q/V \cdot t_0 \cdot I_D \cdot (dI_D/dt_D)^{-1}$ after 15 min. (No. 1).*

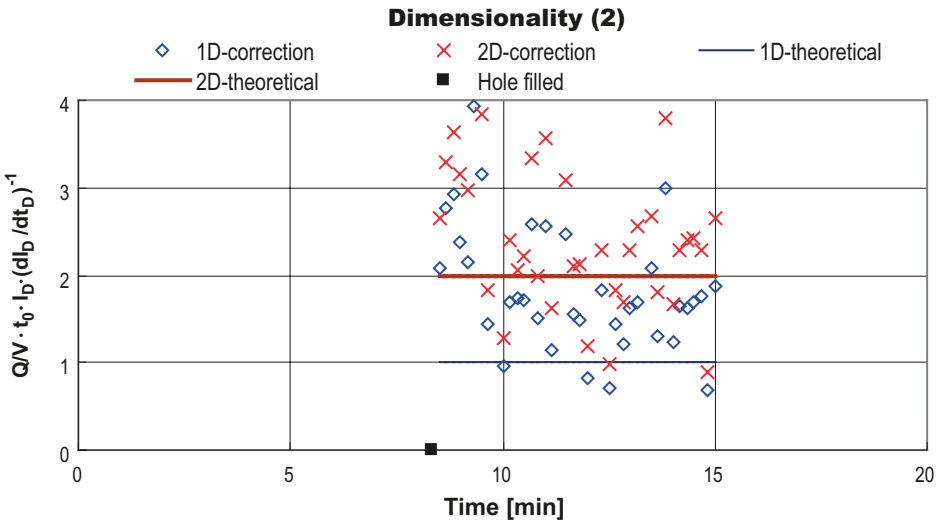

Figure 3-7. *Index for analyzing the dimensionality, $Q/V \cdot t_0 \cdot I_D \cdot (dI_D/dt_D)^{-1}$ after 15 min. (No. 2).*

3.2.4 Calculation of penetration length

Once the dimensionality of the fracture has been determined, the theoretical penetration length can be calculated based on the fracture aperture. Figure 3-8 and Figure 3-9 show the penetration length after 15 min. for Grouting No. 1 and Grouting No. 2.

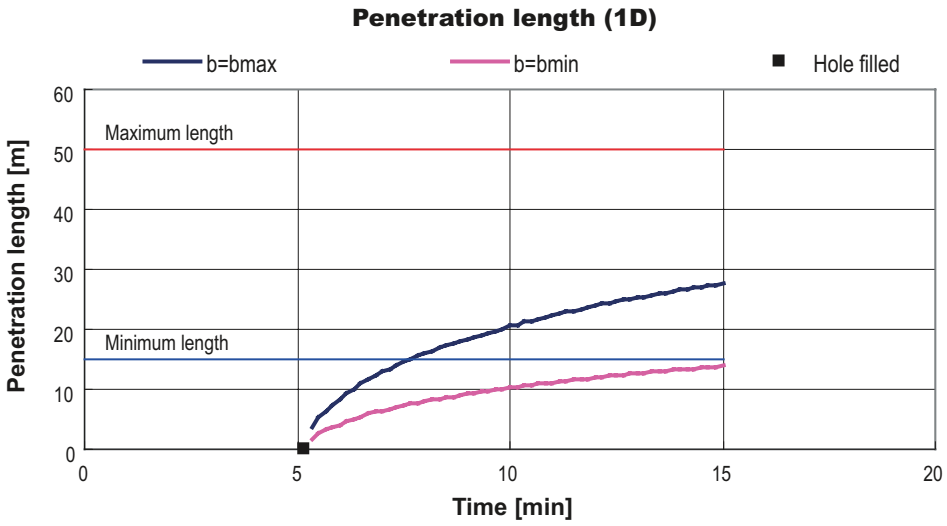

Figure 3-8. *Penetration length for the 1D case after 15 min. (No. 1).*

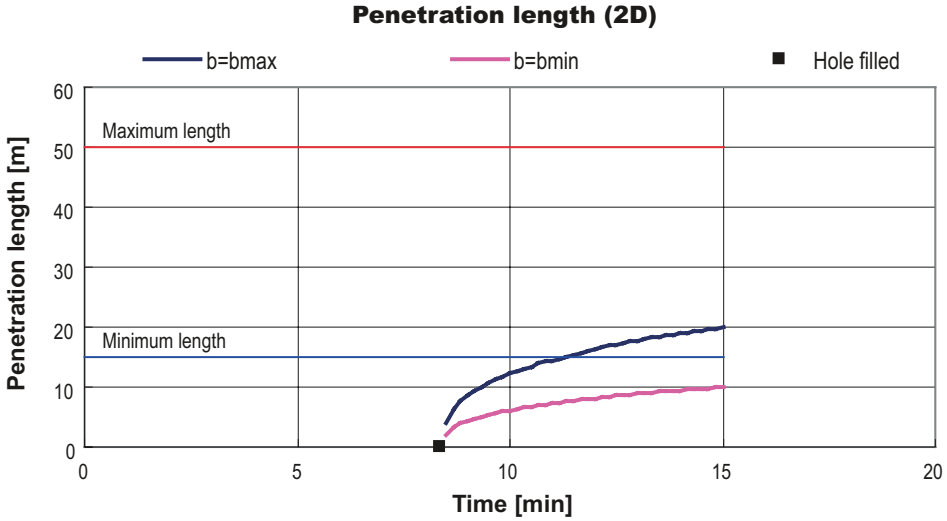

Figure 3-9. *Penetration length for the 2D case after 15 min. (No. 2).*

3.2.5 Estimation of fracture apertures and related theoretical grout flow

As stated in Section 2.2.3, theoretical grout flow can be calculated for both the 1D and 2D cases. For the 1D case, it is expressed as:

$$Q = \frac{dI_D}{dt_D} \cdot \frac{1}{t_0} \cdot \left(\frac{\Delta p}{2\tau_0} \right) \cdot \sum wb^2 \qquad (3\text{-}1)$$

For the 2D case, it is expressed as:

$$Q = 2\pi \cdot I_D \cdot \frac{dI_D}{dt_D} \cdot \frac{1}{t_0} \cdot \left(\frac{\Delta p}{2\tau_0} \right)^2 \cdot \sum b^3 \qquad (3\text{-}2)$$

By making comparisons between measured grout flow and $dI_D/dt_D \cdot (1/t_0) \cdot (\Delta p/2\tau_0)$ for the 1D case, and between recorded grout flow and $2\pi \cdot I_D \cdot dI_D/dt_D \cdot (1/t_0) \cdot (\Delta p/2\tau_0)^2$ for the 2D case, the term $\sum wb^2$ for the 1D case and $\sum b^3$ for the 2D case can be estimated. Both terms are a function of the fracture aperture. Figure 3-10 to Figure 3-13 show an estimation of fracture apertures, and based on these the corresponding theoretical grout flow during the first 15 min. for Grouting No. 1 and Grouting No. 2. In order to evaluate the aperture of single joints, the distribution of the fracture aperture must be known and described e.g. as a Pareto or log normal distribution and in the 1D case also the width of the channel. However, the term given above is in reality dominated by the largest fracture which gives possibility at least in the 2D case to get a first estimation of the largest aperture. This will be further discussed in Sections 3.3.4 and 4.3.2. By definition the regression line has to start from the origin.

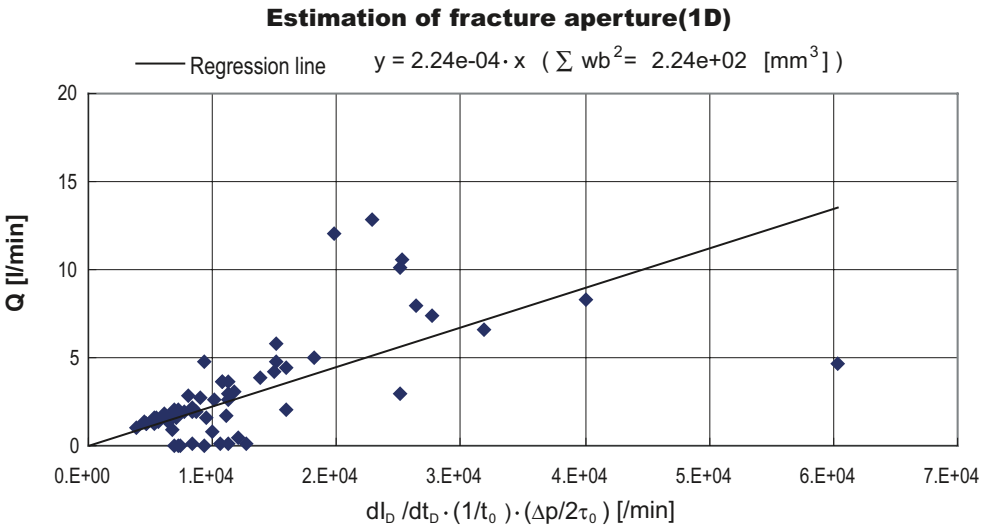

Figure 3-10. *Estimation of fracture aperture for the 1D case after 15 min. (No. 1).*

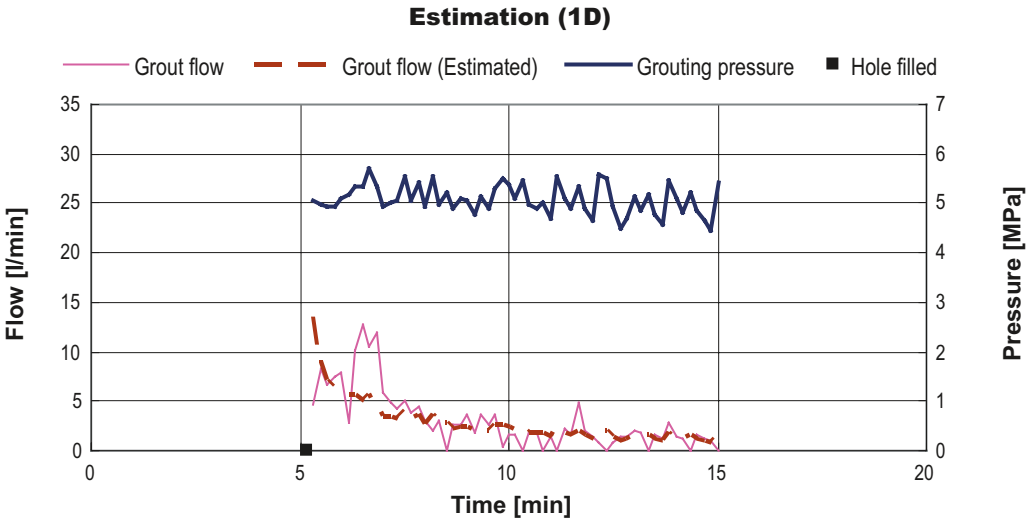

Figure 3-11. *Estimation of grout flow for the 1D case up to 15 min. (No. 1).*

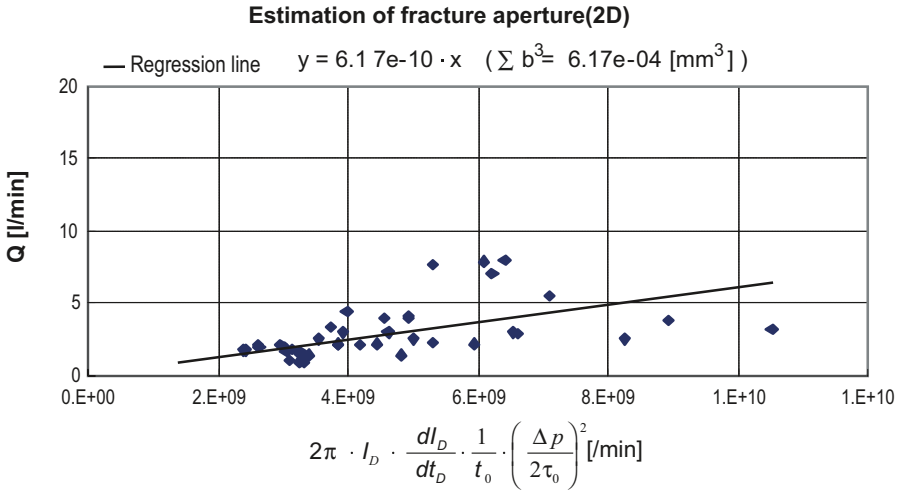

Figure 3-12. *Estimation of fracture apertures for the 2D case after 15 min. (No. 2).*

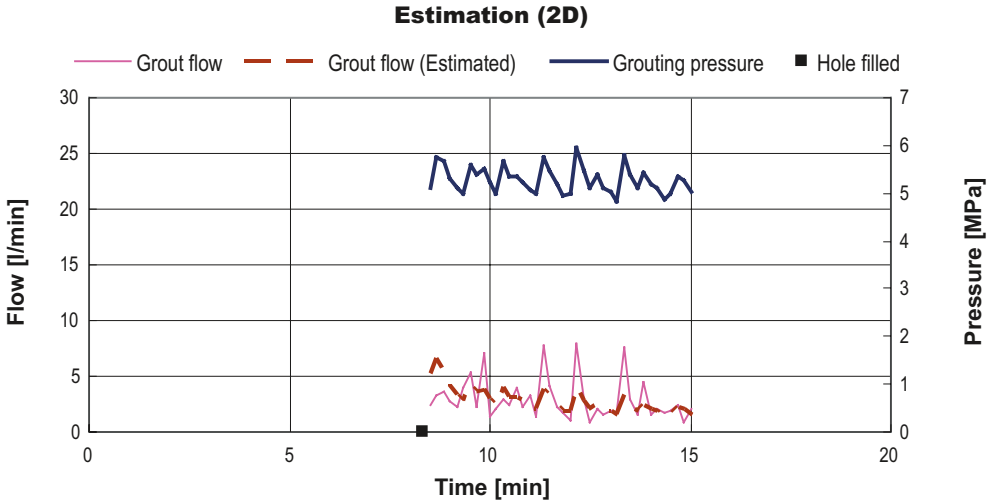

Figure 3-13. *Estimation of grout flow for the 2D case up to 15 min. (No. 2).*

3.2.6 Correction of penetration length

Even if the grout flow has been accurately estimated, there may still be a difference between the measured and the estimated figures. Therefore, it may be necessary to correct the theoretical penetration length based on the difference. Expression, V_{est}, which is the estimated grouted volume derived from the estimated grout flow, Q_{est} as:

$$V_{est} = \int Q_{est} dt \tag{3-3}$$

the corrected penetration length, I_{corr} can be calculated for the 1D case as:

$$I_{corr} = I_{theo} \cdot \frac{V_{mea}}{V_{est}} \tag{3-4}$$

and for the 2D case as:

$$I_{corr} = I_{theo} \cdot \sqrt{\frac{V_{mea}}{V_{est}}} \tag{3-5}$$

where I_{theo} is the theoretical penetration length and V_{mea} is the measured grouted volume.

Figure 3-14 and Figure 3-15 show an estimation of fracture aperture and grout flow after 15 min. for Grouting No. 1 and Grouting No. 2.

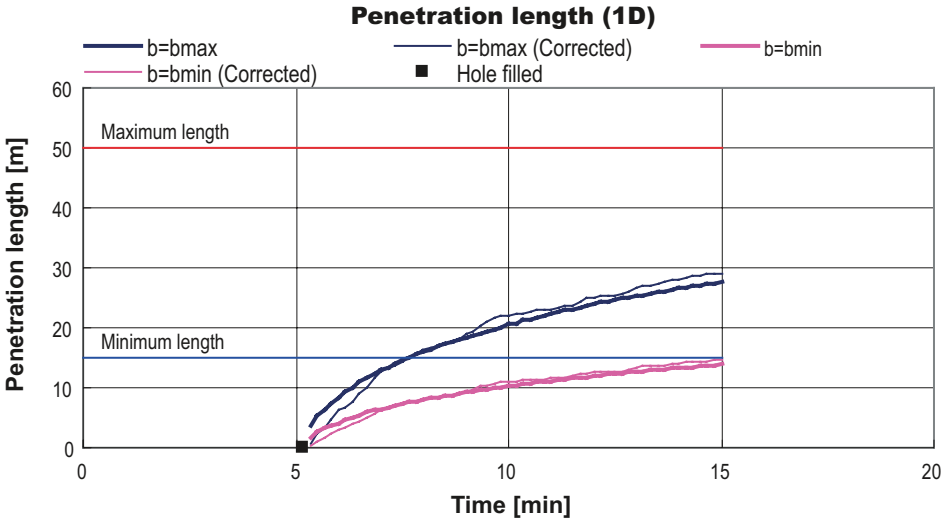

Figure 3-14. *Correction of penetration length for the 1D case after 15 min. (No. 1).*

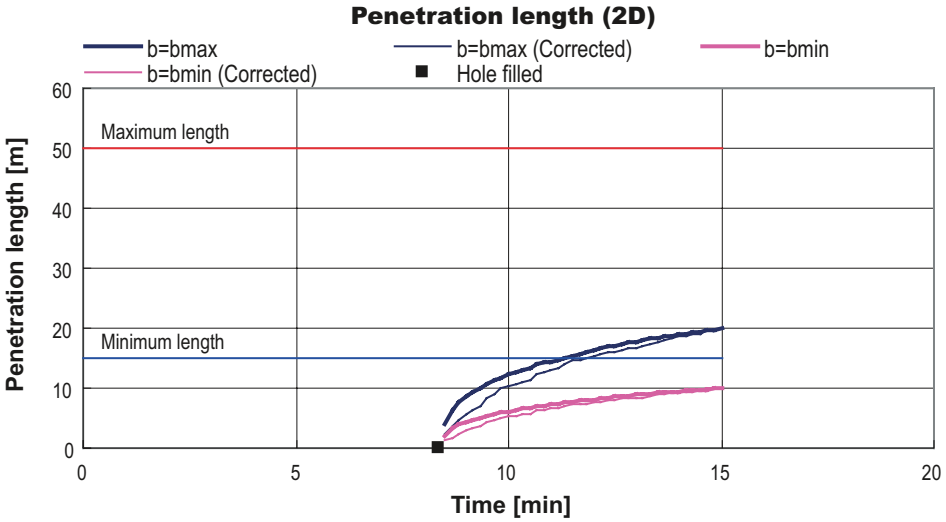

Figure 3-15. *Correction of penetration length for the 2D case after 15 min. (No. 2).*

3.2.7 Stop Criteria

For both Grouting No. 1 and Grouting No. 2 in the example in section 3.2.2 the grouting cannot be considered complete at t = 15 min., as the grout penetration in the smallest fracture aperture to be sealed has not yet reached the target value and the grout penetration in the largest fracture is not above the limit value. As shown in Figure 3-16 and Figure 3-17, for Grouting No. 1 the grout penetration of the smallest fracture aperture reaches the required penetration length after 17 min., so the grouting can be finished. On the other hand, for Grouting No. 2 it appears as though the grout penetration of the minimum fracture aperture will not reach above the required minimum value. Nor will the grout penetration for the maximum fracture aperture reach above the required maximum value for a reasonably long time to come. In this case, the grouting design should be changed by, for example, using a higher grouting pressure or a grout material with a lower viscosity.

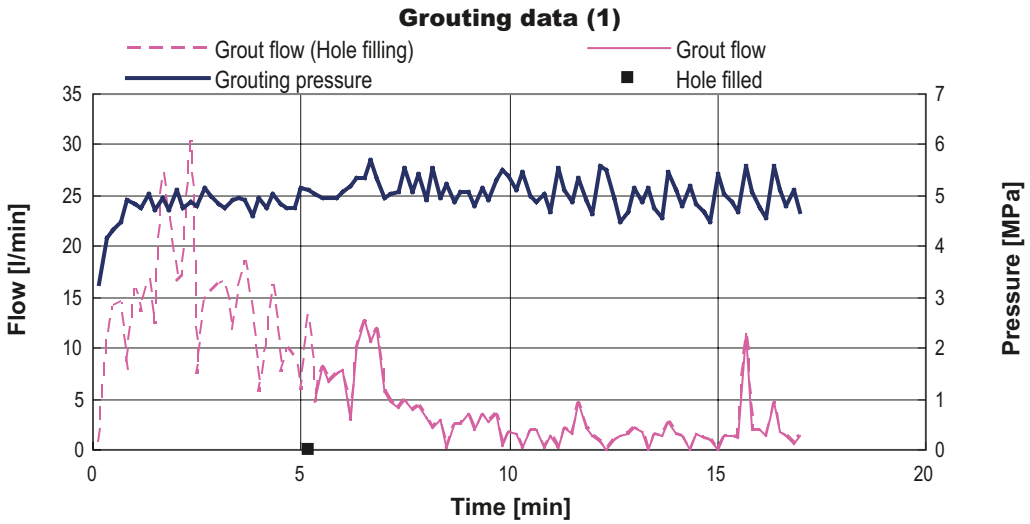

Figure 3-16. Recorded grout flow and grouting pressure after 17 min. (No. 1).

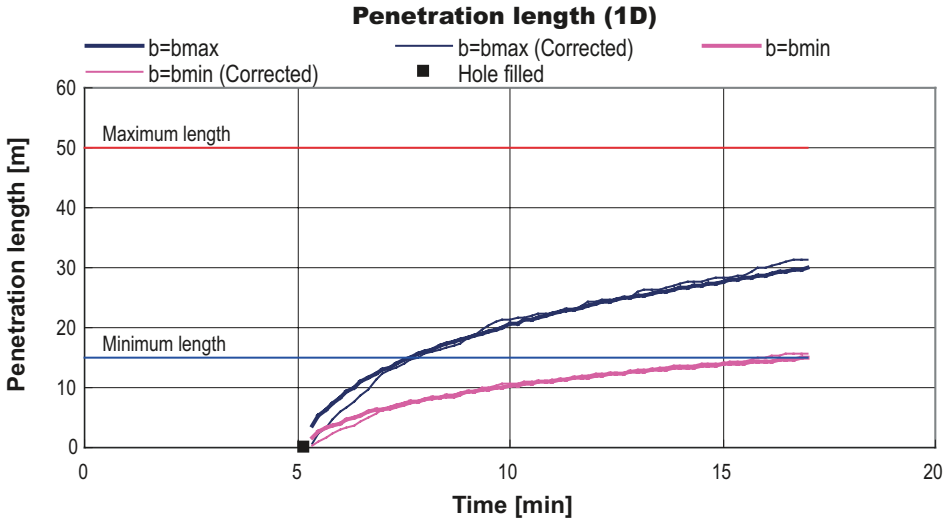

Figure 3-17. Penetration length for the 1D case after 17 min. (No. 1).

3.3 Other options of the "Real Time Grouting Control Method"

3.3.1 Possible other options

Since estimation of fracture aperture and calculation of penetration length are conducted in the "Real Time Grouting Control Method", it is possible to add certain other options to the method such as:

- Prediction of grout flow and grout penetration.
- Calculation of the risk of uplift.
- Prediction of water leakage into the tunnel.

3.3.2 Prediction of grout flow and grout penetration

By using the estimated fracture apertures (grouted fracture "volume") $\sum wb^2$ for the 1D case and $\sum b^3$ for the 2D case at a certain point, it is possible to predict the grouting. However, the grouting pressure must of course be assumed in order to predict the grout flow and the grout penetration. Figure 3-18 to Figure 3-21 show a prediction of the grout flow and grout penetration when the grouting pressure is assumed to be constant As discussed above, the grout spread is not anticipated to be acceptable for Grouting No. 2 (the 2D case). The penetration could be improved by increasing the grout pressure. In this case, a calculation has also been made for a pressure of 7 MPa. as shown in Figure 3-22 and Figure 3-23.

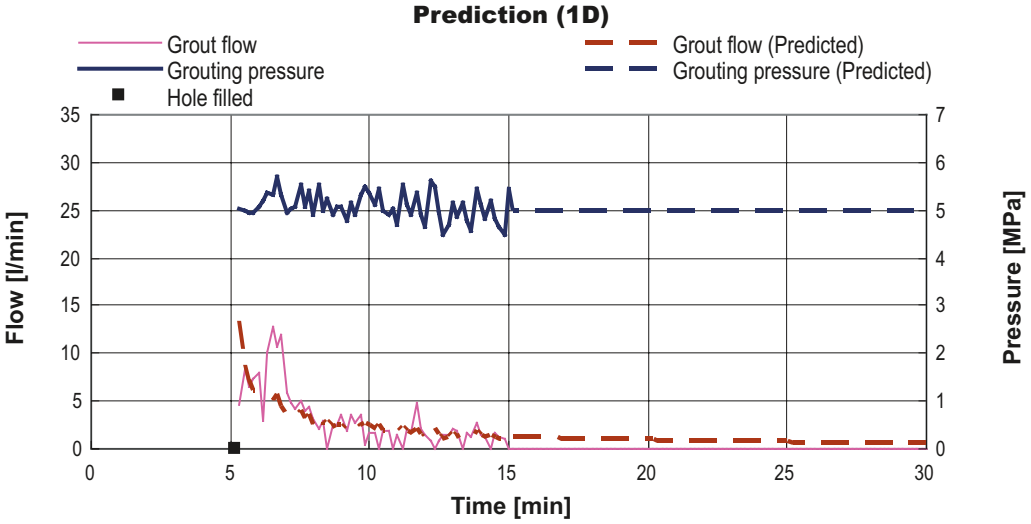

Figure 3-18. *Prediction of grout flow over a period of 30 minutes for the1D case. (No. 1).*

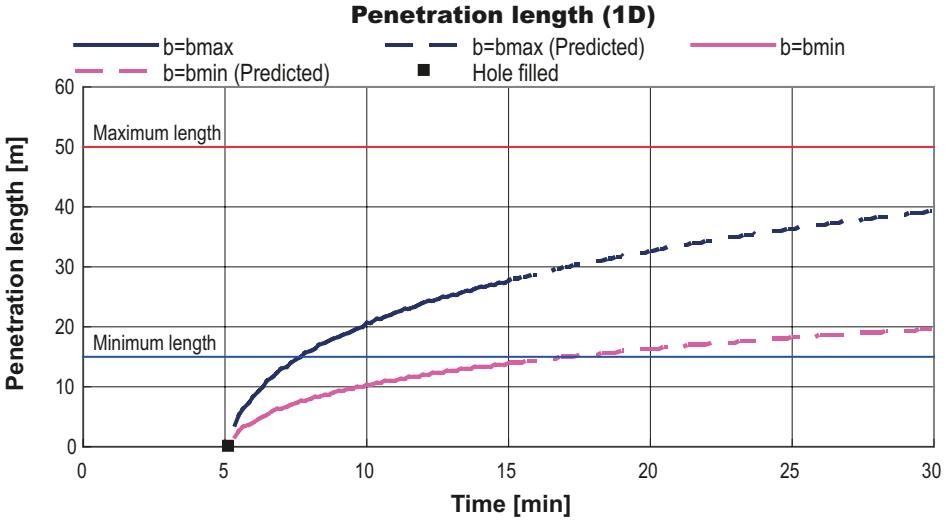

Figure 3-19. *Prediction of penetration length over a period of 30 minutes for the 1D case. (No. 1).*

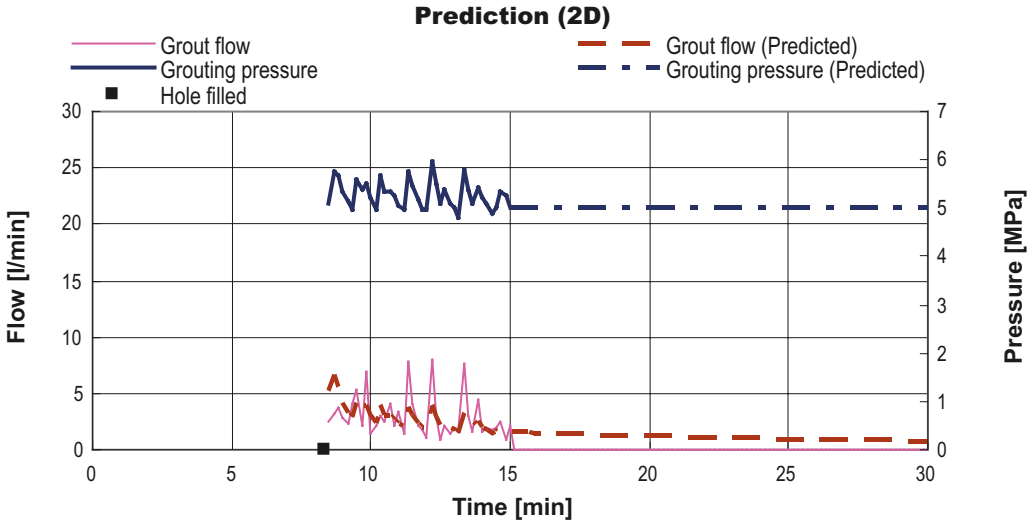

Figure 3-20. *Prediction of grout flow over a period of 30 minutes for the 2D case (No. 2).*

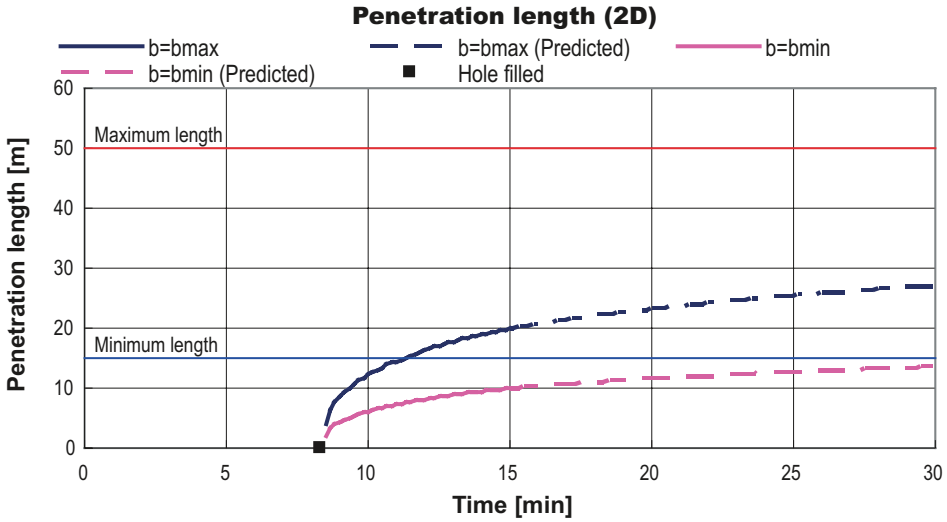

Figure 3-21. *Prediction of penetration length over a period of 30 minutes for the 2D case (No. 2).*

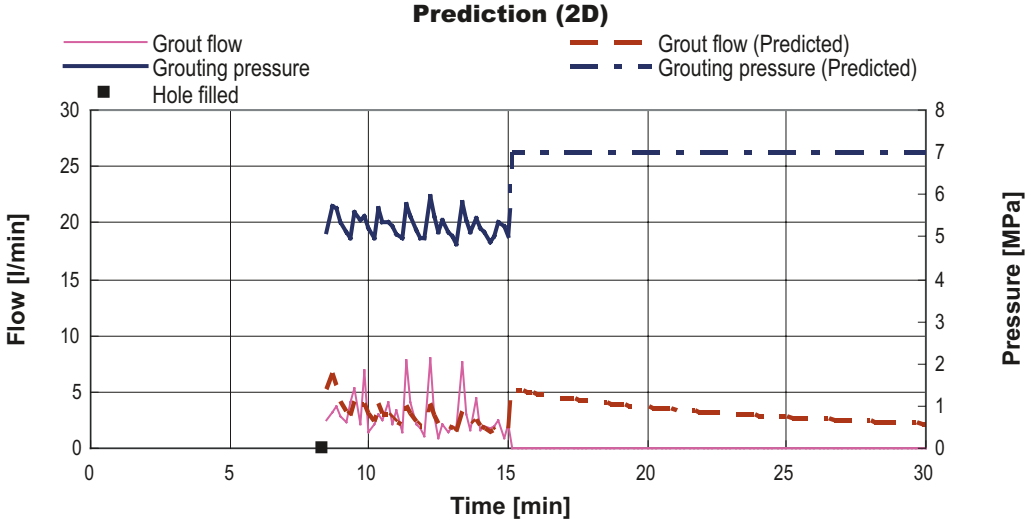

Figure 3-22. *Prediction of grout flow over a period of 30 minutes for the 2D case using the increased grouting pressure. (No. 2).*

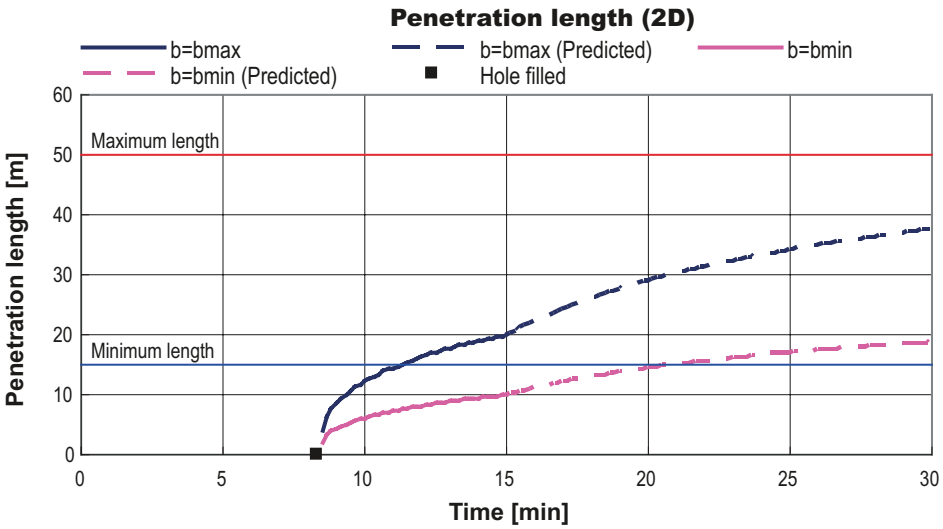

Figure 3-23. *Prediction of penetration length over a period of 30 minutes for the 2D case using the increased grouting pressure (No. 2).*

3.3.3 Calculation of the risk of uplift

Since the penetration length will be estimated during the grouting process in the "Real Time Grouting Control Method", it may be possible to check the risk of uplift in real time. The theory for analyzing the risk of hydraulic uplift, which was studied by /Brantberger et al. 2000/ is used for the calculation. The term uplift in this context corresponds to ultimate bearing capacity of rock mass. Hydraulic jacking may occur at lower level. It is important to point out that there are also other cases such as leakage of grout to the face or jacking the face which also have to be considered. Such risks can be controlled by reviewing the flow-pressure data.

Largest risk for uplift is connected to longest penetration. Therefore the penetration for the largest fracture aperture has been used in the calculations. In /Brantberger et al. 2000/, the allowable lifting force is calculated with an assumption of a circular open fracture so that the lifted rock mass geometry is shown in Figure 3-24. The worst case corresponds to maximum possible penetration. This will be related to largest fracture aperture b_{max} No consideration is given to the shear strength. F_{all}, the allowable uplift force, can be expressed as:

$$F_{all} = k_1 \cdot \rho \cdot g \cdot h \cdot I^2 \cdot \pi \qquad (3\text{-}6)$$

where k_1 is the factor accounting for the geometry of the lifted rock mass, ρ is the density of the rock mass, g is the gravity force, h is the depth of the fracture below ground surface and I is the grout spreading distance.

The factor k_1 depends on the cone angle β in Figure 3-24. According to /Brantberger et al. 2000/, an assumption of β of 45 degrees results in the following equation:

$$k_1 = 1 + \frac{h}{I} + \frac{1}{3}\left(\frac{h}{I}\right)^2 \qquad (3\text{-}7)$$

On the other hand, the uplift force is described with an assumption of a linear pressure fall as:

$$F = \frac{k_2 \cdot \pi \cdot I^2 \cdot p}{3} \qquad (3\text{-}8)$$

where F is the uplift force and k_2 is the factor accounting for the fact that the fracture is not completely open to the grout flow.

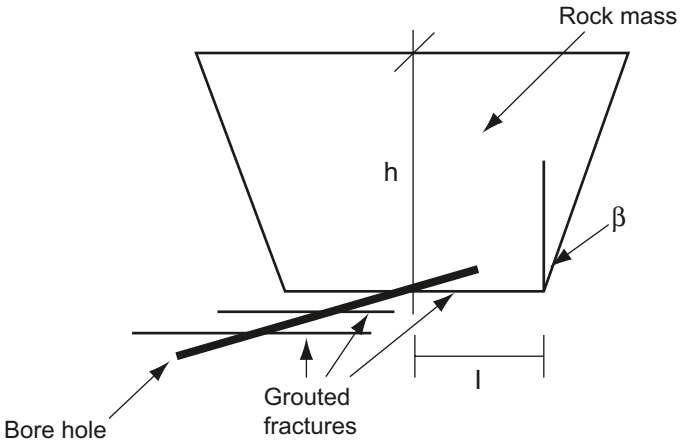

Figure 3-24. *Idealized geometry of a tock mass subject to uplift /Brantberger et al. 2000/.*

In order to prevent hydraulic uplift, the following equation must be satisfied:

$$F < F_{all} \tag{3-9}$$

Equations (3-6) to (3-9) are reformulated as:

$$p < \frac{3 \cdot \rho \cdot g \cdot h}{k_2} \cdot \left(1 + \frac{h}{I} + \frac{1}{3}\left(\frac{h}{I}\right)^2 \right) \tag{3-10}$$

What has been discussed above is only applicable to the 2D case. For the 1D case, the allowable lifting force can be calculated as:

$$F_{all} = k_1 \cdot \rho \cdot g \cdot h \cdot I \cdot w \tag{3-11}$$

where w is the width of the grout spread.

For the 1D case, the factor k_1 depends on the cone angle β_l and β_w in Figure 3-25. As stated in Section 3.2.5, $\sum wb^2$ can be estimated during the grouting procedure. However, w has not been determined. Therefore, an assumption of β_l of 45 degrees and β_w of 90 degrees is used for the 1D case. These values are on the safe side and result in the following equation:

$$k_1 = 1 + \frac{h}{I} \tag{3-12}$$

The uplift force is described with an assumption of a linear pressure fall as:

$$F = \frac{k_2 \cdot w \cdot I \cdot p}{2} \tag{3-13}$$

In order to prevent hydraulic uplift, the following equation must be satisfied from equations (3-9) and (3-11) to (3-13):

$$p < \frac{2 \cdot \rho \cdot g \cdot h}{k_2} \cdot \left(1 + \frac{h}{I} \right) \tag{3-14}$$

Figure 3-26 and Figure 3-27 show examples of how the risk of uplift can be calculated for Grouting No. 1 and Grouting No. 2 after 15min. by using ρ=3 t/m^3 and h=50 m.

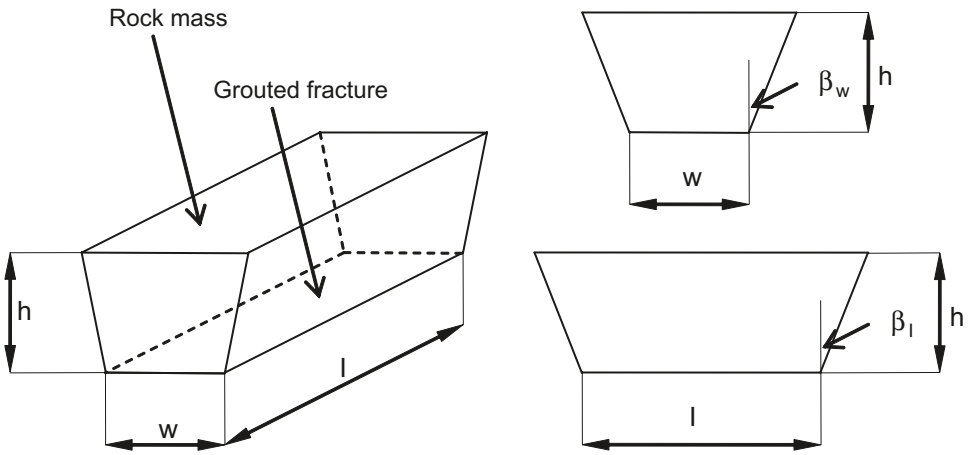

Figure 3-25. *Idealized geometry of a rock mass subject to uplift for the 1D case.*

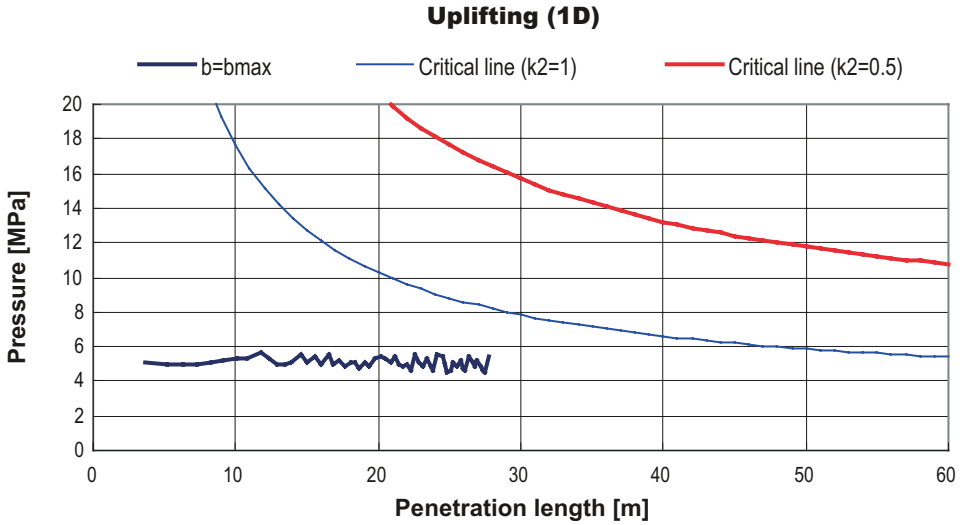

Figure 3-26. *Calculation of the risk of uplift after 15 min. (No. 1). The left-hand area of the critical line indicates the safe zone.*

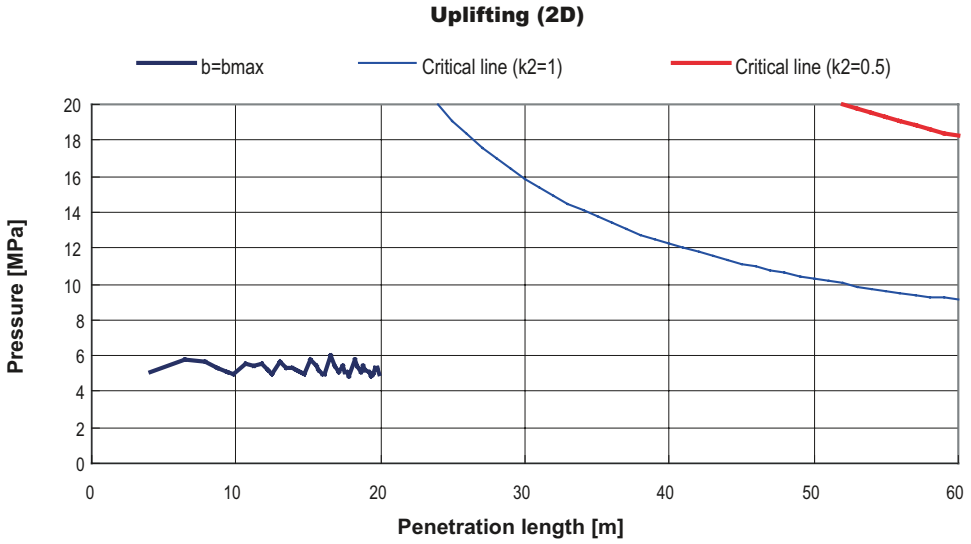

Figure 3-27. *Calculation of the risk of uplift after 15 min. (No. 2). The left-hand area of the critical line indicates the safe zone.*

3.3.4 Prediction of water leakage

If the inflow during drilling from the borehole is measured, $\sum b^3$ can be calculated. According to /Fransson 2001/, the specific capacity (Q/dh) would be approximately equal to the transmissivity and is defined by the inflow during drilling, Q and the hydraulic head measured during a pressure build-up test, dh. Transmissivity T is calculated using the cubic law as:

$$\frac{Q}{dh} = T \tag{3-15}$$

$$T = \frac{\rho_w g \sum b^3}{12\mu_w} \tag{3-16}$$

where ρ_w is the density of water, μ_w is the viscosity of water, g is the acceleration due to gravity and b is the hydraulic aperture of the fracture.

From equations (3-15) and (3-16), $\sum b^3$ can be calculated as:

$$\sum b^3 = \frac{12\mu_w}{\rho_w g} \cdot \frac{Q}{dh} \tag{3-17}$$

If the water loss is measured, transmissivity can be also be calculated according to /Gustafson and Stille 1996/ as:

$$T = \frac{Q_t \rho_w g}{2\pi (P_t - P_w)} \ln \frac{L}{r_w} \tag{3-18}$$

where Q_t and P_t are the water flow and applied water pressure, ρ_w is the density of water, g is the acceleration due to gravity, P_w is the groundwater pressure, L is the length of the test section and r_w is the radius of the borehole. $\sum b^3$ can then be calculated using equation 3-16.

As described in Section 3.2.5, $\sum b^3$ can be calculated from the grouting data for the 2D case. It must be emphasized that these values are only for those fractures with an aperture larger than the groutable aperture size for the injected grout. Thus, non-injected fracture apertures can be calculated for the 2D case as:

$$\sum_{b<b_{groutable}} b^3 = \sum b^3 - \sum_{b>b_{groutable}} b^3 \tag{3-19}$$

Water leakage after grouting, Q_{after} to a control hole with a length equal to the grouting hole can be estimated for the 2D case as:

$$Q_{after} \approx \frac{\rho_w g \cdot dh}{12\mu_w} \cdot \sum_{b<b_{groutable}} b^3 \tag{3-20}$$

If we want to estimate the ingress to the grouted tunnel, we must correct the inflow with a factor that describes the influence of the size of the opening. The ingress to a tunnel is normally estimated to be 3 to 5 times more than to a small borehole. We must also normalize the ingress to flow per meter tunnel.

The problem is that the specific capacity is only defined for the 2D case. For the 1D case the width of the channel has to be estimated before the ingress to the tunnel can be calculated. This issue has to be further studied.

Table 3-2 shows an example of water leakage prediction for Grouting No. 2 by using Q=9 l/min and dh=343 m.

Table 3-2. Prediction of water leakage for Grouting No. 2.

Inflow during drilling Q [l/min]	Hydraulic head dh [m]	Specific capacity Q/dh [m^2/s]	Calculated from inflow Σb^3 [mm^3]	Calculated from grouting Σb^3 ($b > b_{groutable}$) [mm^3]	Non-injected fractures Σb^3 ($b < b_{groutable}$) [mm^3]	Predicted inflow Q_{after} [l/min]
9	343	4.37E–07	0.000696	0.000617	0.000079	1.0

The calculated value of aperture "volume" $\sum b^3$ from the water inflow and from the grouting gives similar results. The largest aperture can be estimated to be $\sqrt[3]{\sum b^3}$ corresponding to 0.085 mm /Gustafson and Fransson 2005/. If the same equation is applied to calculate the largest aperture of the non-injected fractures it will give 0.042 mm. This value corresponds well with the aperture of the smallest penetrable fracture for the cement-based grout mix used.

4 Application using Äspö HRL data

4.1 Field experiment at Äspö HRL

4.1.1 Overview

The field data from the grouting experiments at Äspö HRL is used in order to verify the "Real Time Grouting Control Method" and to demonstrate its applicability. The grouting field experiment was carried out at the 450 m level in the Äspö HRL and reported in /Emmelin et al. 2004/. The experiment has also been analyzed be /Hernqvist et al. 2008/. The main objectives of the experiment were:

- to investigate what can be achieved with the best available technology, material and knowledge under the current conditions, i.e. a relatively tight crystalline rock mass at great depth,
- to collect data and evaluate theories resulting from previous research projects on characterization and predictions of grout spread,
- to collect data to further develop those theories, and
- to contribute to the achievement of good conditions at the experimental site for the pillar stability experiments.

In the grouting experiments, the specific capacity (Q/dh) was assumed to provide a description of the conductive fracture where the median specific capacity would be approximately equal to the transmissivity and the variation in specific capacity would provide an impression of variations in aperture within a conductive feature /Fransson 2001/. Based on the description of the fracture, results and choice of grouting design were predicted using a numerical model /Eriksson 2002/. It was found that the predicted grouting volumes were considerably smaller than the volumes obtained and the predicted grouting times deviated from the times obtained. However, the sealing effect of the grouting was predicted accurately.

4.1.2 Grouting design in the field experiment

In the field experiment, the grouting design was modified according to the modified descriptions of the rock mass. Based on the final third description, the experiment was executed in two grouting fans. The first fan (Fan 1) was grouted using two grouting rounds but the second fan (Fan 2) included only one grouting round. The first grouting round of Fan 1 (Fan 1:1) was to be carried out as follows:

- 11 boreholes, 16 m long.
- Minimum flow 1.0 litre/min.
- Grouting pressure 1 MPa above groundwater pressure.
- Borehole radius 0.032 m.
- Grouting starts with Grout B and continues until 150 litres have been grouted, provided refusal based on the flow criterion is not obtained. After this, a change is made to Grout C. No more than 50 additional litres are grouted, after which grouting is stopped.
- Grouting is carried out in descending order based on specific capacity of respective boreholes.

The second grouting round of Fan 1 (Fan 1:2) was to be carried out as follows:

- 20 boreholes, 16 m long.
- Minimum flow 1.0 litre/min.
- Grouting pressure 2 MPa above groundwater pressure.
- Borehole radius 0.032 m.
- Grouting starts with Grout A and continues until 100 litres have been grouted, provided refusal based on the flow criterion is not obtained. After this, a change is made to Grout B. No more than 50 additional litres are grouted, after which grouting is stopped.
- Grouting is carried out in descending order based on specific capacity.

Fan 2 was to be carried out as follows:

- 21 boreholes, 16 m long.
- Minimum flow 0.2 litres/min.
- Grouting pressure 2 MPa above groundwater pressure.
- Maximum hole distance 2 m.
- Borehole radius 0.032 m.
- Grouting starts with Grout A and, after ~100 litres, the grout is changed to Grout B. Again, after ~50 litres grouting is continued with Grout C. After grouting ~50 litres with this grout, grouting is stopped.

The properties of the two grouts, Grout A and Grout B, were measured both in the laboratory and on site, but the properties of Grout C were not determined since it was only to be used as the final stop grout. The grout properties are listed in Table 4-1. The time, t, is in seconds. Regarding penetrability see /Eriksson and Stille 2003/.

4.1.3 Grouting results measured in previous field experiment

Grout take and grouting time, and evaluated sealing effect recorded in the previous field experiment are shown in Table 4-2. These measured values are presented in detail in Appendix C.

It was found that the predicted grouting volumes were considerably smaller than the volumes obtained, and the predicted grouting times deviated from the times actually obtained. However, the sealing effect of the grouting was predicted accurately.

It should be noted that the practical grouting work for Fan 1:1 was not based on the grouting design shown in Section 4.1.2. According to the measured grouting data, it would appear that the grouting design for Fan 1:1 was changed before operation as follows:

- The grouting starts with Grout B and continues until **100** litres has been grouted, provided refusal based on the flow criterion is not obtained. After this, a change is made to Grout C and no more than **100** additional litres are grouted. After this the grouting is stopped.

Table 4-1. Grout properties valid for t < 3,600sec.

Property		Grout A UF 16, w/c 2.0 0.9% HPM	B UF 16, w/c 1.0 0.9% HPM	C UF 16, w/c 0.8 0.9% HPM
Rheology	Yield value [Pa]	$0.296 \cdot e^{0.0004t}$	$1.5 \cdot e^{0.0004t}$	–
	Viscosity [Pas]	$0.0056 \cdot e^{0.0004t}$	$0.017 \cdot e^{0.0004t}$	–
Penetrability	b_{min} [µm]	37	41	–
	$b_{critical}$ [µm]	$0.0032t+60$	$0.0032t+75$	–
Density	[kg/m^3]	1,290	1,480	–
Bleed	[%]	15	5	–

Table 4-2. Summary of measured and evaluated grouting results.

Fan	Grout take [l] Including hole filling/ excluding hole filing	Grouting time [min] Including hole filling/ excluding hole filing	Sealing effect [%]
1:1	1633/863	196/160	97
1:2	2537/1137	854/800	97
2	2456/1470	480/420	95

4.2 Verification of “Real Time Grouting Control Method”

4.2.1 Input data

Input data are mainly set according to /Emmelin et al. 2004/. As for the grout properties, there are two methods of using the properties for the calculation. One is that the properties are described as time-dependent, which was used in the experiment at the Äspö HRL, (see Table 4-1). The other method is to use constant properties, which is shown in, for example, /Dalmalm 2004/. In this report, both time-independent and time-dependent grout properties are used for the calculation. As can be seen from Table 4-1, since the properties of Grout C were not determined in the experiment at the Äspö HRL, the grout data from /Dalmalm 2004/ had to be used. Input data used for the calculation are as follows:

- Grout properties Table 4-3.
- Groudwater pressure 3.36 Mpa.
- Hole filling volume 70 l.

Table 4-3. Grout properties used for the calculation.

Property Rheology		Grout A UF 16, w/c 2.0 0.9% HPM	B UF 16, w/c 1.0 0.9% HPM	C UF 16, w/c 0.8 0.9% HPM
Case 1	Yield value [Pa]	0.296	1.5	10.3
Time-independent	Viscosity [Pas]	0.0056	0.017	0.093
Case 2	Yield value [Pa]	$0.296 \cdot e^{0.0004t}$	$1.5 \cdot e^{0.0004t}$	$10.3 \cdot e^{0.0004t}$
Time-dependent	Viscosity [Pas]	$0.0056 \cdot e^{0.0004t}$	$0.017 \cdot e^{0.0004t}$	$0.093 \cdot e^{0.0004t}$

Time , *t*, is in seconds.

4.2.2 Calculation

All recorded grouting data in Fan 1:1 and Fan 1:2, except for the holes in which the grouted volume is below the hole-filling volume, are used for the calculation (see Appendix A to Appendix C). In order to verify the "Real Time Grouting Control Method", calculated dimensionality, fracture aperture and grout flow have been discussed and compared with measured or in other way estimated results when possible. Figure 4-1 shows the verification procedure.

4.3 Comparison of calculated and measured results

4.3.1 Dimensionality

In order to determine the flow dimension of the fracture, the index, $Q/V{\cdot}t_0{\cdot}I_D{\cdot}(dI_D/dt_D)^{-1}$ is used. Figure 4-2 and Figure 4-3 show an example of the 1D case, Figure 4-4 and Figure 4-5 show an example of the 2D case, and Figure 4-5 and Figure 4-6 show an example of the 2D to 1D (2→1) case. Due to fluctuations in the grouting pressure and grout flow, determination of the dimensionality was no easy matter, and therefore dimensionality was evaluated on the basis of the general trend. A filtration of the pressure and flow data would have given more clear plots. For example, in Figure 4-3, dimensionality looks 1D before changing grout and thereafter between 1D and 2D, however, it is determined to be 1D.

Frequency distributions of the index for analyzing the dimensionality,

$Q/V{\cdot}t_0{\cdot}I_D{\cdot}(dI_D/dt_D)^{-1}$ in Fan 1:1 and Fan 1:2 for using both time-independent and time-dependent grout properties are shown in Figure 4-8 and Figure 4-9 (see also Appendix D).

According to /Emmelin et al. 2004/, fractures are assumed to be planes which are perpendicular to the tunnel and intersect with boreholes, which means that the dimensionality of the fracture is 2D. Judging from this, the calculations using time-independent grout properties were more accurate than time-dependent and well estimated in this case. It is interesting to note that for the first Fan1:1 the majority of the spread is 2D. For the second Fan 1:2 the spread is more of type 1D or 3D indicating that the secondary joint system filled at the end of the grouting had a more random orientation.

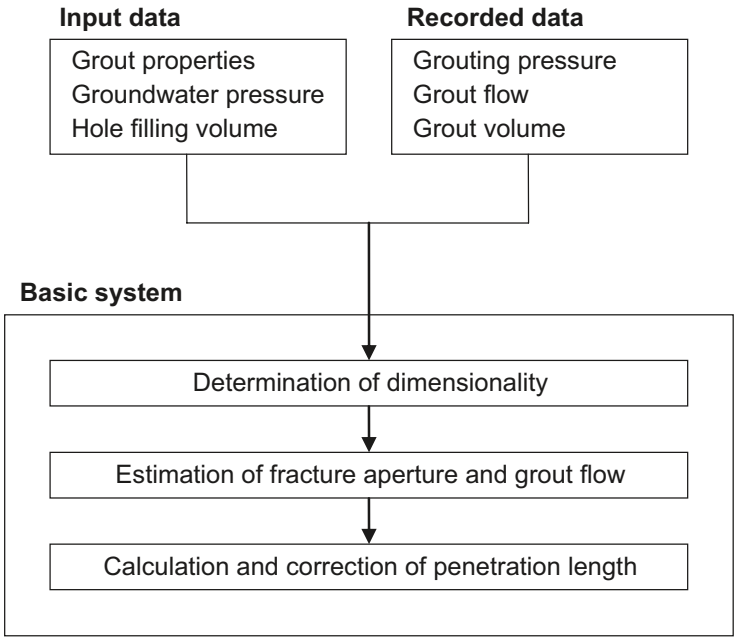

Figure 4-1. *Basic system used for verification of the "Real Time Grouting Control Method".*

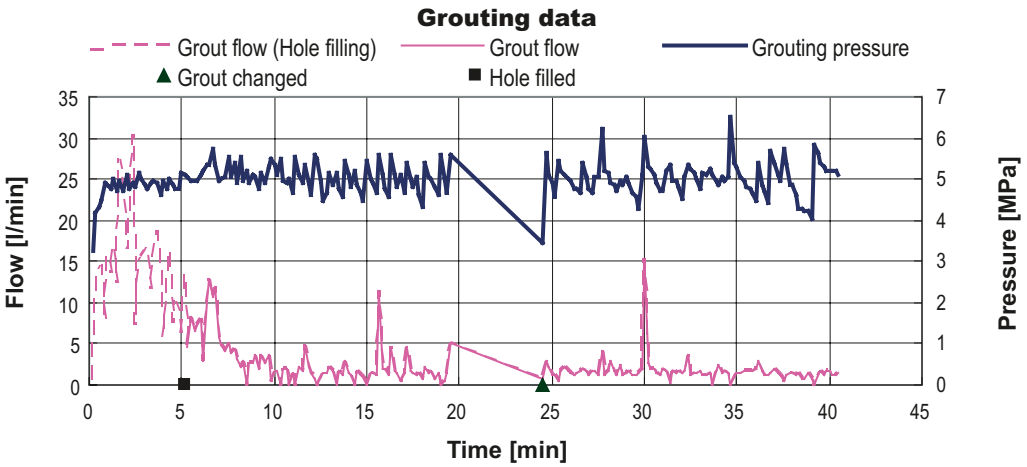

Figure 4-2. *An example of recorded grout flow and grouting pressure for the 1D case: Borehole B24 in Fan 1:2.*

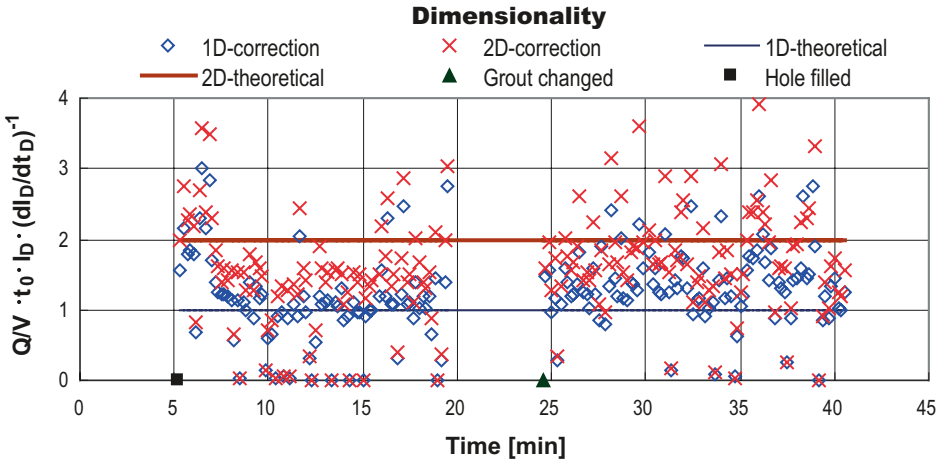

Figure 4-3. *An example of the index for analyzing the dimensionality, $Q/V \cdot t_0 \cdot I_D \cdot (dI_D/dt_D)^{-1}$ for the 1D case: Grouting data from borehole B24 in Fan 1:2 using time-independent grout properties.*

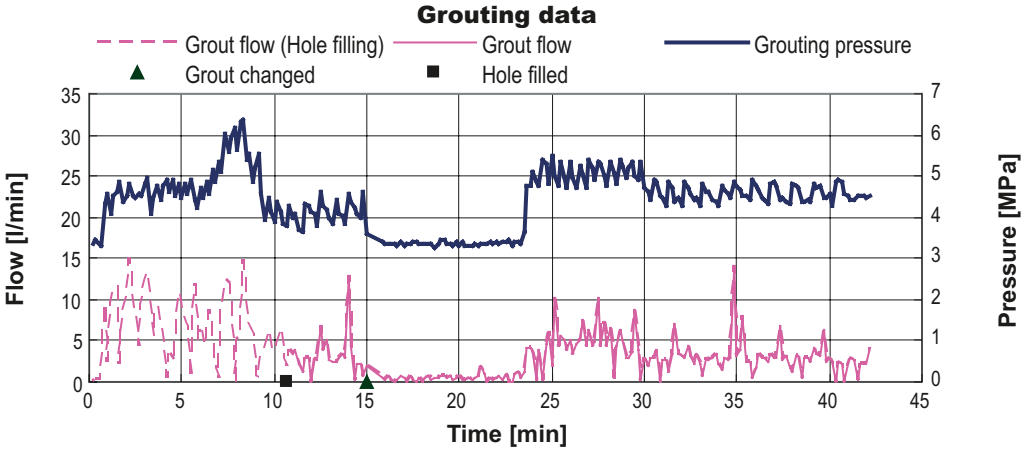

Figure 4-4. *An example of recorded grout flow and grouting pressure for the 2D case: Borehole A1 in Fan 1:1.*

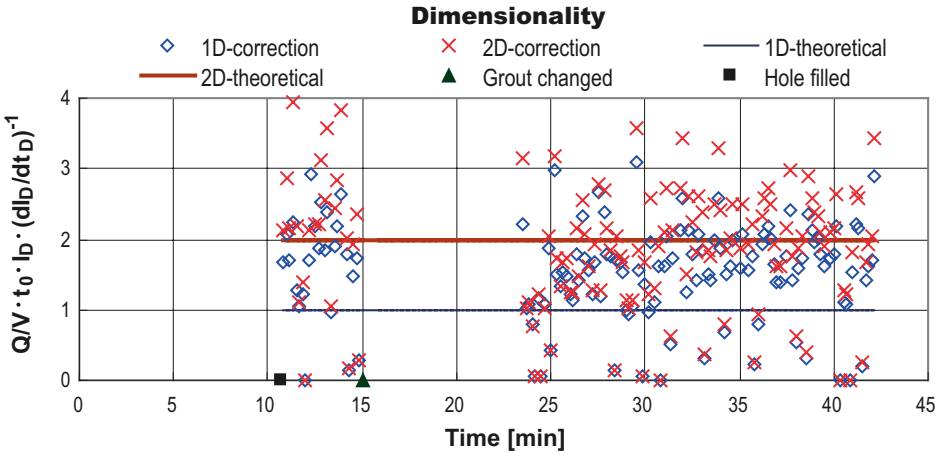

Figure 4-5. *An example of the index for analyzing the dimensionality, $Q/V \cdot t_0 \cdot I_D \cdot (dI_D/dt_D)^{-1}$ for the 2D case: Borehole A1 in Fan 1:1 using time-independent grout properties.*

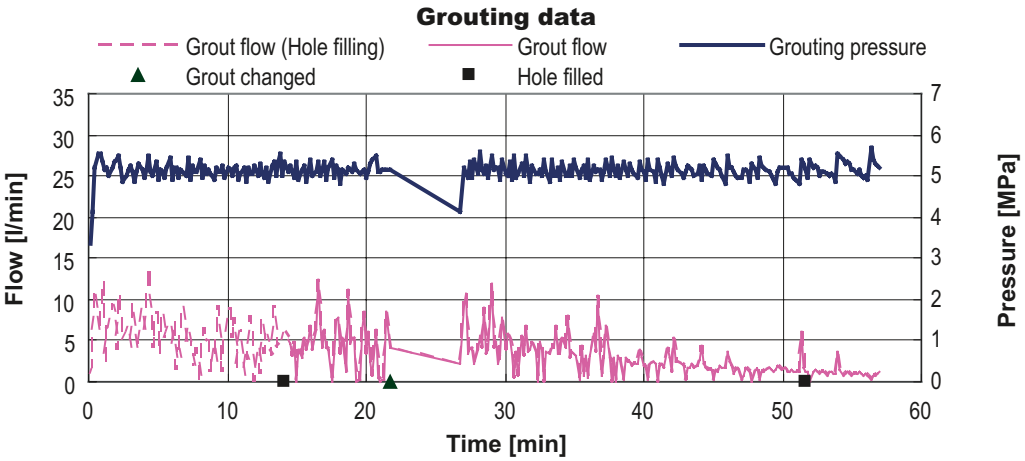

Figure 4-6. *An example of recorded grout flow and grouting pressure for the 2D to 1D case: Grouting data from borehole G27 in Fan 1:2 using time-independent grout properties.*

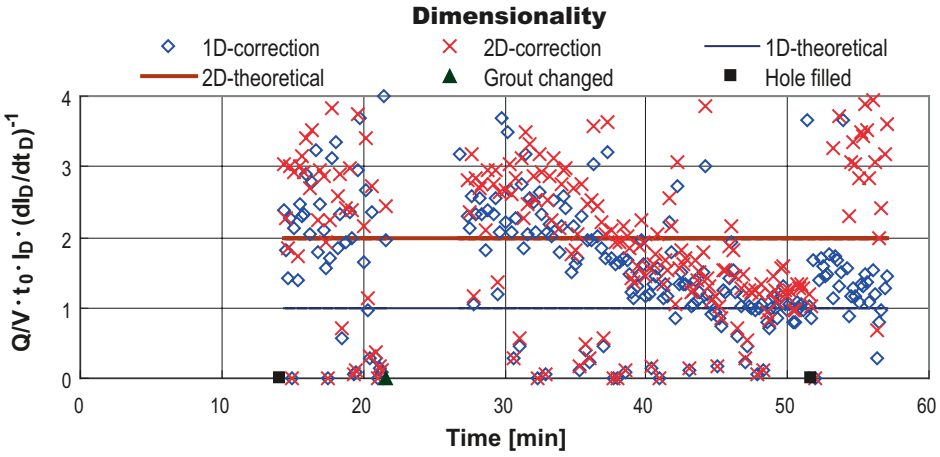

Figure 4-7. *An example of the index for analyzing the dimensionality, $Q/V \cdot t_0 \cdot I_D \cdot (dI_D/dt_D)^{-1}$ for the 2D to 1D case: Grouting data from borehole G27 in Fan 1:2 using time-independent grout properties.*

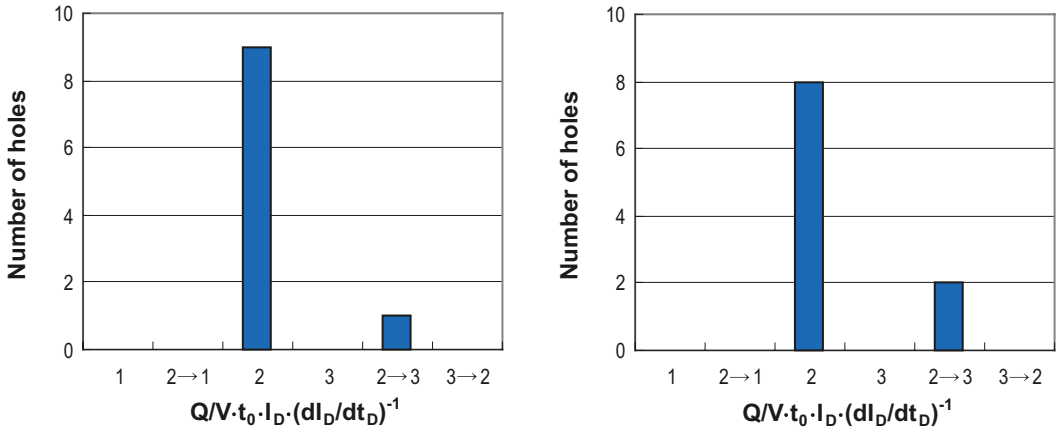

Figure 4-8. *Frequency distribution of the index for analyzing the dimensionality, $Q/V \cdot t_0 \cdot I_D \cdot (dI_D/dt_D)^{-1}$ in Fan 1:1. Time-independent grout properties are used in the graph on the left and time-dependent grout properties are used in the graph on the right.*

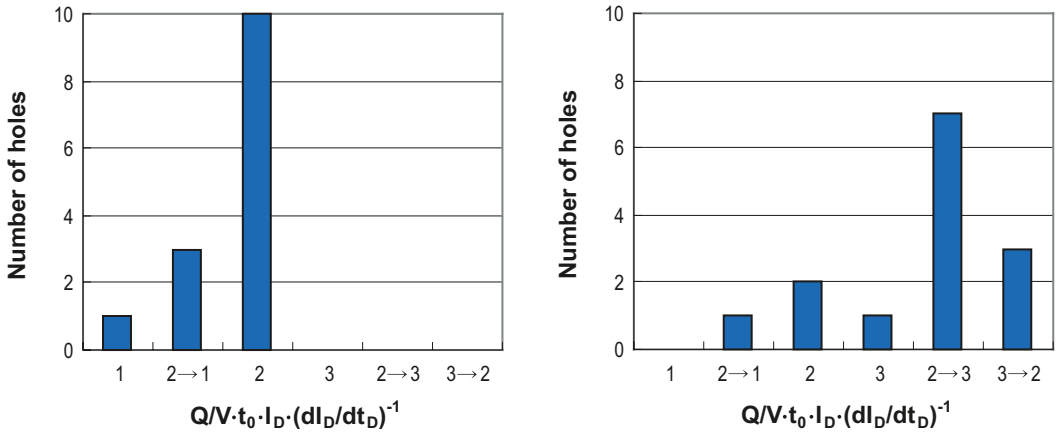

Figure 4-9. *Frequency distribution of the index for analyzing the dimensionality, $Q/V \cdot t_0 \cdot I_D \cdot (dI_D/dt_D)^{-1}$ in Fan 1:2. Time-independent grout properties are used in the graph on the left and time-dependent grout properties are used in the graph on the right.*

4.3.2 Fracture aperture

The calculate apertures from the grouting can be compared with measured aperture from hydraulic testing. In Figure 4-10 to 4-12 three examples of estimation from the grouting is given. Figure 4-10 shows an example of the estimated fracture aperture $\sum wb^2$ for the 1D case. Figure 4-11 shows an example of the estimated fracture aperture, $\sum b^3$ for the 2D case. Figure 4-12 shows an example of the 2D to 1D case. The geological interpretation of the results has not been carried out in this study.

The calculated fracture apertures have been compared with measured hydraulic apertures. Two types of measurements have been used. One is based on inflow during drilling, which was estimated in /Emmelin et al. 2004/ and the other is based on water loss measurement (WLM), which was estimated in /Kobayashi and Stille 2007/. Figure 4-13 and Figure 4-14 show the comparison of the calculated fracture apertures and those measured for the 2D case (see also Appendix D). The calculated results include more than the 2D cases because $\sum b^3$ can be calculated as a 2D case.

For Fan 1:1, the calculated results were close to the fracture apertures based on WLM. On the other hand, the calculated results were good at predicting the fracture apertures based on inflow (water loss measurements were not performed in Fan 1:2).

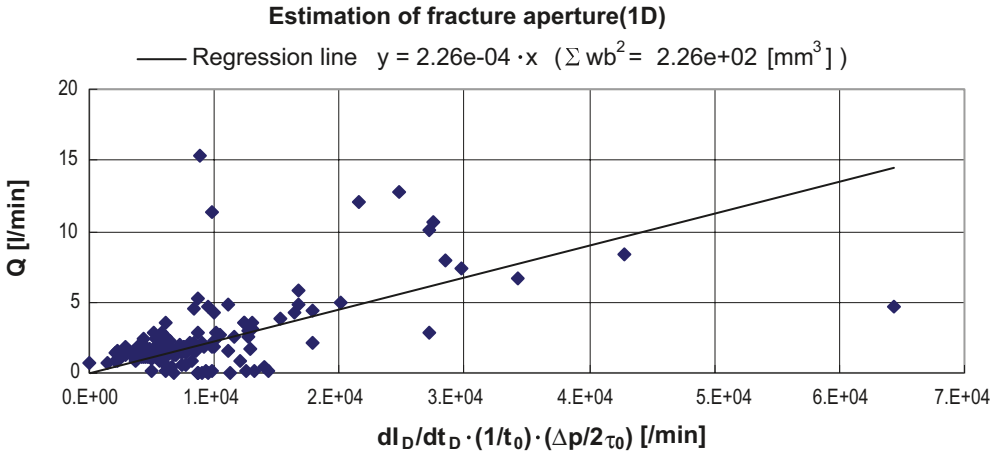

Figure 4-10. *An example of estimated fracture aperture for the 1D case: Grouting data from borehole B24 in Fan 1:2 using time-independent grout properties.*

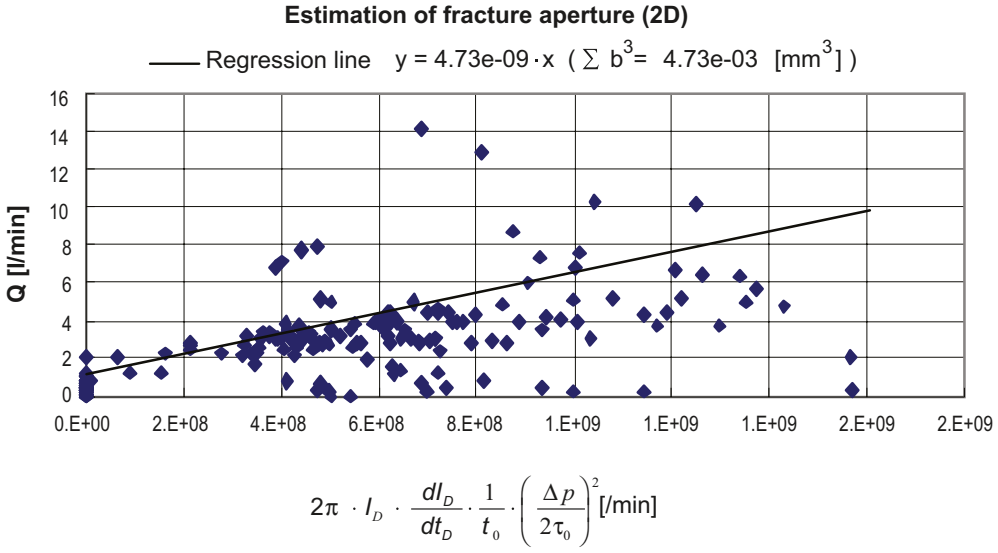

Figure 4-11. *An example of estimated fracture aperture for the 2D case: Grouting data from borehole A1 in Fan 1:1 using time-independent grout properties.*

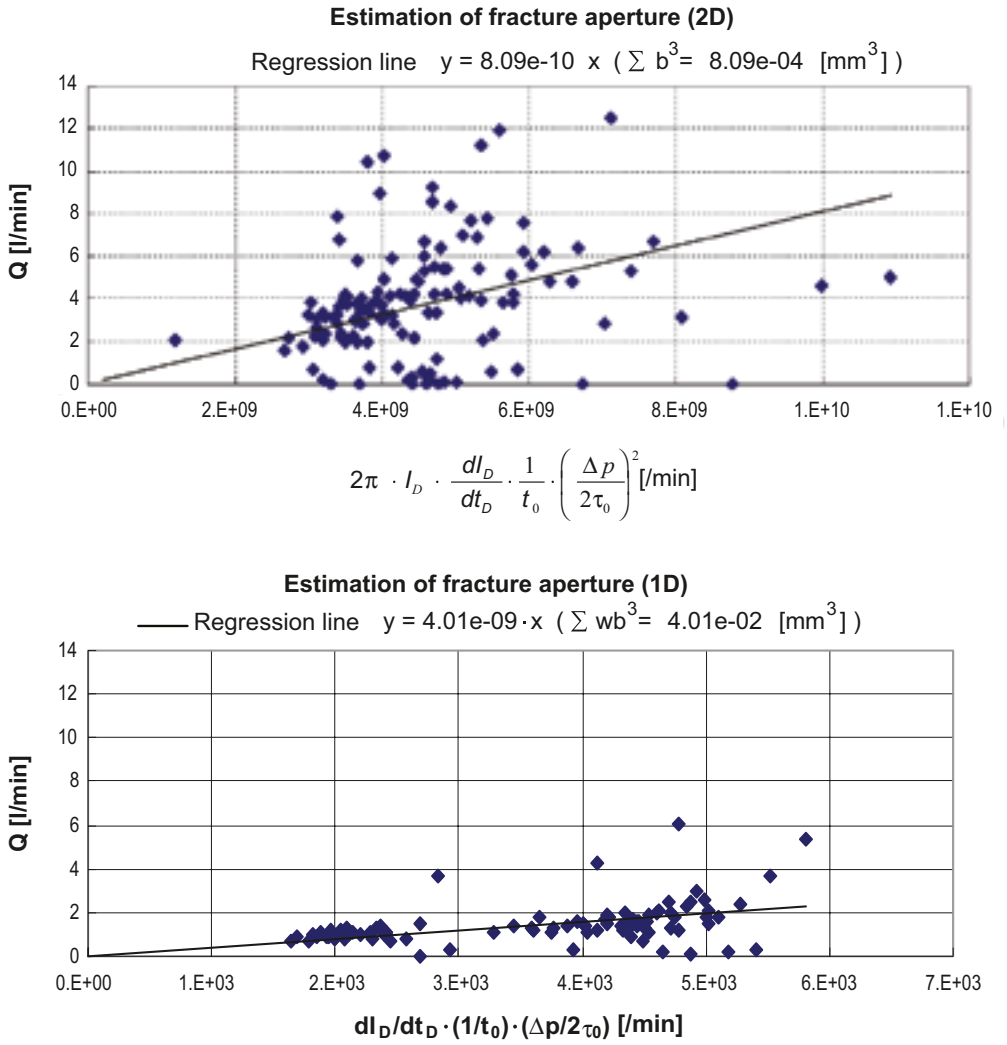

Figure 4-12. *An example of estimated fracture aperture for the 2D to 1D case: Grouting data from borehole G27 in Fan 1:2 using time-independent grout properties. The top graph shows the estimated fracture aperture during 2D and the bottom graph shows the estimated fracture aperture during 1D.*

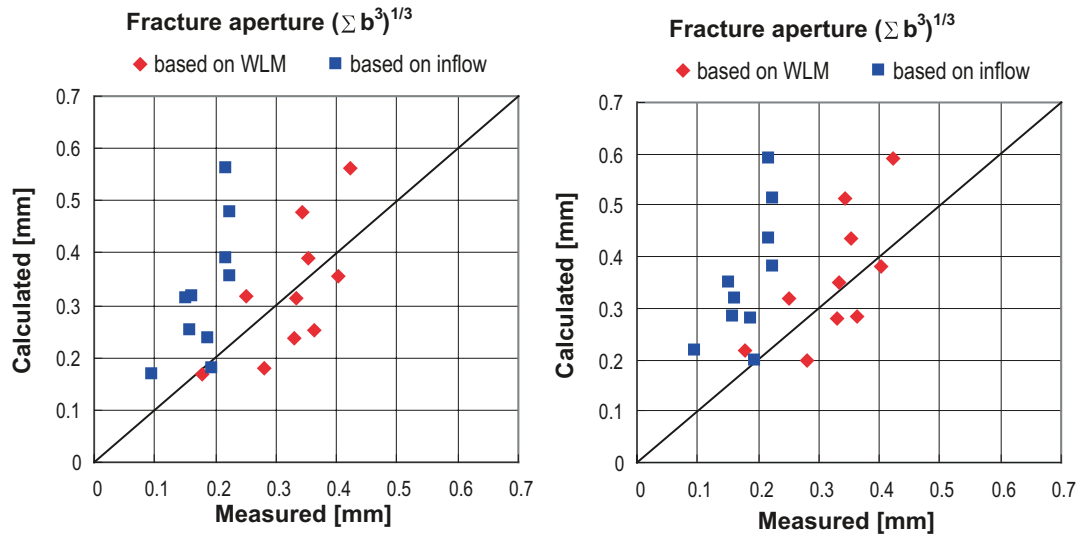

Figure 4-13. *Relationship between calculated fracture apertures for the 2D case and measured results from hydraulic apertures based on inflow and WLM for Fan 1:1. Time-independent grout properties are used in the graph on the left and time-dependent grout properties are used in the graph on the right.*

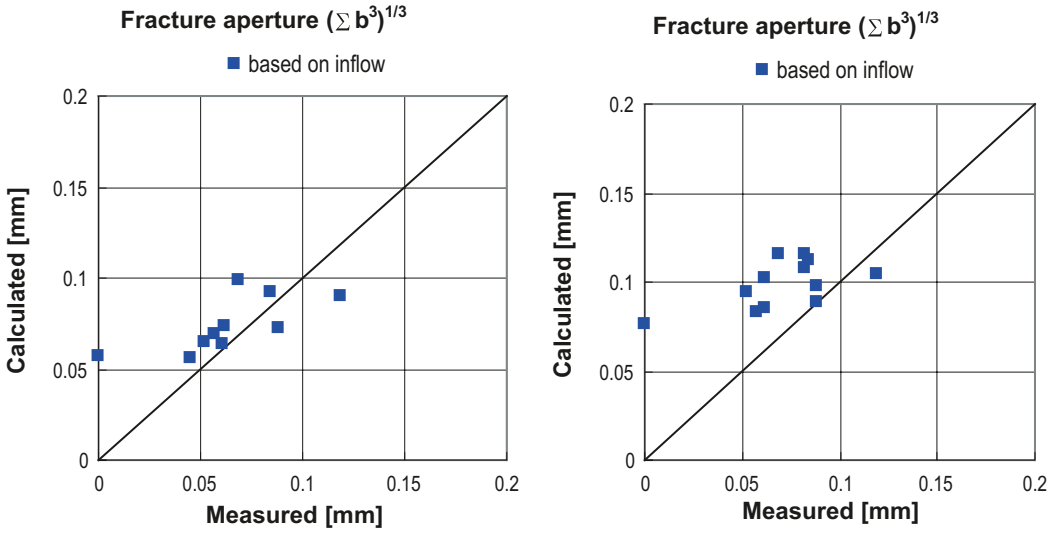

Figure 4-14. *Relationship between calculated fracture apertures for the 2D case and measured results from hydraulic apertures based on inflow for Fan 1:2.Time-independent grout properties are used in the graph on the left and time-dependent grout properties are used in the graph on the right.*

For the 2D to 1D cases, $\sum b^3$ and $\sum wb^2$ can be calculated during the 2D flow and 1D flow respectively. Table 4-4 show the calculated fracture apertures for the 2D to 1D cases. The fracture apertures and width of 1D flow are calculated assuming that the number of fractures is one. As can be seen from Table 4-5, it was estimated that there was one fracture along borehole C15 in Fan 1:2. As regards boreholes C27 and C28 in Fan 1:2, only inflows during drilling from total borehole length were measured. Therefore it was assumed that the number of fractures is one.

Table 4-4. Calculated hydraulic aperture for the 2D to 1D case.

Fan	Borehole	Grout properties	Fracture aperture 2D→1D				
			Σb^3 [mm³]	Σwb^2 [mm³]	n	b [mm]	w [m]
Fan 1:2	C15	Time-independent	0.00259	276.6	1	0.137	14.7
Fan 1:2	C15	Time-dependent	0.00396	567.6	1	0.158	22.7
Fan 1:2	G27	Time-independent	0.00081	401.2	(1)	(0.093)	(46.2)
Fan 1:2	G28	Time-independent	0.00068	209.7	(1)	(0.088)	(27.2)

Table 4-5. Estimated hydraulic apertures based on inflow for the 2D to 1D case.

Borehole/ Section	Estimated hydraulic aperture based on inflow [µm]					
	0–4.6m	4.6–7.6m	7.6–10.6m	10.6–13.6m	13.6–15.6m	Total
Fan 1:2, C15	0	0	0	123	0	
Fan 1:2, C27						(82)
Fan 1:2, C28						(82)

Figure 4-15 shows a comparison between the calculated fracture apertures and those measured for the 2D to 1D case. The calculated results were close to those measured.

There is only one 1D case. Table 4-6 shows the calculated results. Unlike the 2D and 2D to 2D cases, it is impossible to make a comparison between calculated results and measured results since the width of the fracture is unknown. Using the measured fracture apertures shown in Table 4-7, the average width can be calculated.

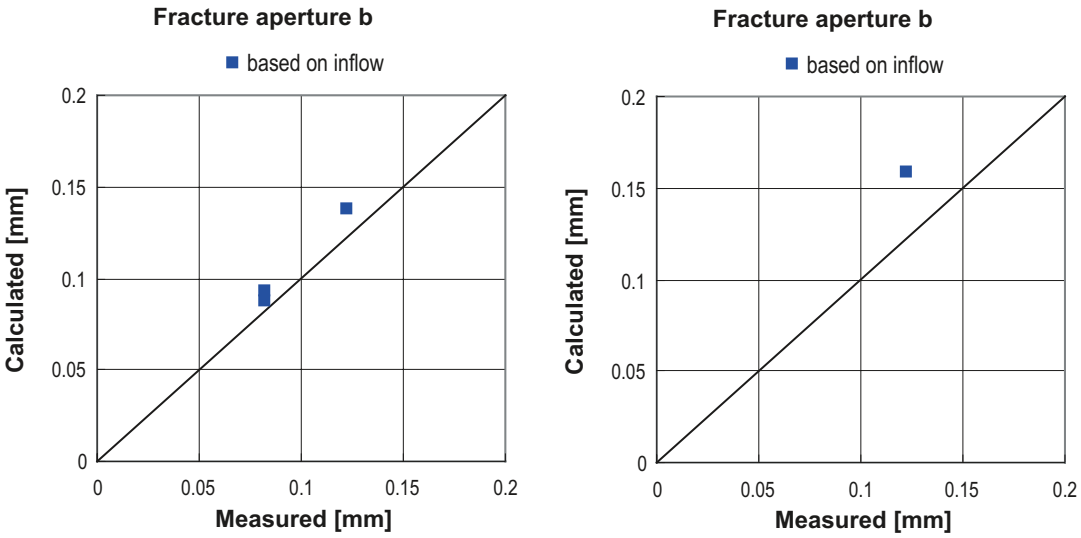

Figure 4-15. *Relationship between calculated fracture apertures for the 2D to 1D case and measured results based on inflow for Fan 1:2.Time-independent grout properties are used in the graph on the left and time-dependent grout properties are used in the graph on the right.*

Table 4-6. Calculated hydraulic aperture for the 1D case.

Fan	Borehole	Grout properties	Fracture aperture 1D		
			Σwb^2 [mm^3]	n	w (average) [m]
Fan 1:2	B24	Time-independent	225.7	2	10.6

Table 4-7. Estimated hydraulic aperture based on inflow for the 1D case.

Borehole/ Section	Estimated hydraulic aperture based on inflow [µm]				
	0–4.6m	4.6–7.6m	7.6–10.6m	10.6–13.6m	13.6–15.6m
Fan 1:2, B24	0	43	0	0	85

4.3.3 Grout flow

Figure 4-16, Figure 4-17 and Figure 4-18 show examples of calculated grout flow for the 1D, 2D and 2D to 1D cases respectively. In Appendix E, all the calculated grout flows according to the flow dimensionality are shown. There are various kinds of grouting logs but the calculated grout flows appear to be very similar to those measured. It can be observed that the "Real Time Grouting Control Method" may be applicable to a wide range of different grouting situations.

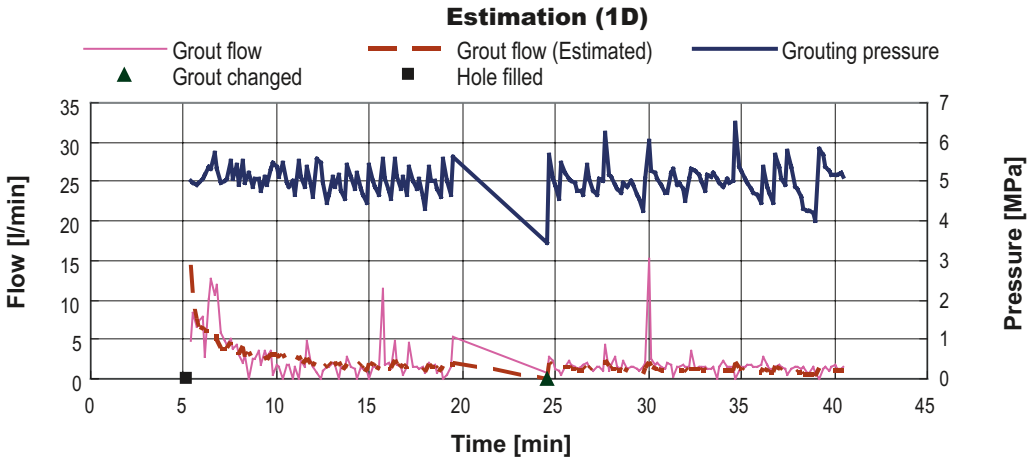

Figure 4-16. *An example of estimated grout flow for 1D case: Grouting data from borehole B24 in Fan 1:2 using time-independent grout properties.*

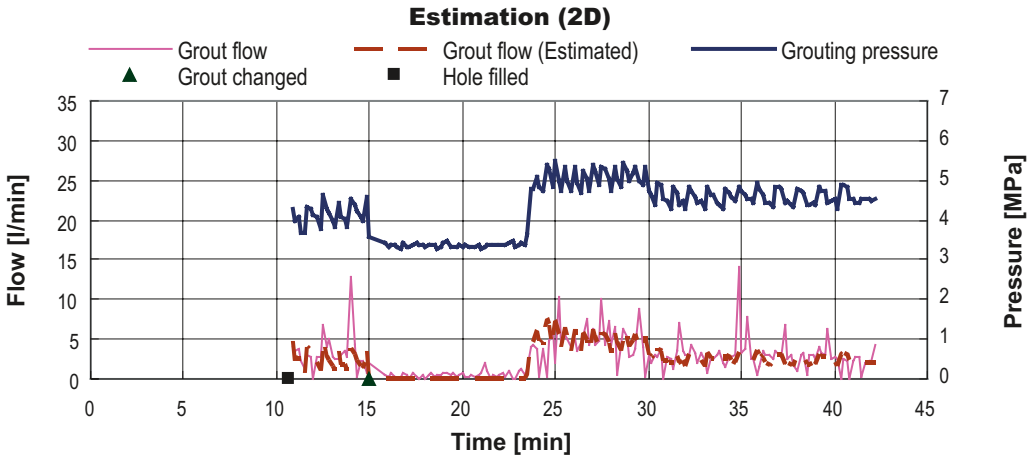

Figure 4-17. *An example of estimated grout flow for the 2D case: Grouting data from borehole A1 in Fan 1:1 using time-independent grout properties.*

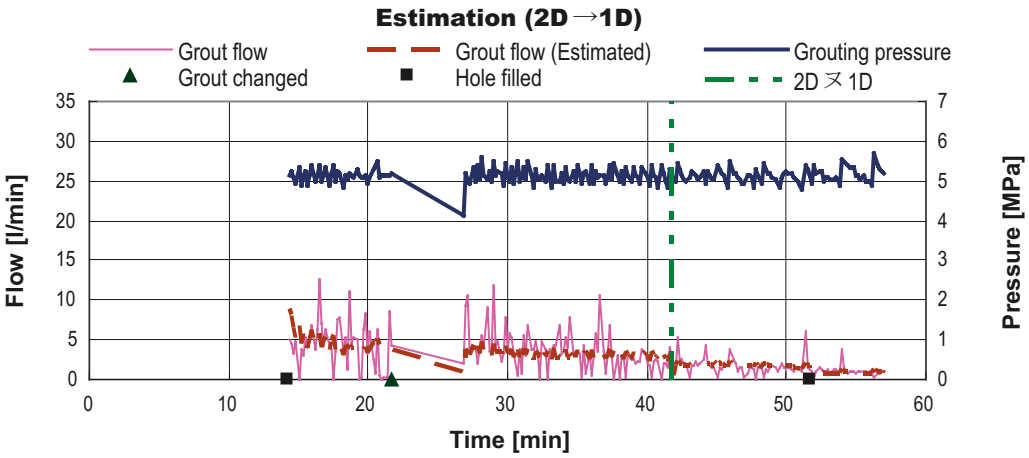

Figure 4-18. *An example of estimated grout flow for the 2D to 1D case: Grouting data from borehole G27 in Fan 1:2 using time-independent grout properties.*

4.3.4 Penetration length

Penetration length is difficult to measure directly. The grouting experiments at Äspö HRL, can therefore not be used for verification of the estimated penetration length according to the "Real Time Grouting Control Method". In this case, penetration length has been calculated only for reference purposes.

As can be seen from Figure 4-13 to Figure 4-15, calculated fracture apertures and measured fracture apertures differ somewhat. Therefore, fracture apertures have been modified to better describe actual penetration length according to the following equations:

$$b^* = b \times \sum_{b>b_{groutable}}^{Measured} b^3 \Big/ \sum_{b>b_{groutable}}^{Calculated} b^3 \qquad (2D) \qquad \text{(4-1a)}$$

$$b^* = b \times \sum_{b>b_{groutable}}^{Measured} b^3 \Big/ \sum_{b>b_{groutable}}^{Calculated} b^3 \qquad (1D) \qquad \text{(4-1b)}$$

Figure 4-19 to Figure 4-21 show calculated penetration length (see Appendix F). Figure 4-22 and Figure 4-23 show the locations of grouting holes.

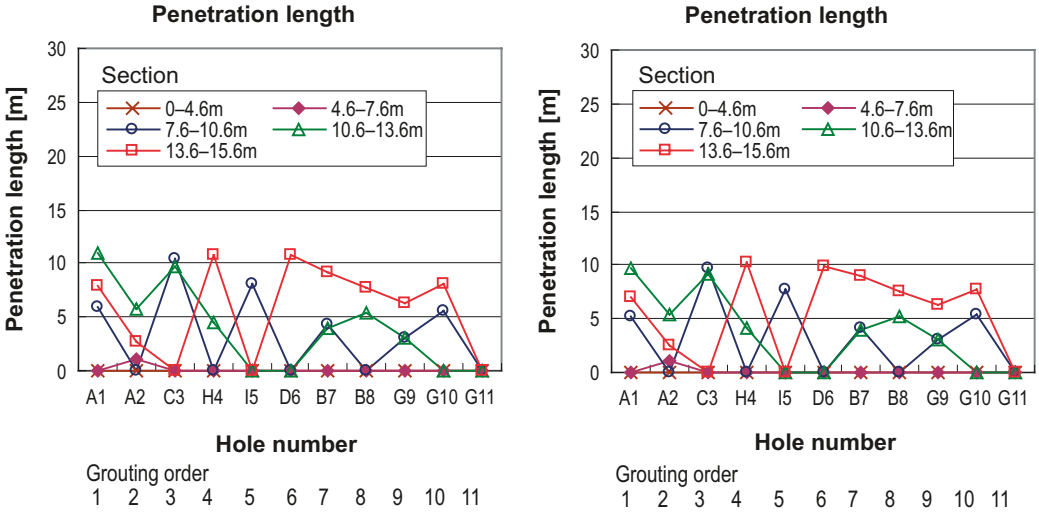

Figure 4-19. *Calculated penetration length in Fan 1:1. The left graph uses time-independent grout properties. The right graph shows time-dependent grout properties.*

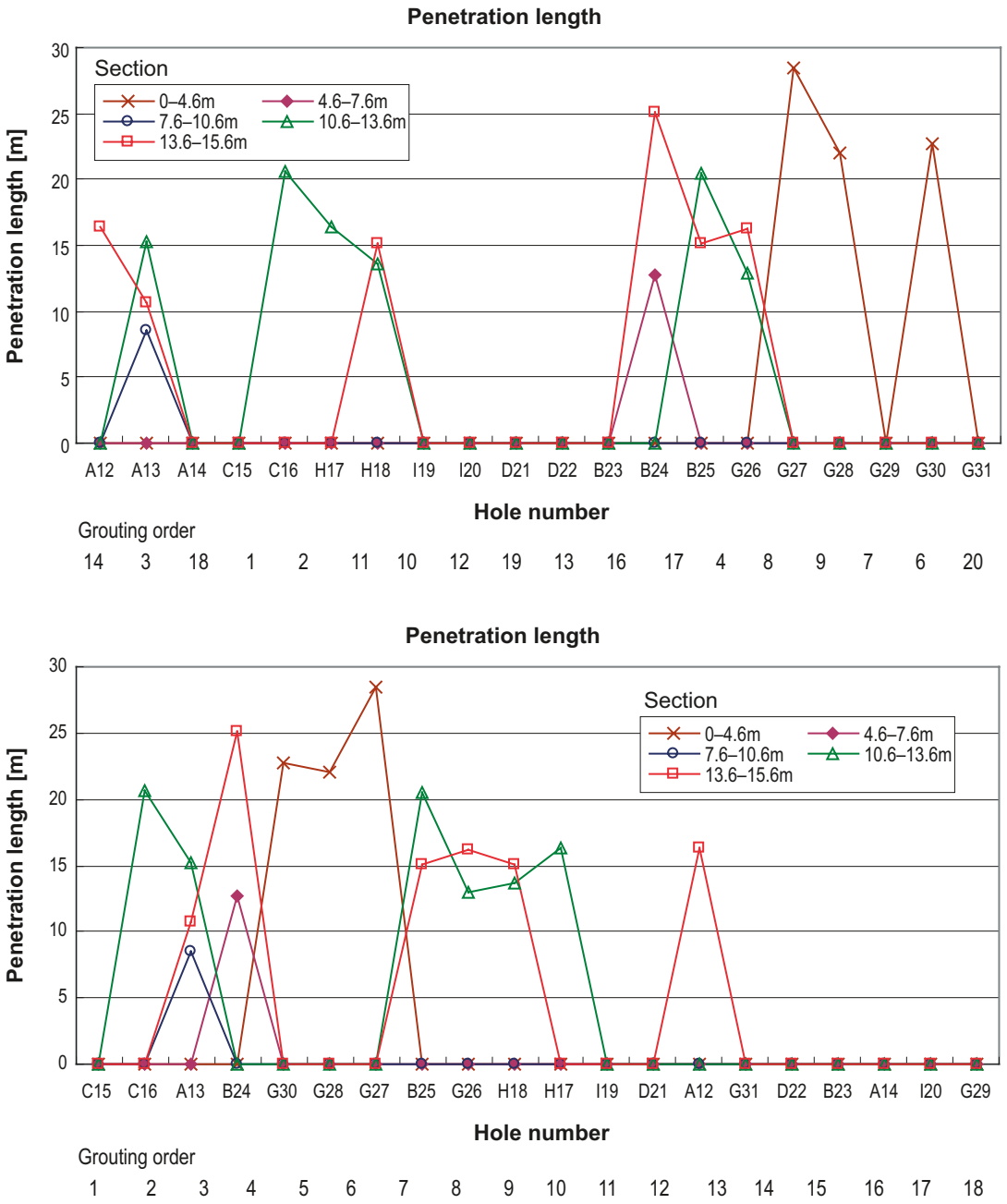

Figure 4-20. *Calculated penetration length in Fan 1:2 using time-independent grout properties. The top graph shows the results in borehole order. The bottom graph shows them in grouting order.*

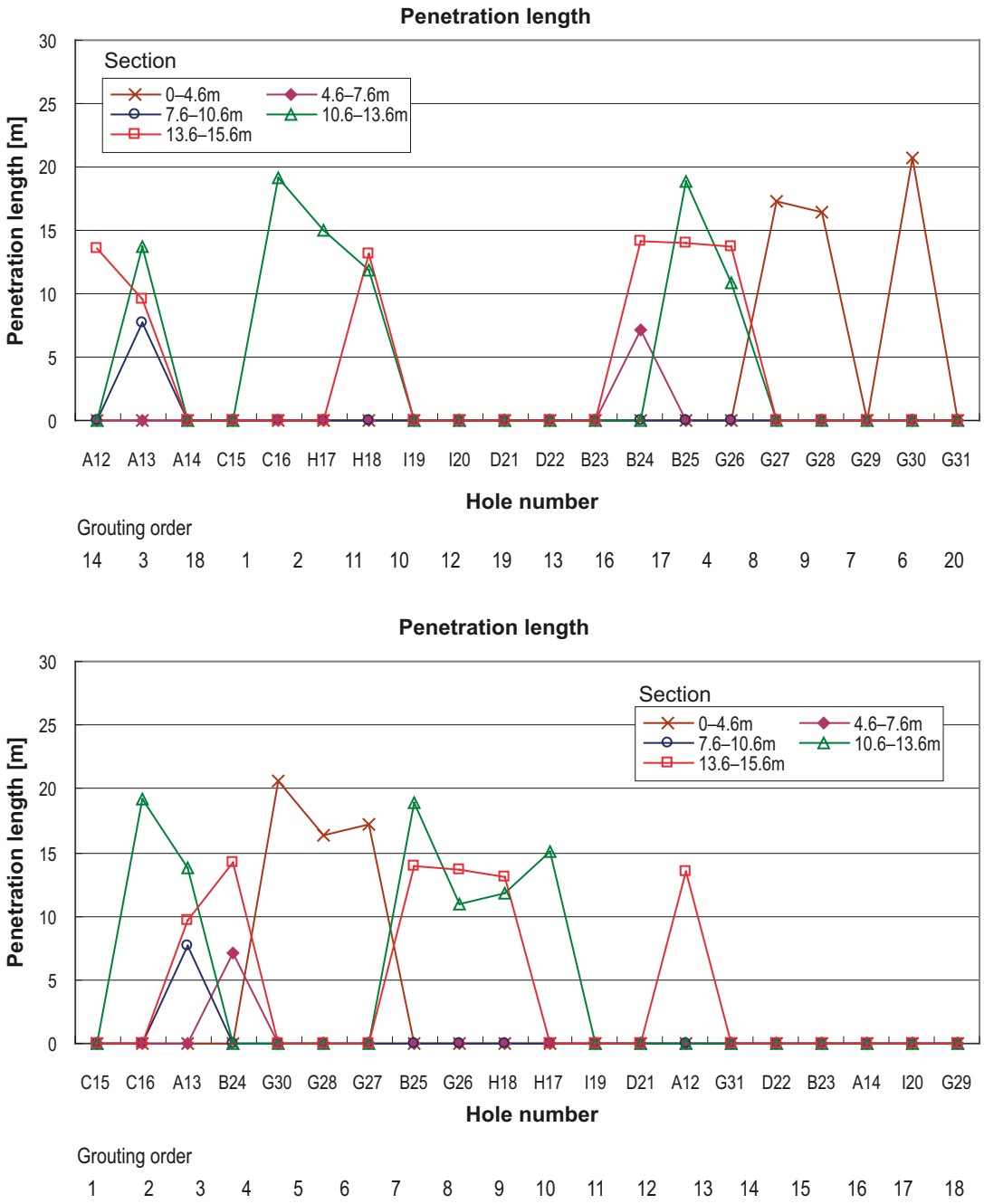

Figure 4-21. *Calculated penetration length in Fan 1:2 using time-dependent grout properties. The top graph shows the results in borehole order. The bottom graph shows them in grouting order.*

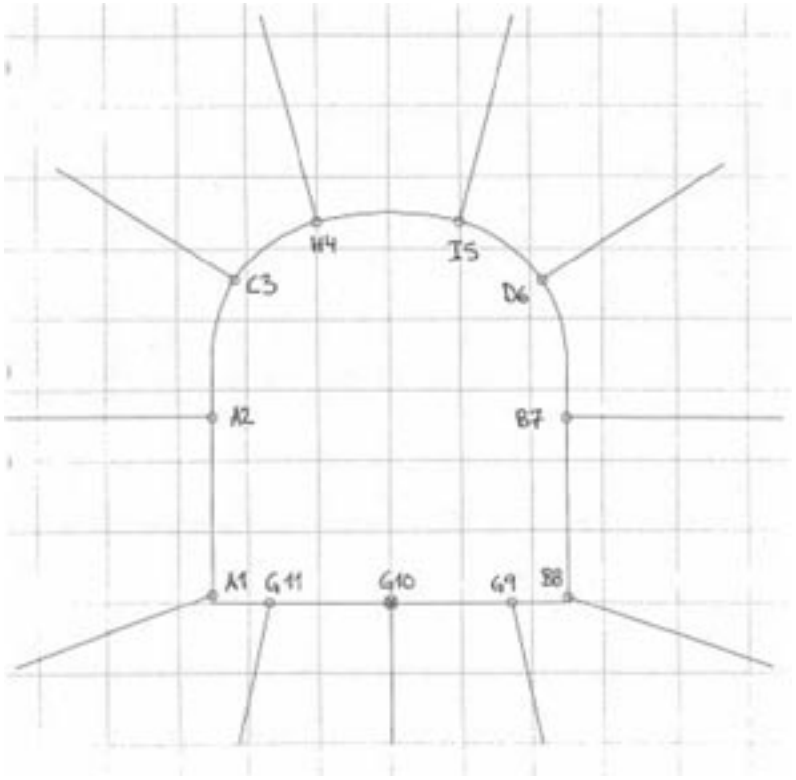

Figure 4-22. *Grouting holes in Fan 1:1 /Emmelin et al. 2004/.*

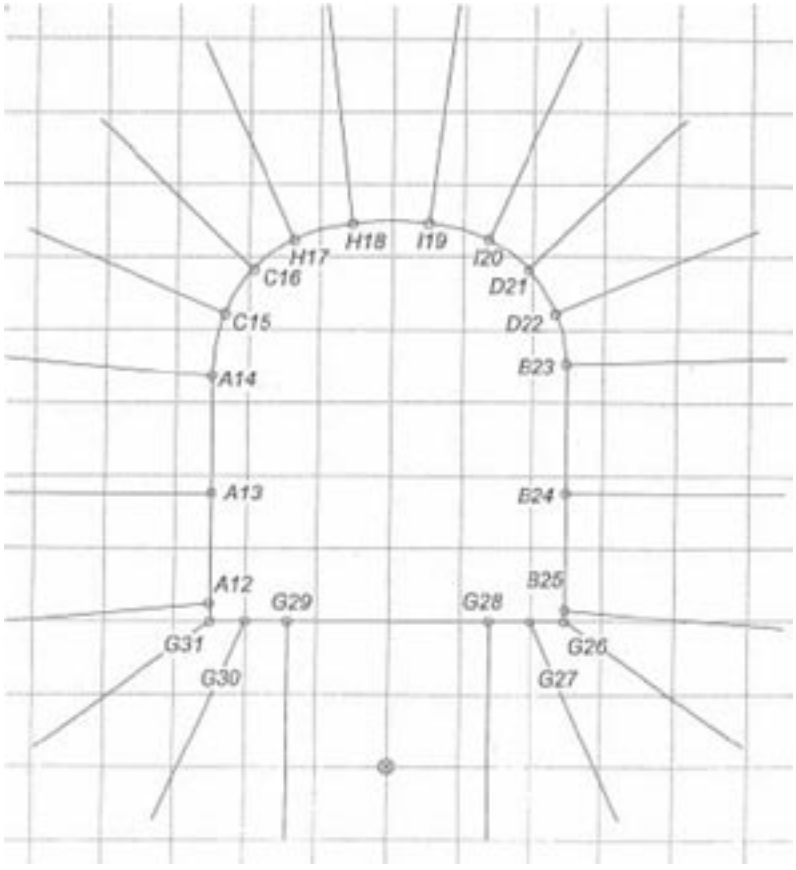

Figure 4-23. *Grouting holes in Fan 1:2 /Emmelin et al. 2004/.*

4.4 Conclusions regarding verification

In order to verify the "Real Time Grouting Control Method", the field data from the grouting field experiment at the 450 m level in the Äspö HRL is used. Use is made of all recorded grouting data in Fan 1:1 and Fan 1:2, except for the holes in which the grouted volume is below the hole-filling volume. For the verification of the "Real Time Grouting Control Method", differences in dimensionality, fracture aperture and grout flow between calculated and measured results are compared. The conclusions of the verification can be summarized as follows:

- The calculated flow dimensionality showed 2D for almost all boreholes in both Fan 1:1 and Fan 1:2 when time-independent grout properties were used for the calculations. This is a good estimation since fractures were assumed to be planes in the field experiment. It was found that time-independent grout properties gave better predictions in this case.
- The calculated fracture apertures from the measured grout flows were close to the estimated fracture apertures based on water loss measurements for Fan 1:1. On the other hand, the calculated fracture apertures were close to the estimated fracture apertures based on inflow for Fan 1:2 (water loss measurements were not performed in Fan 1:2). It can be concluded that the calculations were fairly well conducted but a deeper understanding is needed in order to describe the fracture aperture.
- Although all the grouting data were used for the calculations, the calculated grout flows according to the flow dimensionality were quite close to the measured grouting flow. It can be concluded that the "Real Time Grouting Control Method" could be applicable to a wide range of grouting logs.
- Penetration length cannot be used for the verification of the "Real Time Grouting Control Method" since it was not measured in the grouting experiments at Äspö HRL. Normally it is not visible. In order to confirm the calculated penetration, a field test will be needed where the penetration length is directly measured.

5 Conclusions and proposals

5.1 Conclusions

In this report the "Real Time Grouting Control Method" has been described in order to calculate grout penetration and make it possible to control grouting in real time by applying further developed theories for grout spread. The underlying analytical solutions have been verified as well as the possibility to use them in an active way during grouting in order to govern the process and establish the stop criterion.

For the "Real Time Grouting Control Method", the stop criterion is related to achieved grout spread. Grouting is completed when the grout penetration of the smallest fracture that has to be sealed is above a certain minimum value (target value) or before the grout penetration for the largest fracture aperture reaches a certain maximum value (limiting value). Based on the calculated penetration length it may be possible to add certain other options to the method such as:

- Estimation of joint aperture.
- Prediction of grout flow and grout penetration.
- Calculation of the risk of uplift.
- Prediction of water leakage to the tunnel.

These are essential aspects of a grouting design and important factors for a successful grouting operation.

The data for the system can be derived from the ordinary testing and investigations carried out for a modern tunnel project. Hydraulic testing will give the groundwater level, the transmissivity and largest fracture aperture before grouting. Testing the grout mix will give important flow properties such as density, viscosity and yield value. It will also give us the finest fracture aperture the grout will be able to penetrate. Furthermore, the requirements of maximum allowable ingress of water, ban of drips and grout spread have to be established on the basis of hydrogeological analysis.

In order to verify the "Real Time Grouting Control Method", the field data from the grouting field experiment at the 450 m level in the Äspö HRL has been used. The calculated flow dimensionality, the calculated fracture apertures and the calculated grout flows were quite close to the values measured. It may be concluded that the "Real Time Grouting Control Method" is applicable for real grouting design and control.

5.2 Proposals

Nowadays a computerized logging tool, which records grouting parameters such as grouting time, grouting pressure, grout flow and grouted volume, is often used in grouting projects. Our intention is to combine our method with the computerized logging tool to acquire an active tool in order to be able to govern the grout spread in real time during grouting operations. This we see as being an important step in creating an active process.

The method must also be further tested and evaluated in real tunnel grouting operations to gain a clearer understanding of its practical application. It is also proposed that Real Time Grouting Concept could be further developed by incorporate the theories of dimensionality according to /Hässler 1991/.

A better understanding of the deformations of the fractures and the risk of jacking the rock mass during grouting operations is essential. It is suggested that by analyzing the flow versus pressure, it will be possible to identify the point at which the joints start to open up when the pressure is increased. In the report, a rough method for estimate the ultimate uplift pressure is proposed based on simple relations between ultimate bearing capacity and the load from grout pressure.

References

Brantberger M, Stille H, Eriksson M, 2000. Controlling the grout spread in tunnel grouting – Analyses and developments of the GIN-method, Tunneling and Underground Space Technology, Vol 15, No. 4, pp 343–352.

Dalmalm T, 2004. Choice of grouting method for jointed hard rock based on sealing time predictions. PhD Thesis, Division of Soil and Rock Mechanics, Royal Institute of Technology, Stockholm.

Eklund D, Stille H, 2007. Penetrability due to filtration tendency of cement-based grouts, Tunnelling and Underground Space Technology.

Emmelin A, Eriksson M, Fransson Å, 2004. Characterisation, design and execution of two grouting fans at 450 m level, Äspö HRL. R-04-58, Svensk Kärnbränslehantering AB.

Eriksson M, Stille H, Andersson J, 2000. Numerical calculations for prediction of grout spread with account for filtration and varying aperture, Tunnelling and Underground Space Technology, Vol 15, No. 4, pp 353–364.

Eriksson M, Stille H, 2003. A method for measuring and evaluating the penetrability of grouts, Grouting and ground treatment. Proc. of third int. conference, New Orleans, USA.

Eriksson M, Stille H, 2005. Cementinjektering i hårt berg (Grouting with cement based grout in hard jointed rock) SveBeFo, Stockholm, Sweden.

Eriksson M, 2002. Prediction of grout spread and sealing effect. A probabilistic approach. PhD Thesis, Division of Soil and Rock Mechanics, Royal Institute of Technology, Stockholm.

Fransson Å, 2001. Characterisation of fractured rock for grouting using hydrogeological methods. PhD Thesis, Department of Geology, Chalmers University of Technology, Göteborg.

Gustafson G, Claesson J, 2005. Steering Parameters for Rock Grouting, Submitted to Journal of Rock Mechanics and Mining Science.

Gustafson G, Fransson Å, 2005. The use of the Pareto distribution for fracture transmissivity assessment. Hydrogeology Journal (2005) 14: 15–20.

Gustafson G, Stille H, 1996. Prediction of groutability from grout properties and hydro geological data, Tunnelling and Underground Space Technology 11(3), pp 325–332.

Gustafson G, Stille H, 2005. Stop criteria for cement grouting, Felsbau 23(3), pp 62–68.

Hernqvist L, Fransson Å, Gustafson G, Emmelin A, Eriksson M, Stille H, 2008. Analyses of the grouting results for a section of the APSE tunnel at Äspö Hard Rock Laboratory, Journal of Rock Mechanics and Mining Sciences. http://dx.doi.org/10.1016/j.ijrmms.2008.02.003.

Houlsby A C, 1990. Construction and design of cement grouting, ISBN 0-471-51629-5, John Wiley & Sons, Inc., USA.

Hässler L, Stille H, Håkansson U, 1987. Simulation of grouting in jointed rock, Proc. 6th International Congress on Rock Mechanics, Vol. 2, pp 943-946, Montreal.

Hässler L, 1991. Grouting of rock – Simulation and classification. PhD Thesis, Division of Soil and Rock Mechanics, Royal Institute of Technology, Stockholm.

Kobayashi S, Stille H, 2007. Design for rock grouting based on analysis of grout penetration. Verification using Äspö HRL data and parameter analysis. R-07-13, Svensk Kärnbränslehantering AB.

Lombardi G, 1985. The role of cohesion in cement grouting of rock, 15th ICOLD Congress, Vol. III, pp 235–261, Lausanne.

Lombardi G, Deere D, 1993. Grouting design and control using the GIN principle, Water Power and Dam Construction, June 1993, pp 15–22.

Appendix A

Inflow during drilling and estimated hydraulic apertures

Table A-1. Inflow during drilling, Fan 1:1.

Borehole/ Section	Inflow [l/min] 0–4.6 m	4.6–7.6 m	7.6–10.6 m	10.6–13.6 m	13.6–15.6 m	Qtot
H4	0	0	0	3	42	45
C3	0	0	28	23	0	51
A2	0	1	0	119	12	132
A1	0	0	1	8	3	12
I5	0	0	132	0	0	132
G11	0	0	48	0	12	60
G10	0	0	24	0	72	96
D6	0	0	0	0	84	84
B7	0	0	12	10	122	144
B8	0	0	0	36	108	144
G9	0	0	5	5	44	54

Table A-2. Estimated hydraulic apertures based on inflow, Fan 1:1.

Borehole/ Section	Estimated hydraulic aperture [µm] 0–4.6 m	4.6–7.6 m	7.6–10.6 m	10.6–13.6 m	13.6–15.6 m
H4	0	0	0	61	148
C3	0	0	129	121	0
A2	0	43	0	210	98
A1	0	0	45	84	61
I5	0	0	217	0	0
G11	0	0	155	0	98
G10	0	0	123	0	177
D6	0	0	0	0	187
B7	0	0	98	92	211
B8	0	0	0	141	203
G9	0	0	73	73	150

Table A-3. Inflow during drilling, Fan 1:2.

Borehole/ Section	Inflow [l/min] 0–4.6 m	4.6–7.6 m	7.6–10.6 m	10.6–13.6 m	13.6–15.6 m	Qtot
I19	0	0	0	1.5	0.9	2.4
C15	0	0	0	24	0	24
I20	0	0	0	0	0.3	0.3
C16	0	0	0	21.6	0	21.6
D21	0	0	1	0	1.8	2.8
A14	0	0	0	0	0.1	0.1
D22	0	0	0	1	0	1
H17	0	0	0	2.4	0	2.4
B23	0	0	0.48	0	0.7	1.2
A13	0	0	1	6	2	9
B24	0	1	0	0	8	9
H18	0	0	0	1.3	1.7	3
B25	0	0	0	3	1.2	4.2
A12	0	0	0	0	1.8	1.8
G26	0	0	0	1	2	3
G31	0	0	0	0	0	0
G30						7.8
G29						0
G27						7.2
G28						7.2

Table A-4. Estimated hydraulic apertures based on inflow, Fan 1:2.

Borehole/ Section	Estimated hydraulic aperture [µm] 0–4.6 m	4.6–7.6 m	7.6–10.6 m	10.6–13.6 m	13.6–15.6 m
I19	0	0	0	49	41
C15	0	0	0	123	0
I20	0	0	0	0	29
C16	0	0	0	119	0
D21	0	0	43	0	52
A14	0	0	0	0	21
D22	0	0	0	43	0
H17	0	0	0	57	0
B23	0	0	33	0	38
A13	0	0	43	77	54
B24	0	43	0	0	85
H18	0	0	0	46	51
B25	0	0	0	61	45
A12	0	0	0	0	52
G26	0	0	0	43	54
G31	0	0	0	0	0

Appendix B

Inflow during drilling and estimated hydraulic apertures

Table B-1. Water loss measurements in Fan 1:1.

Borehole no	Inflow natural [l]	Borehole length [m]	Water loss Length [m]	Time [min]	Final pressure [MPa]	Volume [l]	Flow, V/t [l/min]	Lugeon Value
H4	45	15.6	15	1	0.2	29	29	9.7
C3	45	15.6	15	1	0.15	28	28	12.5
A2	132	15.6	15	1	0.2	35	35	11.7
A1	7.2	15.6	15	1	0.5	11	11	1.5
I5	132	15.6	15	1	0.15	45	45	20
G11	60	15.6	15	1	0.65	42	42	4.3
G10	96	15.6	15	1	0.5	44	44	5.9
D6	84	15.6	15	1	0.4	56	56	9.3
B7	144	15.6	15	1	0.2	52	52	17.3
B8	144	15.6	15	1	0.35	56	56	10.7
G9	60	15.6	15	1	0.65	40	40	4.1

Table B-2. Estimated hydraulic apertures based on water loss measurements, Fan 1:1.

Borehole/ Section	Estimated hydraulic aperture [µm] 0–4.6 m	4.6–7.6 m	7.6–10.6 m	10.6–13.6 m	13.6–15.6 m
H4	0	0	0	134	325
C3	0	0	296	278	0
A2	0	70	0	342	160
A1	0	0	82	154	112
I5	0	0	424	0	0
G11	0	0	236	0	149
G10	0	0	178	0	256
D6	0	0	0	0	329
B7	0	0	178	167	382
B8	0	0	0	217	312
G9	0	0	114	114	233

Appendix C

Inflow during drilling and estimated hydraulic apertures

Table C-1. Grouting data in Fan 1:1.

Hole number	Grouted volume [l]	Grouting time [min]
A1	154	41
A2	113	5
C3	198	26
H4	189	14
I5	184	5
D6	156	28
B7	177	8
B8	180	5
G9	115	31
G10	115	17
G11	53	17
Total	1,634	197

Table C-2. Grouting data in Fan 1:2.

Hole number	Grouted volume [l]	Grouting time [min]
A12	124	67
A13	140	49
A14	51	9
C15	224	56
C16	191	51
H17	129	43
H18	136	71
I19	78	35
I20	47	2
D21	87	39
D22	45	24
B23	77	38
B24	137	35
B25	232	59
G26	149	71
G27	178	52
G28	161	45
G29	54	7
G30	220	66
G31	77	35
Total	2,537	854

Appendix D

Inflow during drilling and estimated hydraulic apertures

Table D-1. Calculated dimensionality and hydraulic aperture in Fan 1:1 (time-dependent grout properties).

Hole number	Dimensionality	hydraulic aperture			
		1D Σwb^2 [mm^3]	> 2D Σb^3 [mm^3]	2D→1D Σb^3 [mm^3]	Σwb^2 [mm^3]
A1	2→3		0.01022		
A2	2		0.08177		
C3	2→3		0.02329		
H4	2		0.04292		
I5	2		0.20817		
D6	2		0.02216		
B7	2		0.05614		
B8	2		0.13557		
G9	2		0.03220		
G10	2		0.00792		
G11	—				

Table D-2. Calculated dimensionality and hydraulic aperture in Fan 1:2 (time-dependent grout properties).

Hole number	Dimensionality	hydraulic aperture			
		1D Σwb^2 [mm^3]	> 2D Σb^3 [mm^3]	2D→1D Σb^3 [mm^3]	Σwb^2 [mm^3]
A12	2→3		0.00084		
A13	2→3		0.00070		
A14	—				
C15	2→1			0.00396	567.6
C16	2→3		0.00115		
H17	2→3		0.00057		
H18	2→3		0.00061		
I19	—				
I20	—				
D21	—				
D22	—				
B23	2		0.00047		
B24	2→3		0.00093		
B25	3		0.00153		
G26	2→3		0.00107		
G27	3→2		0.00156		
G28	3→2		0.00124		
G29	—				
G30	3→2		0.00140		
G31	2		0.00045		

Table D-3. Calculated dimensionality and hydraulic aperture in Fan 1:1 (time-independent grout properties).

Hole number	Dimensionality	hydraulic aperture			
		1D Σwb^2 [mm^3]	> 2D Σb^3 [mm^3]	2D→1D Σb^3 [mm^3]	Σwb^2 [mm^3]
A1	2		0.00473		
A2	2		0.05967		
C3	2→3		0.01589		
H4	2		0.03104		
I5	2		0.17877		
D6	2		0.01303		
B7	2		0.04565		
B8	2		0.11021		
G9	2		0.03220		
G10	2		0.00590		
G11	—				

Table D-4. Calculated dimensionality and hydraulic aperture in Fan 1:2 (time-independent grout properties).

Hole number	Dimensionality	hydraulic aperture			
		1D Σwb^2 [mm^3]	> 2D Σb^3 [mm^3]	2D→1D Σb^3 [mm^3]	Σwb^2 [mm^3]
A12	2		0.00027		
A13	2		0.00038		
A14	—				
C15	2→1			0.00259	276.6
C16	2		0.00074		
H17	2		0.00034		
H18	2		0.00026		
I19	—				
I20	—				
D21	—				
D22	—				
B23	2		0.00017		
B24	1	225.7			
B25	2		0.00096		
G26	2		0.00039		
G27	2→1			0.00081	401.2
G28	2→1			0.00068	209.7
G29	—				
G30	2		0.00080		
G31	2		0.00018		

Appendix E

Inflow during drilling and estimated hydraulic apertures

Fan 1:1

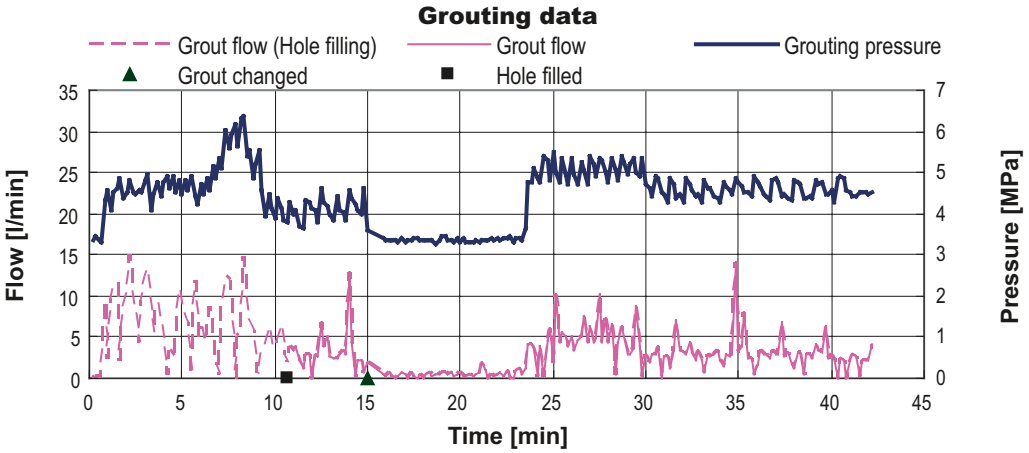

Figure E-1. *Grouting data on borehole A1 in Fan 1:1.*

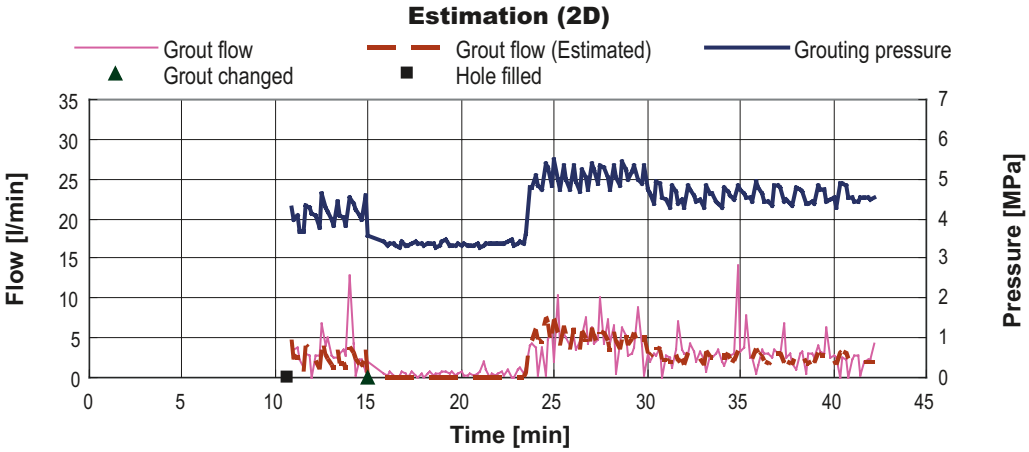

Figure E-2. *Estimated grout flow of borehole A1 in Fan 1:1 (time-independent grout properties).*

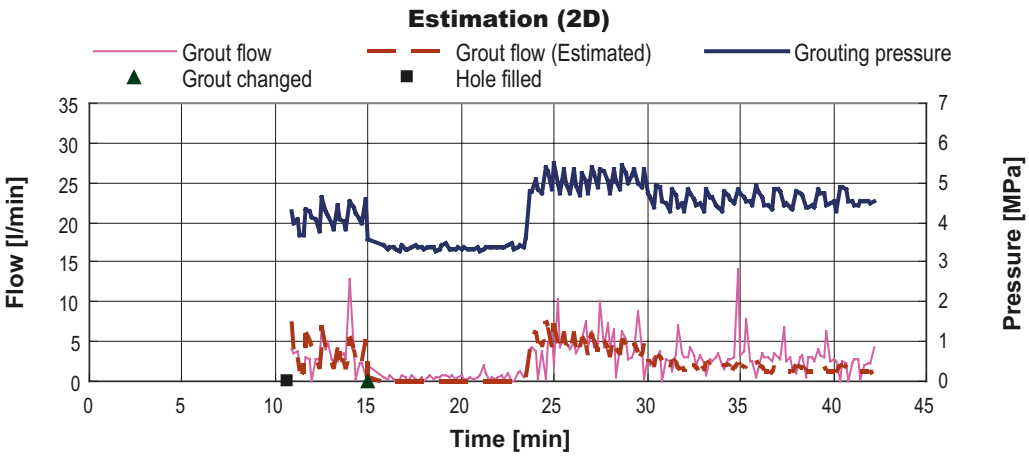

Figure E-3. *Estimated grout flow of borehole A1 in Fan 1:1 (time-dependent grout properties).*

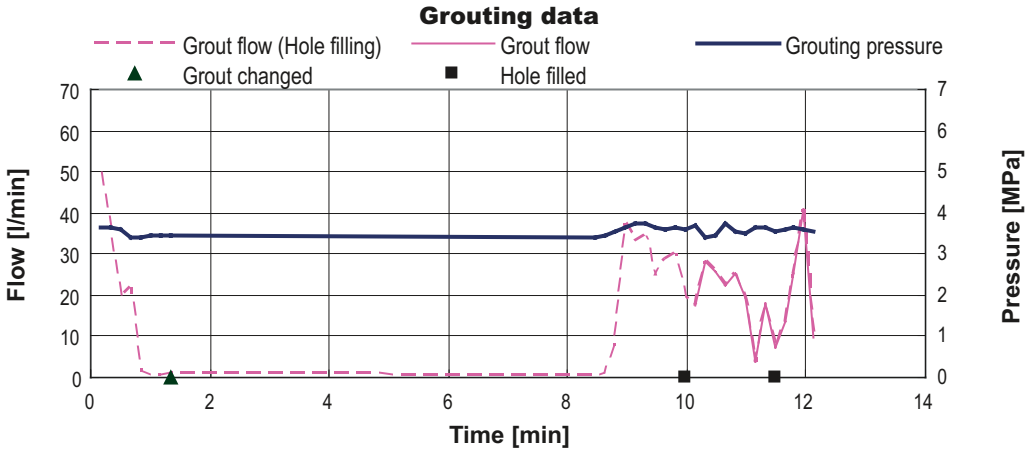

Figure E-4. *Grouting data on borehole A2 in Fan 1:1.*

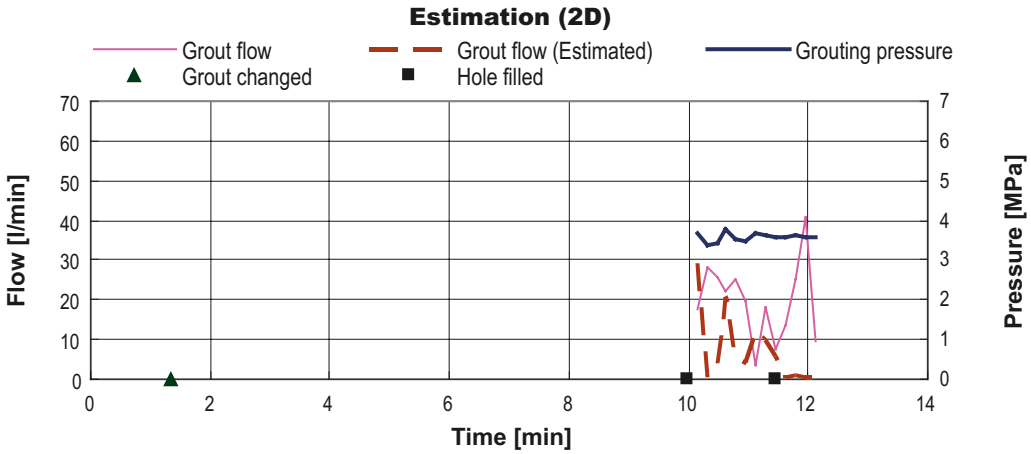

Figure E-5. *Estimated grout flow of borehole A2 in Fan 1:1 (time-independent grout properties).*

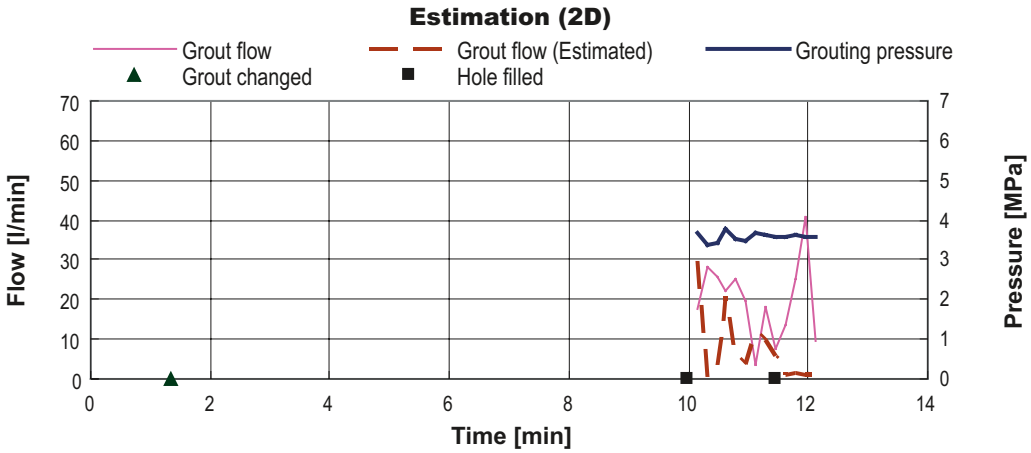

Figure E-6. *Estimated grout flow of borehole A2 in Fan 1:1 (time-dependent grout properties).*

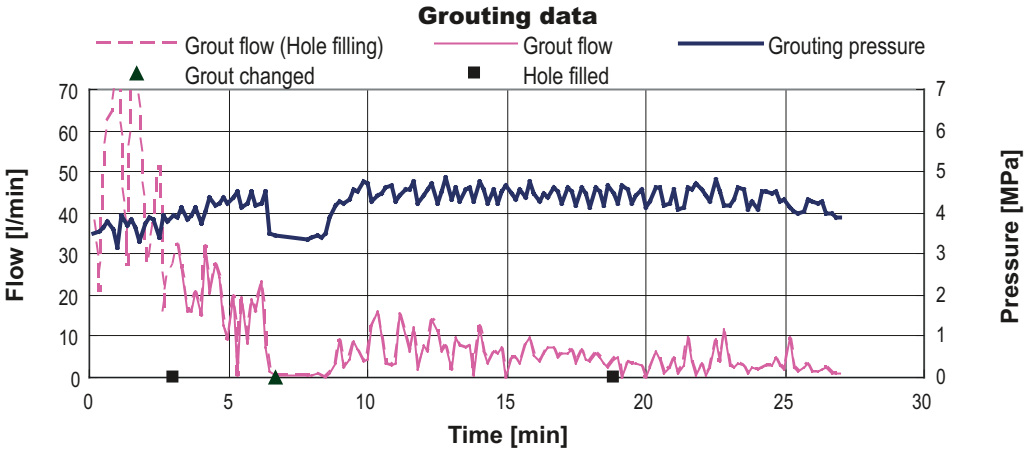

Figure E-7. *Grouting data on borehole C3 in Fan 1:1.*

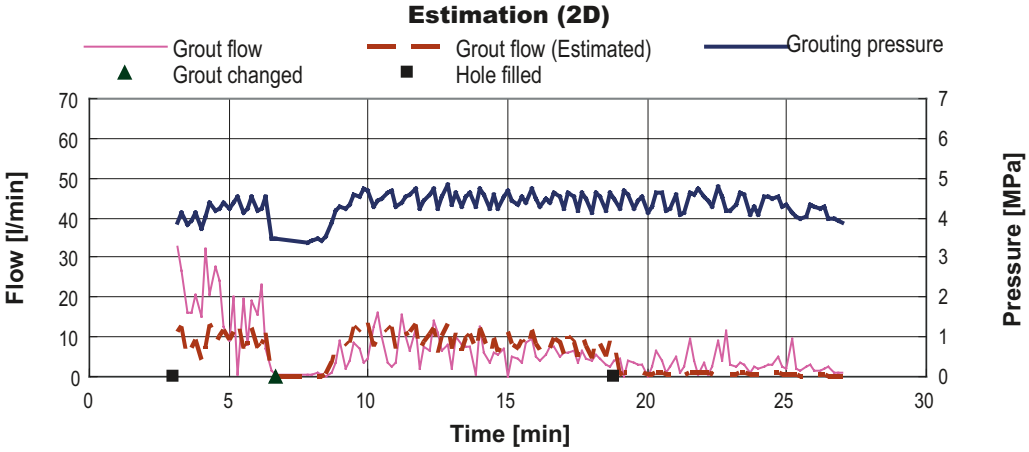

Figure E-8. *Estimated grout flow of borehole C3 in Fan 1:1 (time-independent grout properties).*

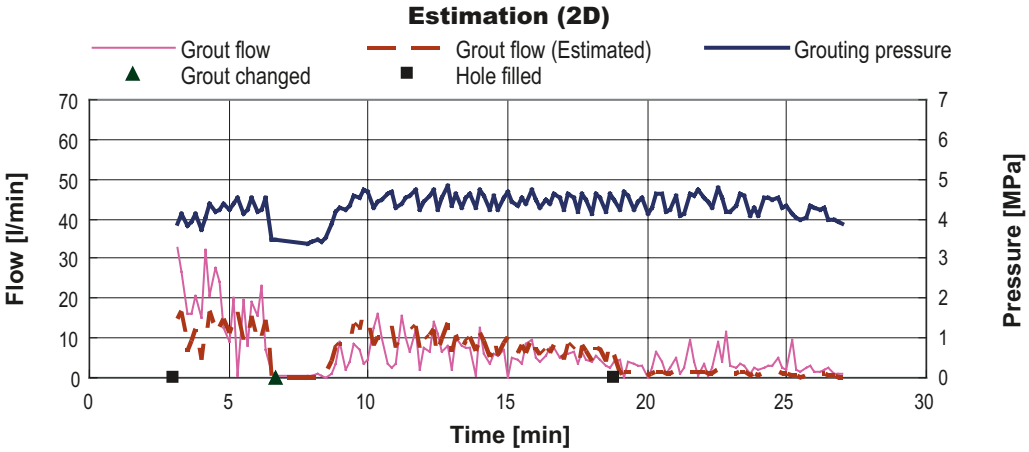

Figure E-9. *Estimated grout flow of boreholeC3 in Fan 1:1 (time-dependent grout properties).*

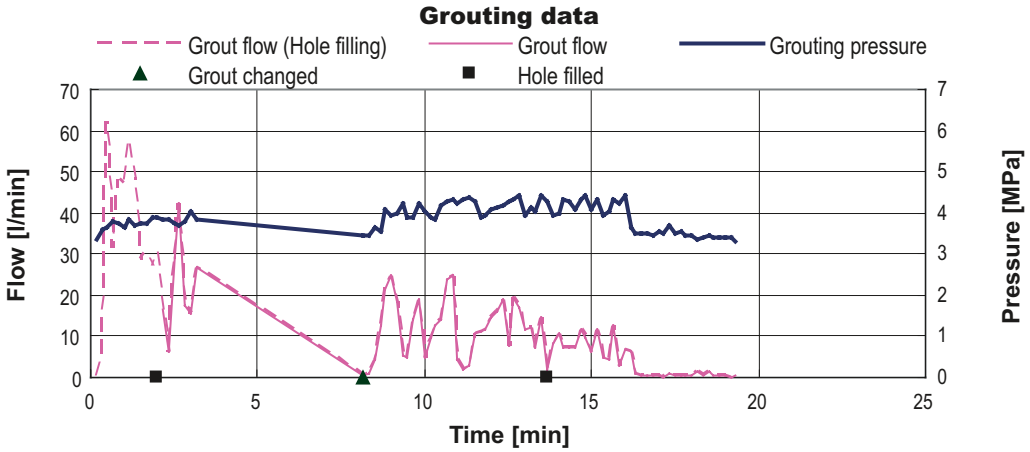

Figure E-10. *Grouting data on borehole H4 in Fan 1:1.*

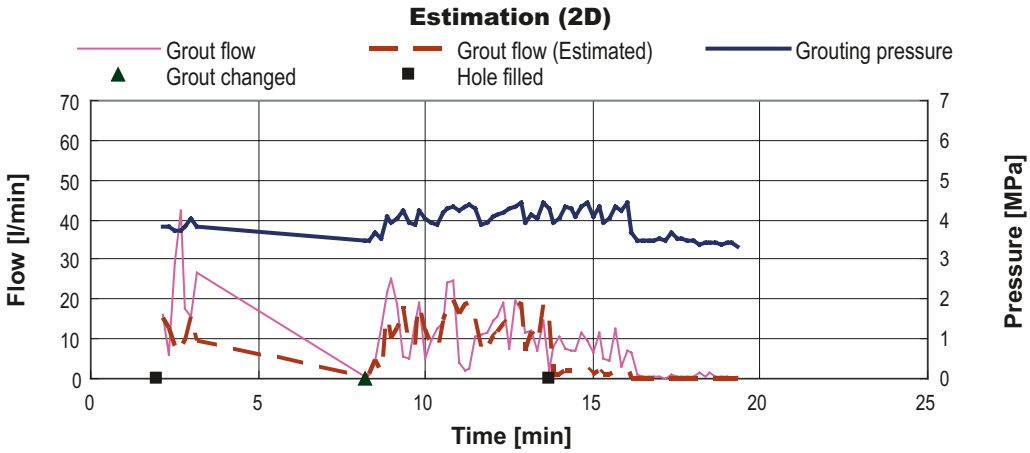

Figure E-11. *Estimated grout flow of borehole H4 in Fan 1:1 (time-independent grout properties).*

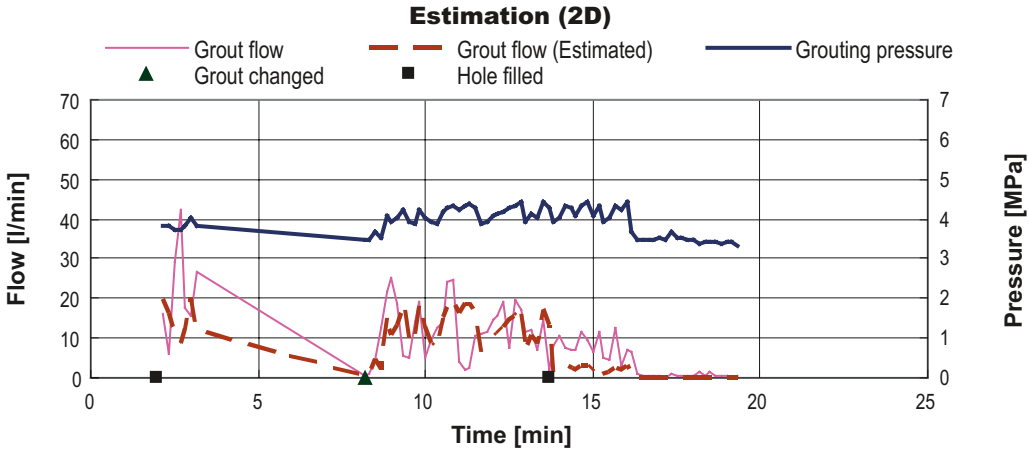

Figure E-12. *Estimated grout flow on borehole H4 in Fan 1:1 (time-dependent grout properties).*

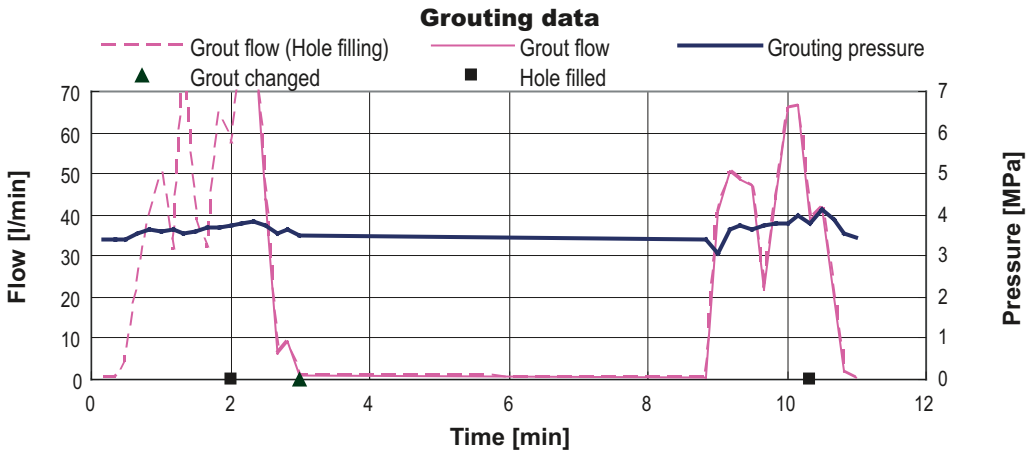

Figure E-13. *Grouting data on borehole I5 in Fan 1:1.*

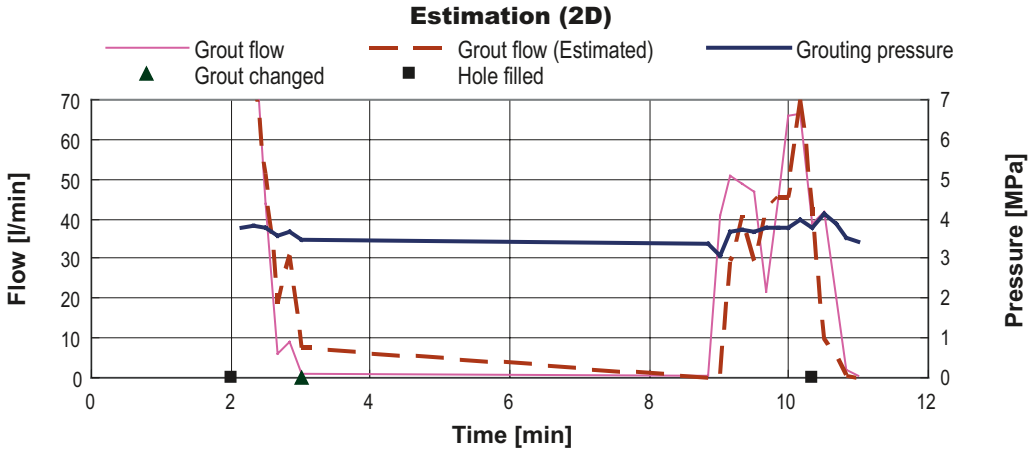

Figure E-14. *Estimated grout flow of borehole I5 in Fan 1:1 (time-independent grout properties).*

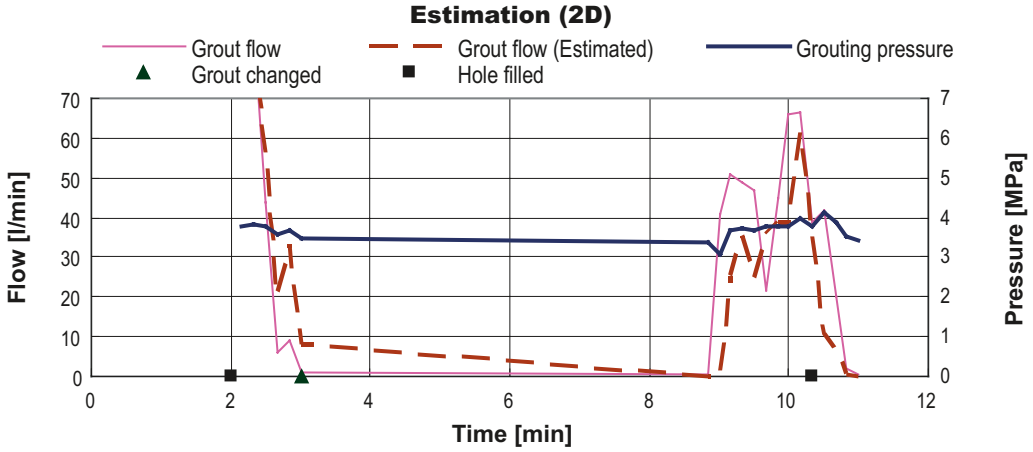

Figure E-15. *Estimated grout flow of borehole I5 in Fan 1:1 (time-dependent grout properties).*

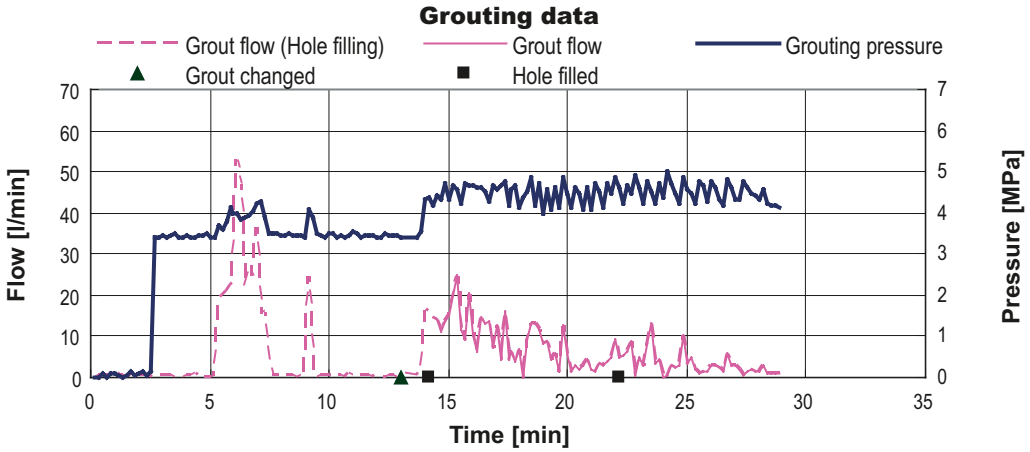

Figure E-16. *Grouting data on borehole D6 in Fan 1:1.*

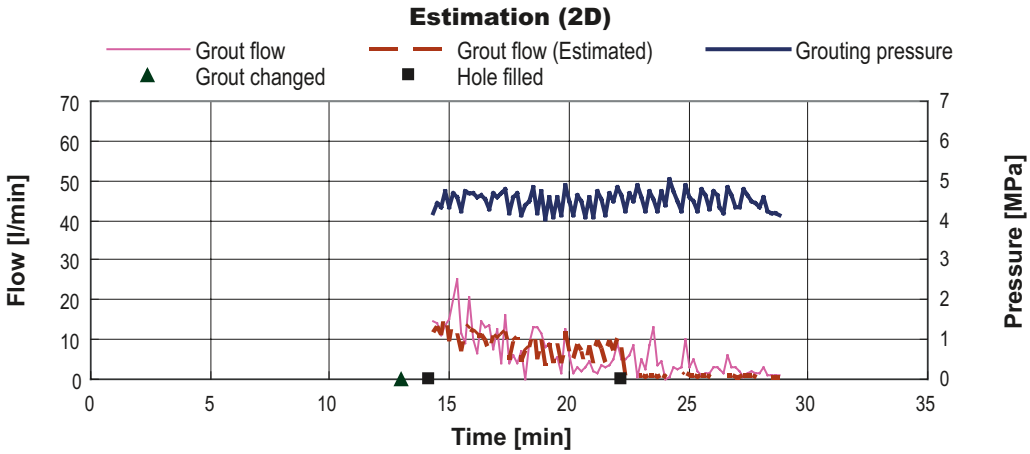

Figure E-17. *Estimated grout flow of borehole D6 in Fan 1:1 (time-independent grout properties).*

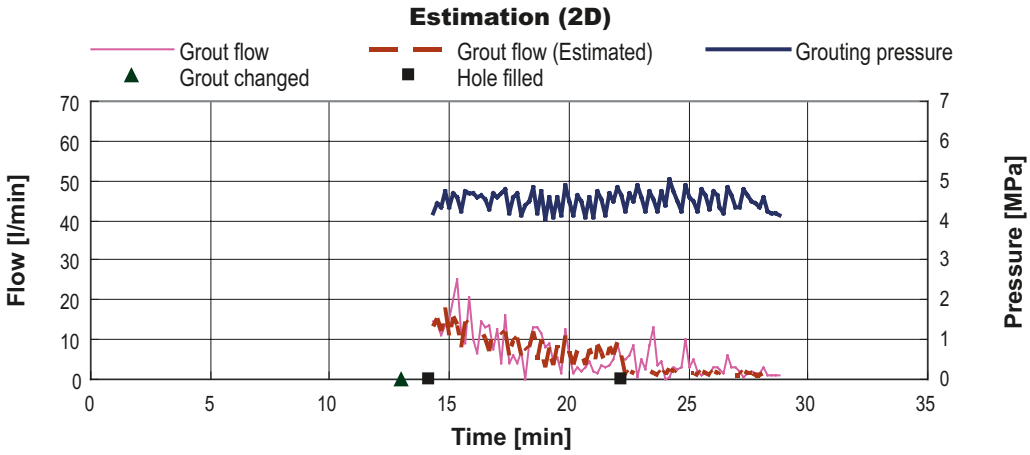

Figure E-18. *Estimated grout flow of borehole D6 in Fan 1:1 (time-dependent grout properties).*

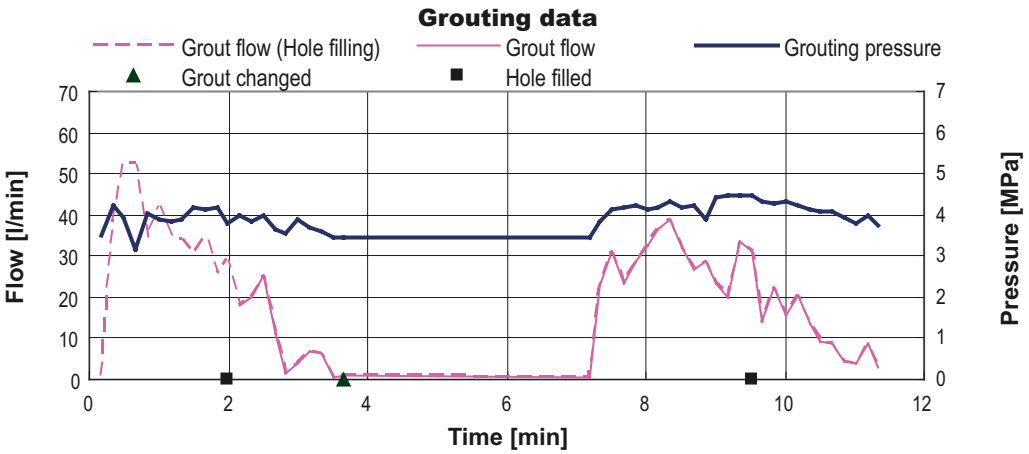

Figure E-19. *Grouting data on borehole B7 in Fan 1:1.*

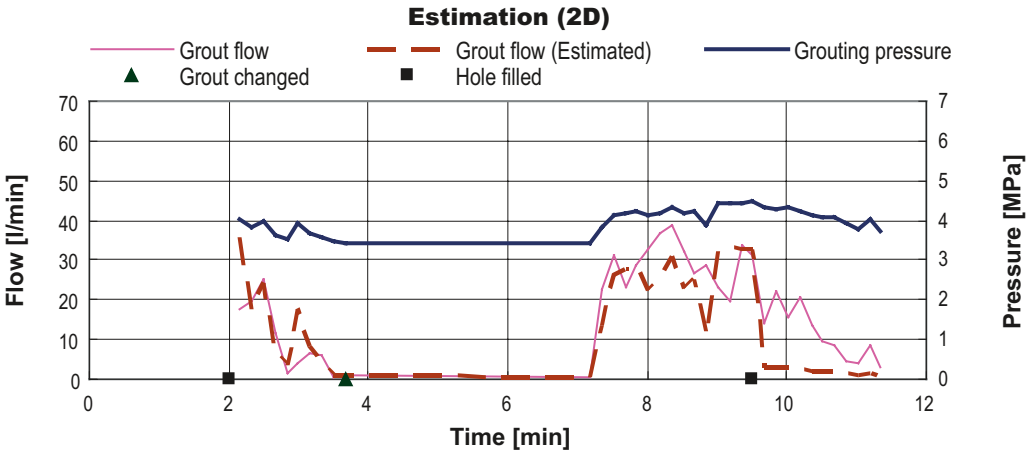

Figure E-20. *Estimated grout flow of borehole B7 in Fan 1:1 (time-independent grout properties).*

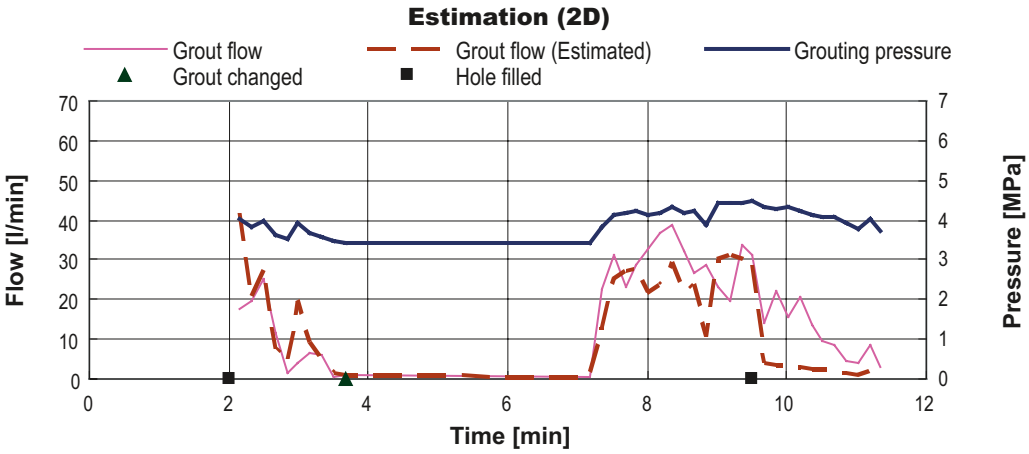

Figure E-21. *Estimated grout flow of borehole B7 in Fan 1:1 (time-dependent grout properties).*

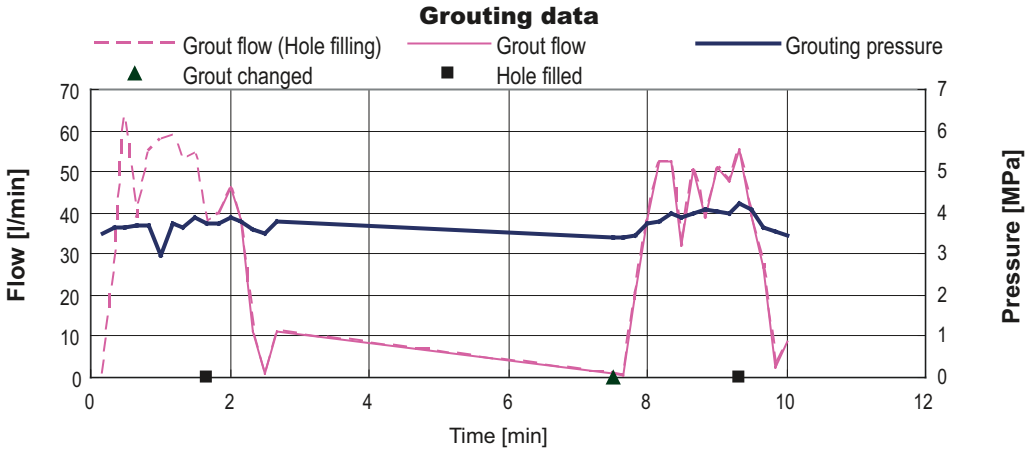

Figure E-22. *Grouting data on borehole B8 in Fan 1:1.*

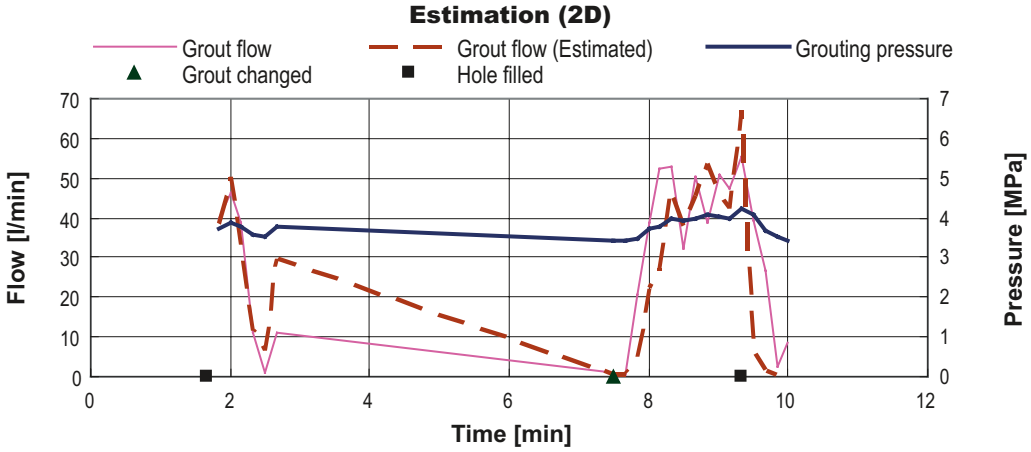

Figure E-23. *Estimated grout flow of borehole B8 in Fan 1:1 (time-independent grout properties).*

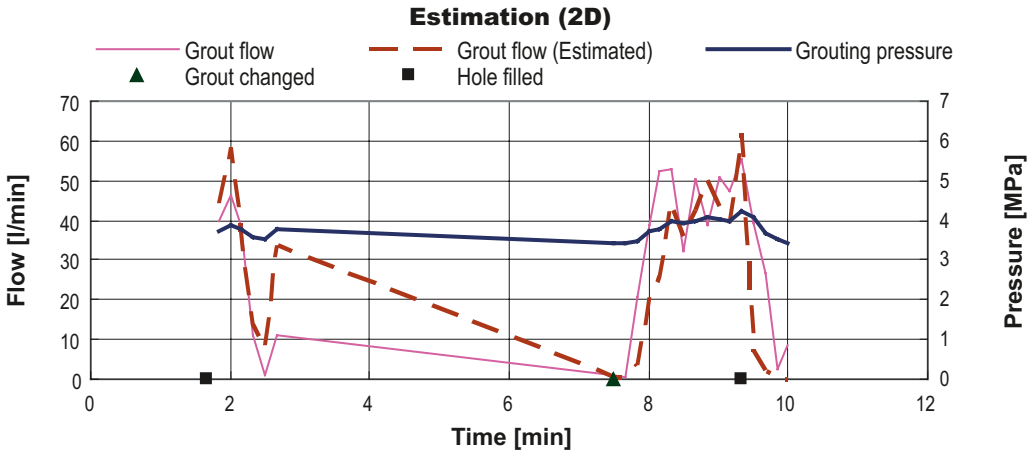

Figure E-24. *Estimated grout flow of borehole B8 in Fan 1:1 (time-dependent grout properties).*

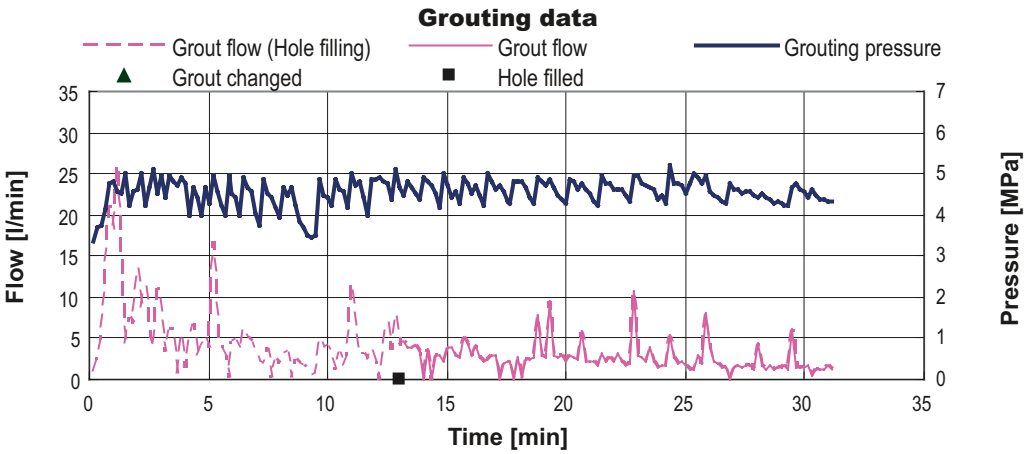

Figure E-25. *Grouting data on borehole G9 in Fan 1:1.*

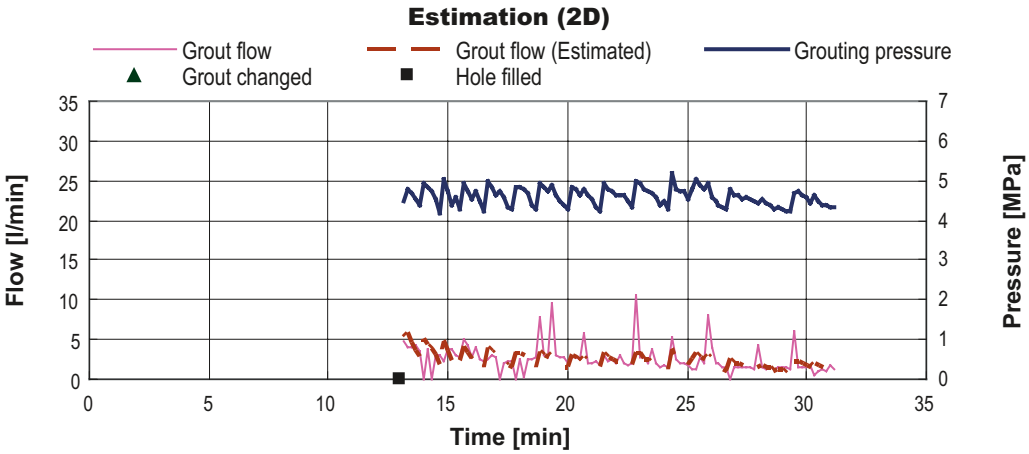

Figure E-26. *Estimated grout flow of borehole G9 in Fan 1:1 (time-independent grout properties).*

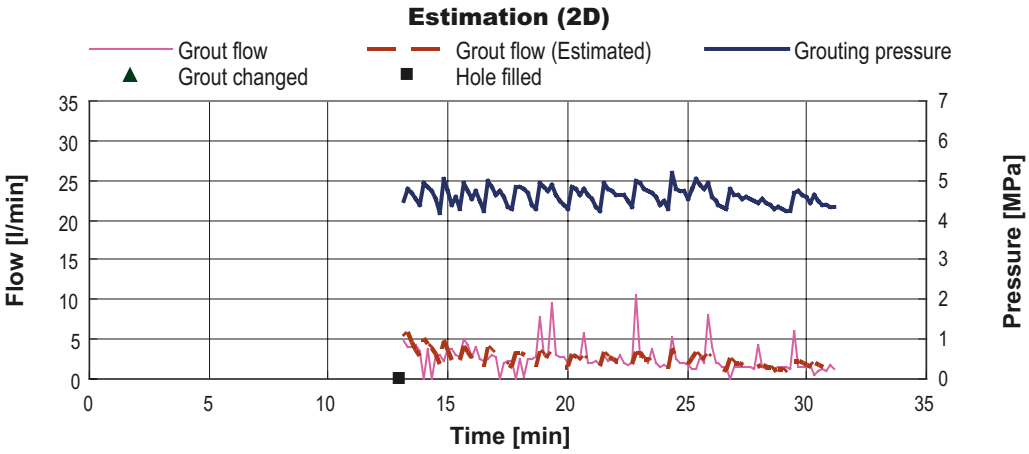

Figure E-27. *Estimated grout flow of borehole G9 in Fan 1:1 (time-dependent grout properties).*

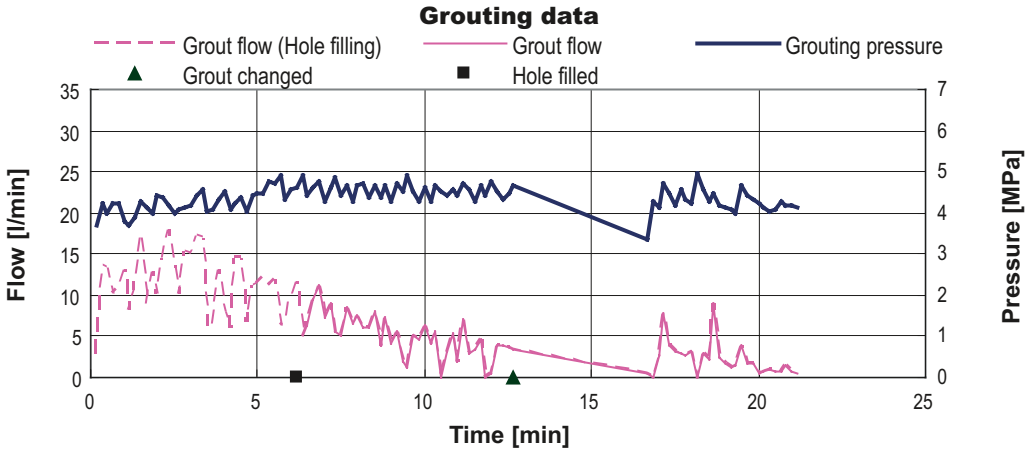

Figure E-28. *Grouting data on borehole G10 in Fan 1:1.*

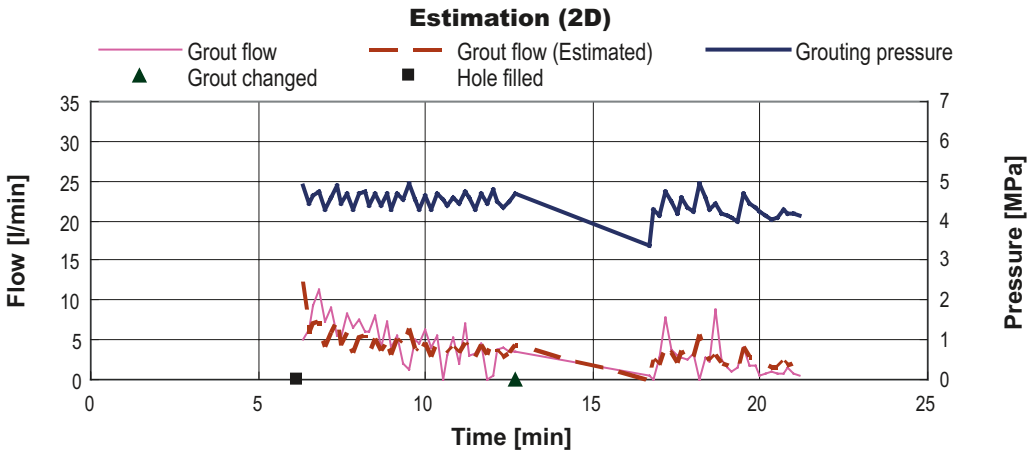

Figure E-29. *Estimated grout flow of borehole G10 in Fan 1:1 (time-independent grout properties).*

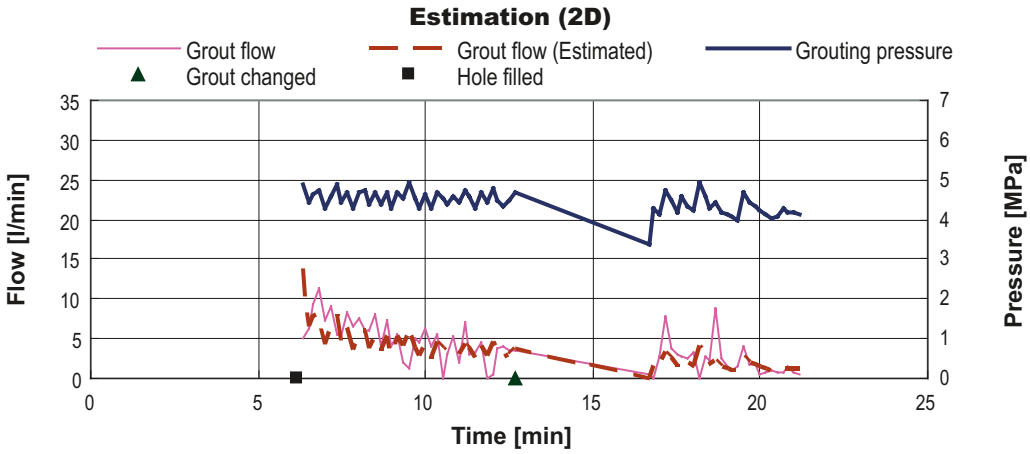

Figure E-30. *Estimated grout flow of borehole G10 in Fan 1:1 (time-dependent grout properties).*

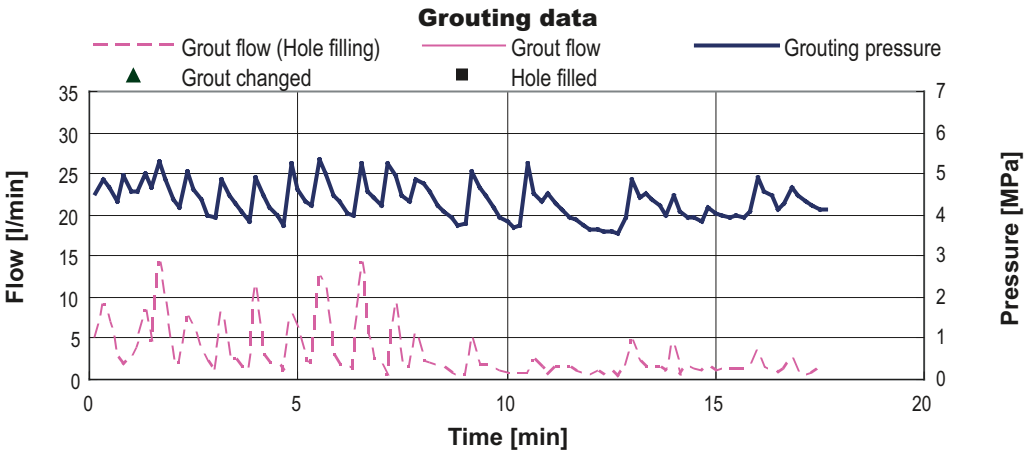

Figure E-31. *Grouting data on borehole G11 in Fan 1:1.*

Fan 1:2

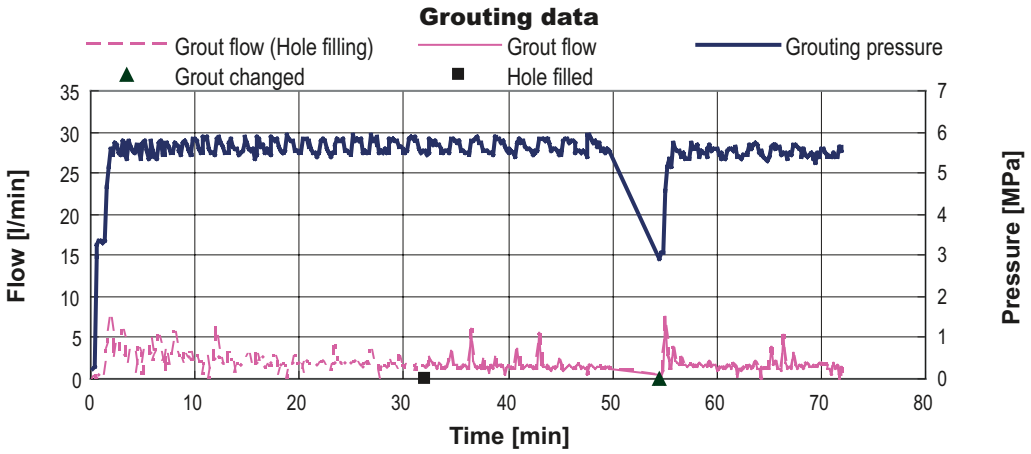

Figure E-32. *Grouting data on borehole A12 in Fan 1:2.*

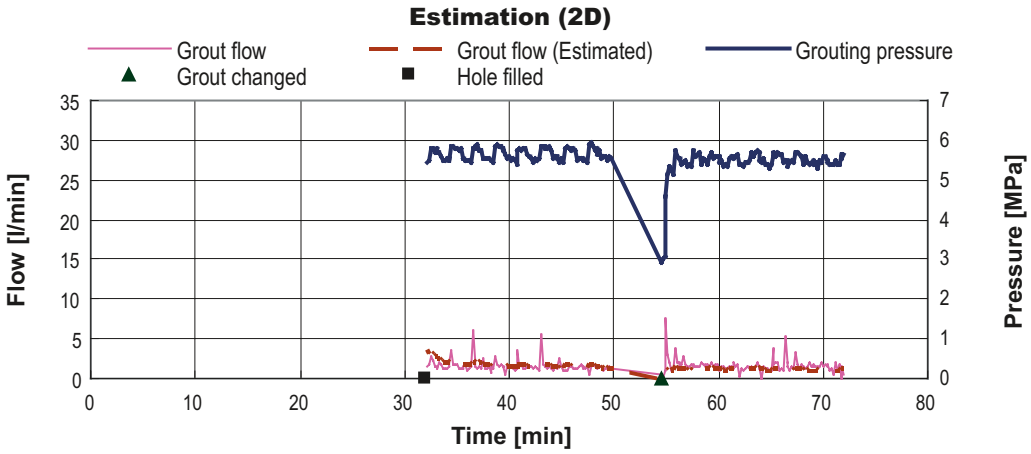

Figure E-33. *Estimated grout flow of borehole A12 in Fan 1:2 (time-independent grout properties).*

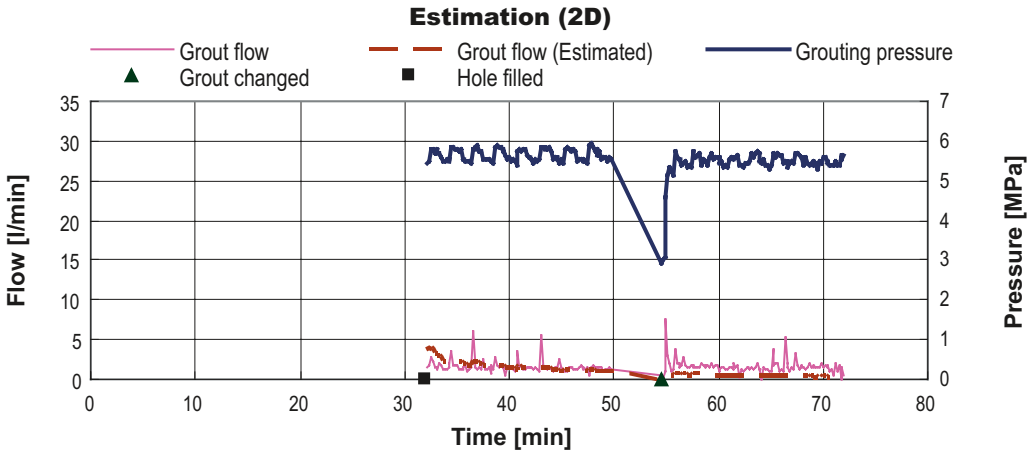

Figure E-34. *Estimated grout flow of borehole A12 in Fan1:2 (time-dependent grout properties).*

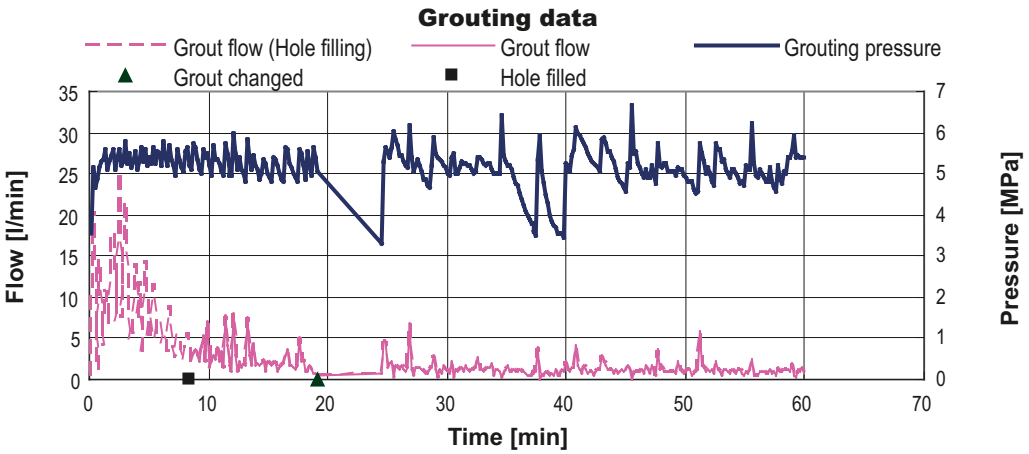

Figure E-35. *Grouting data on borehole A13 in Fan 1:2.*

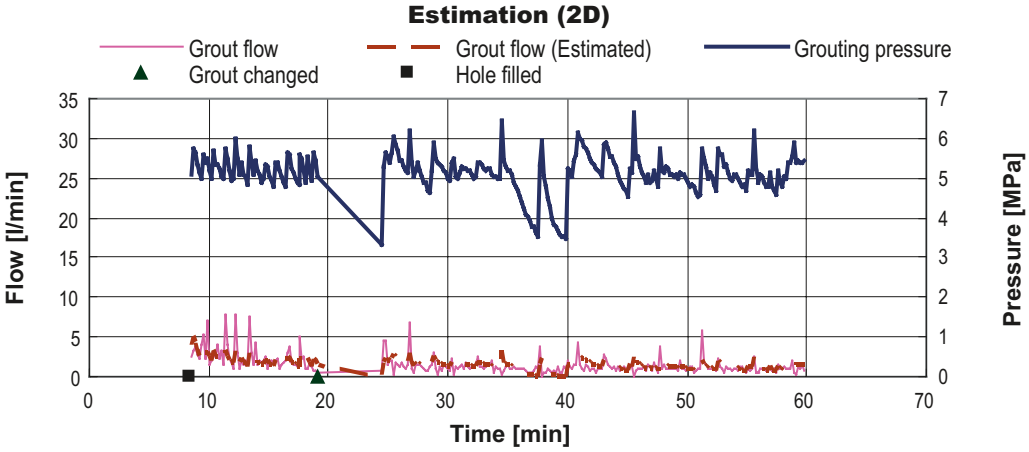

Figure E-36. *Estimated grout flow of borehole A13 in Fan 1:2 (time-independent grout properties).*

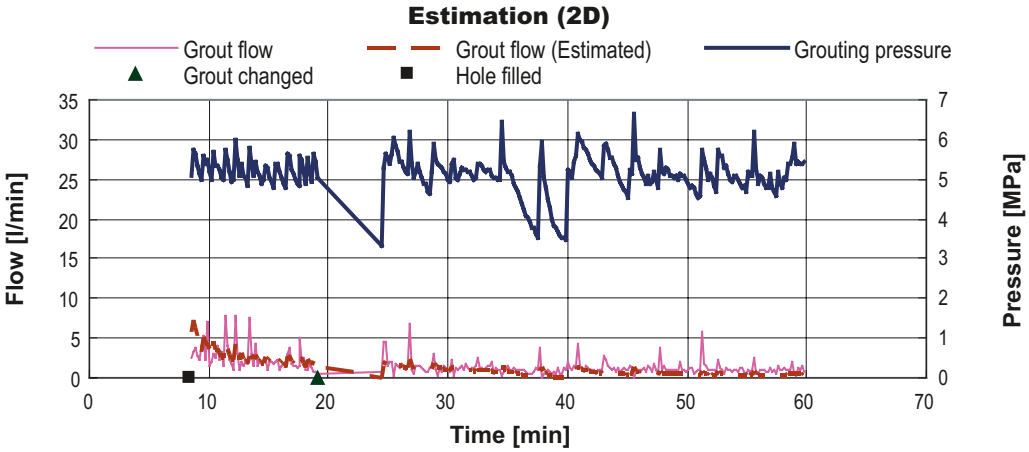

Figure E-37. *Estimated grout flow of borehole A13 in Fan1:2 (time-dependent grout properties).*

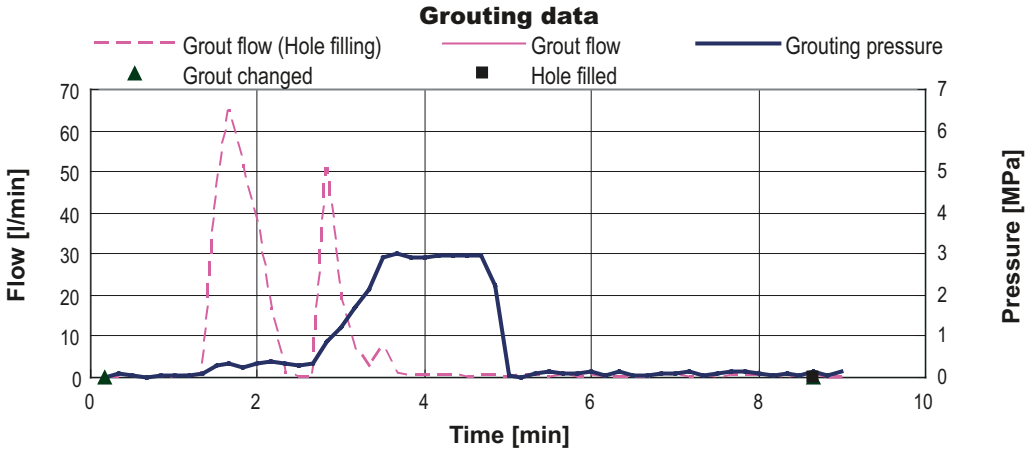

Figure E-38. *Grouting data on borehole A14 in Fan 1:2.*

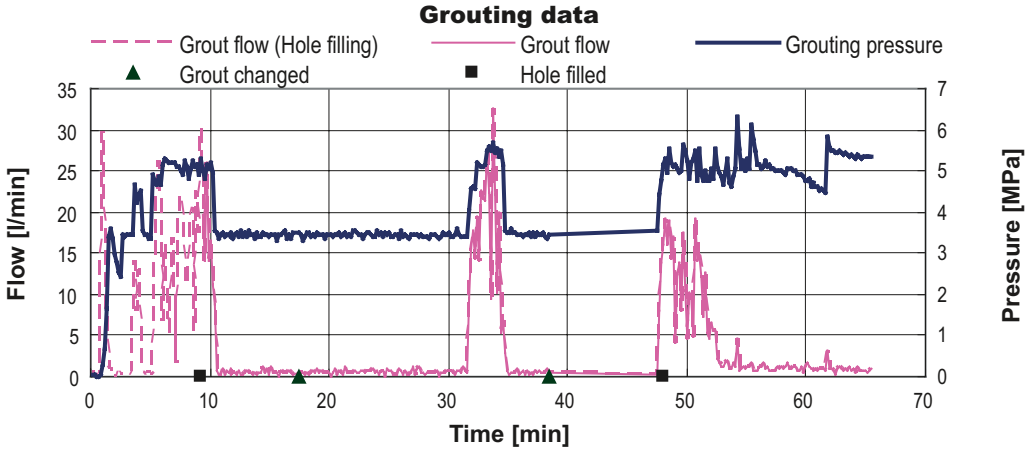

Figure E-39. *Grouting data on borehole C15 in Fan 1:2.*

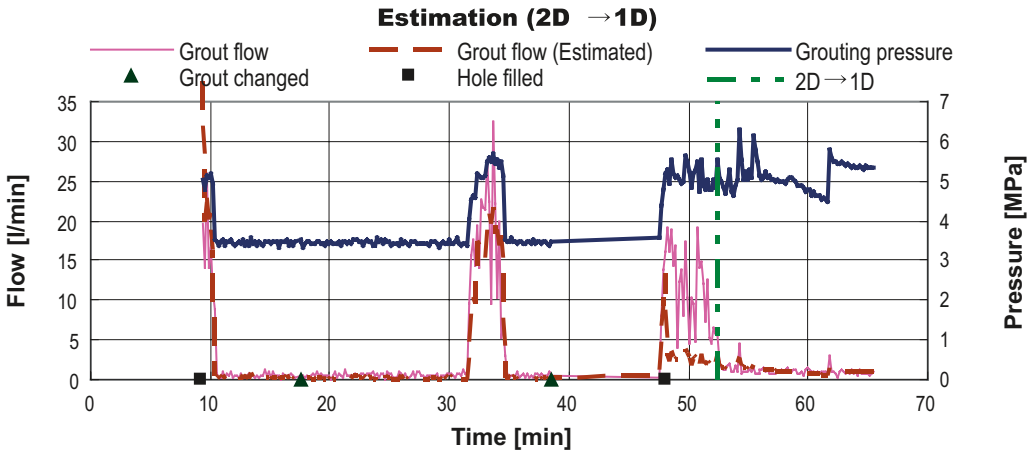

Figure E-40. *Estimated grout flow of borehole C15 in Fan 1:2 (time-independent grout properties).*

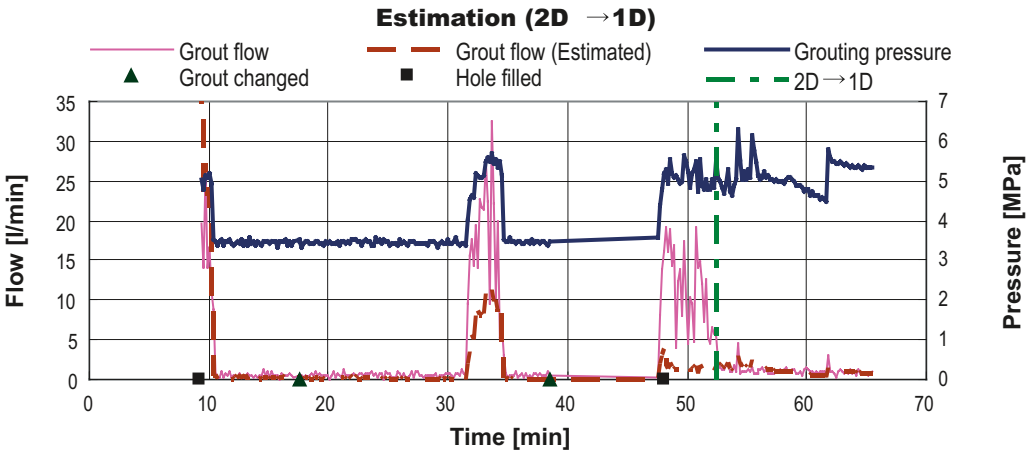

Figure E-41. *Estimated grout flow of borehole C15 in Fan1:2 (time-dependent grout properties).*

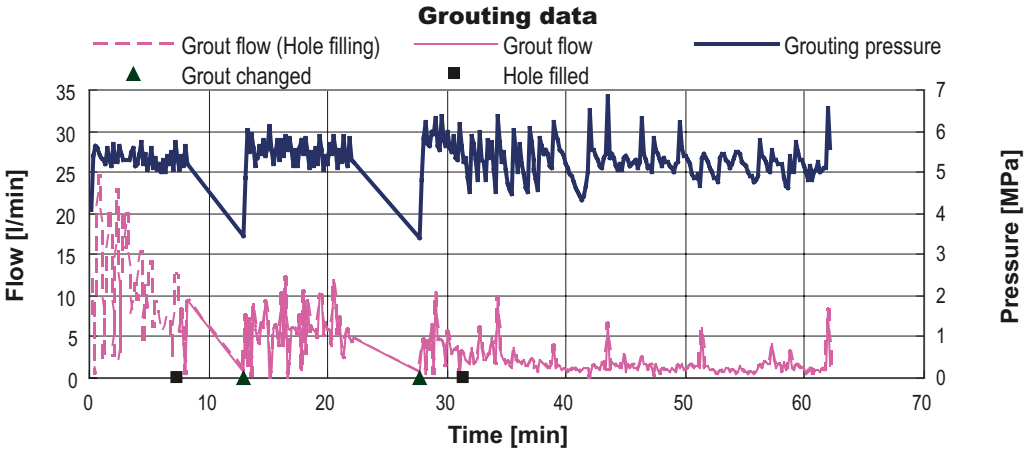

Figure E-42. *Grouting data on borehole C16 in Fan 1:2.*

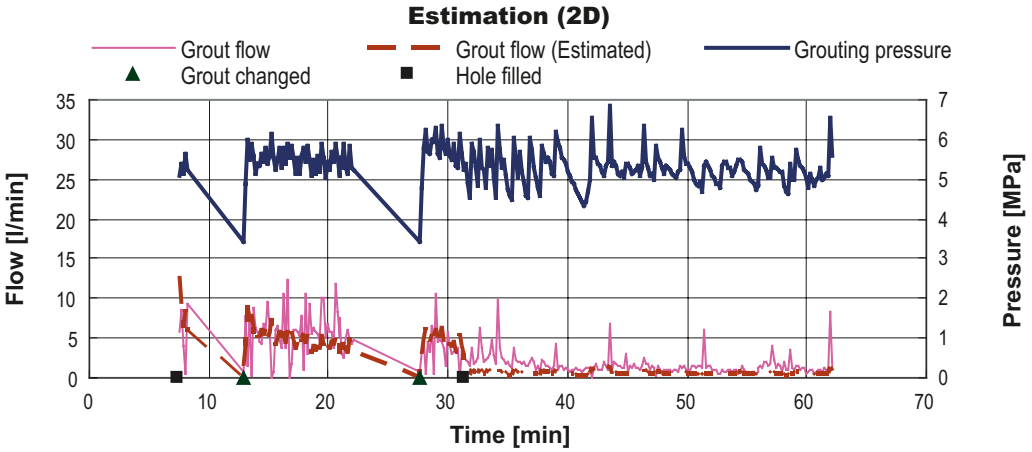

Figure E-43. *Estimated grout flow of borehole C16 in Fan 1:2 (time-independent grout properties).*

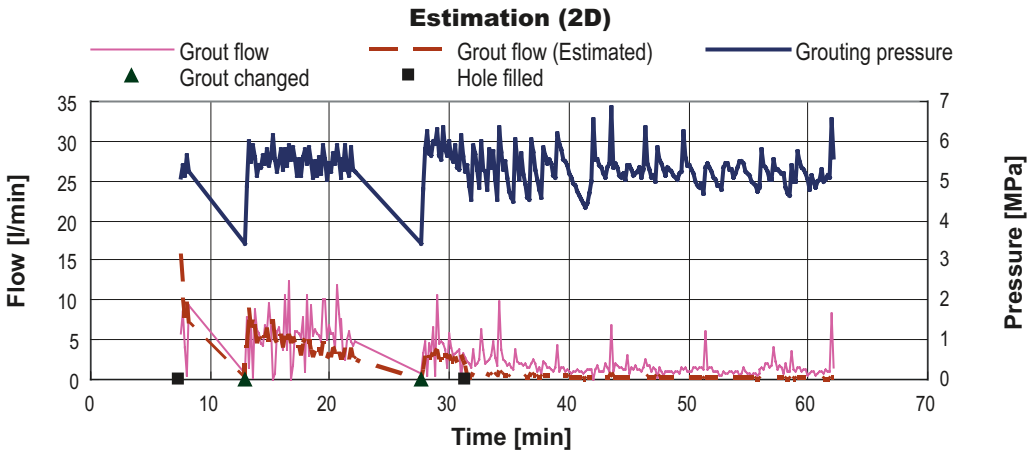

Figure E-44. *Estimated grout flow of borehole C16 in Fan1:2 (time-dependent grout properties).*

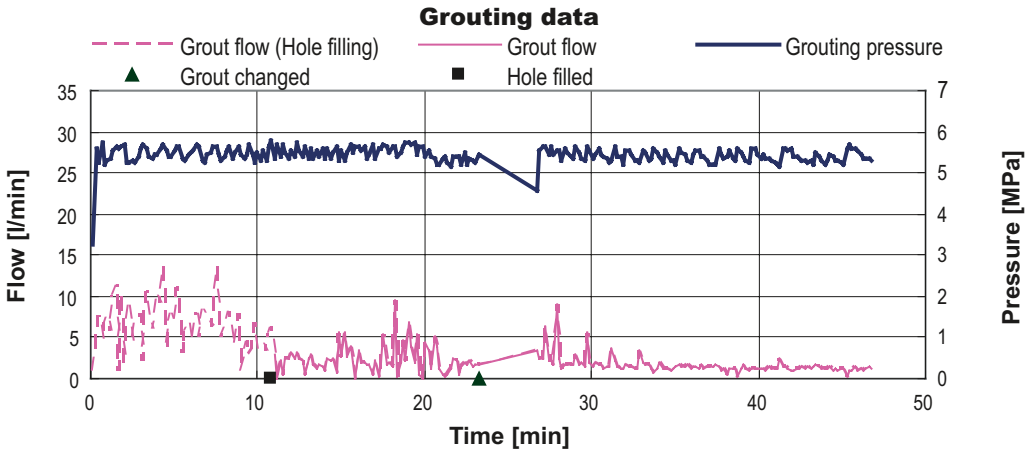

Figure E-45. *Grouting data on borehole H17 in Fan 1:2.*

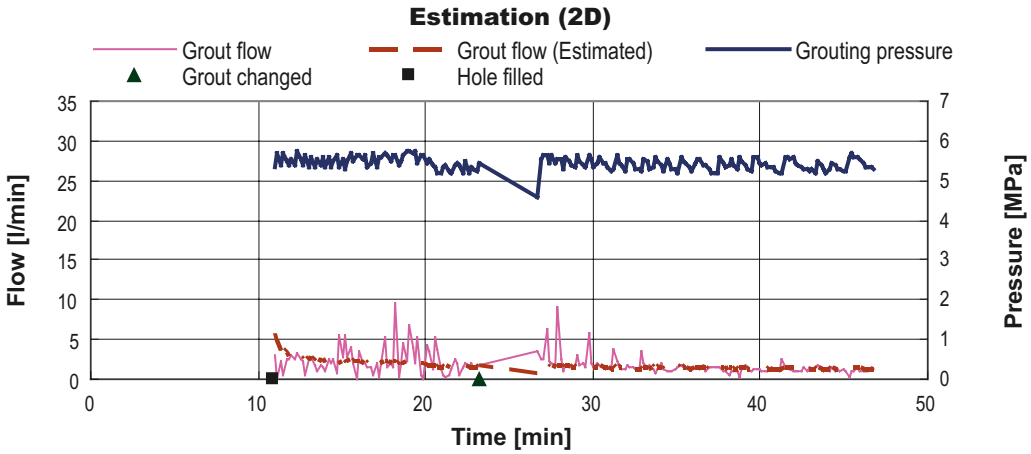

Figure E-46. *Estimated grout flow of borehole H17 in Fan 1:2 (time-independent grout properties).*

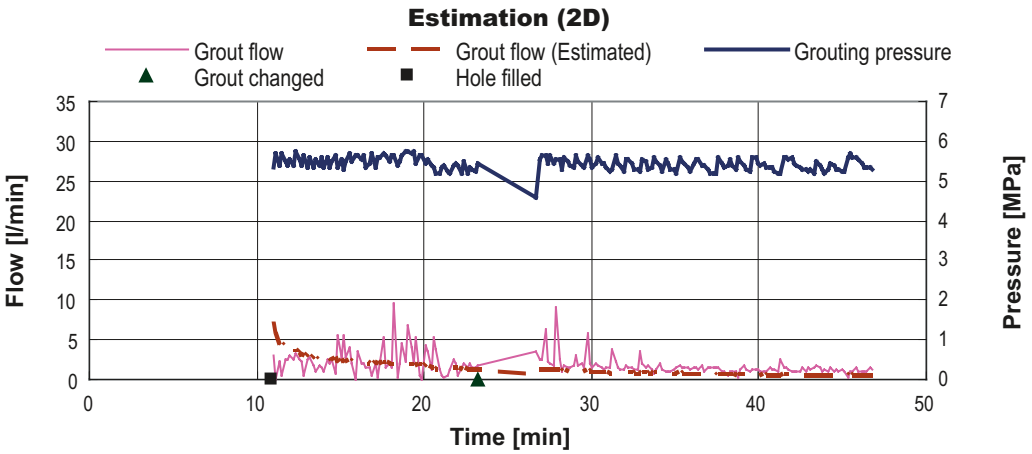

Figure E-47. *Estimated grout flow of borehole H17 in Fan1:2 (time-dependent grout properties).*

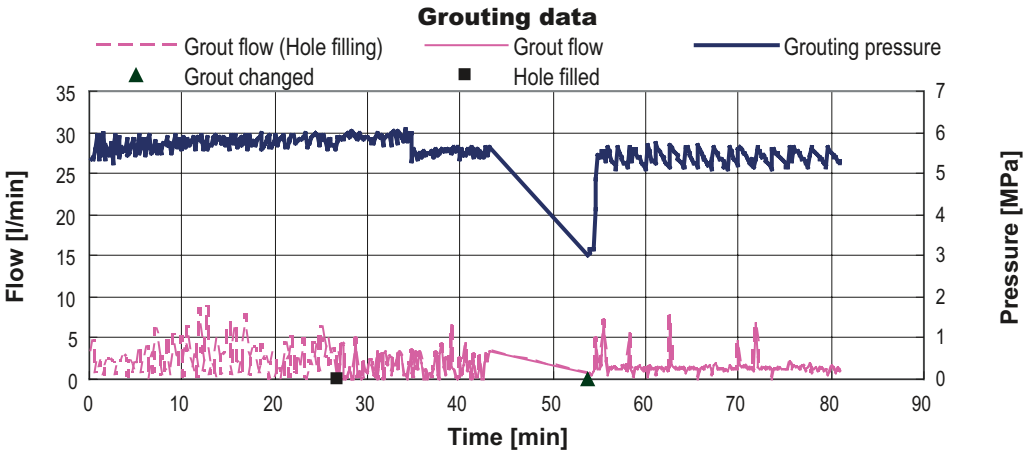

Figure E-48. *Grouting data on borehole H18 in Fan 1:2.*

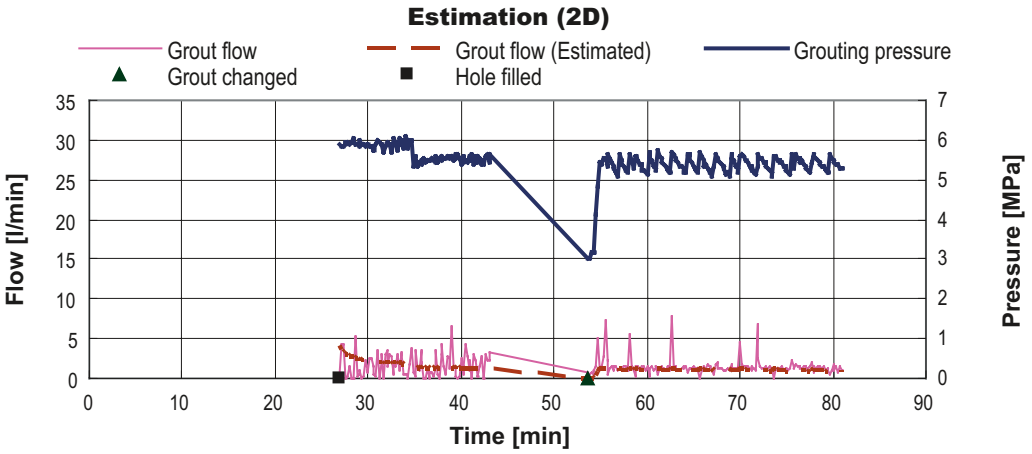

Figure E-49. *Estimated grout flow of borehole H18 in Fan 1:2 (time-independent grout properties).*

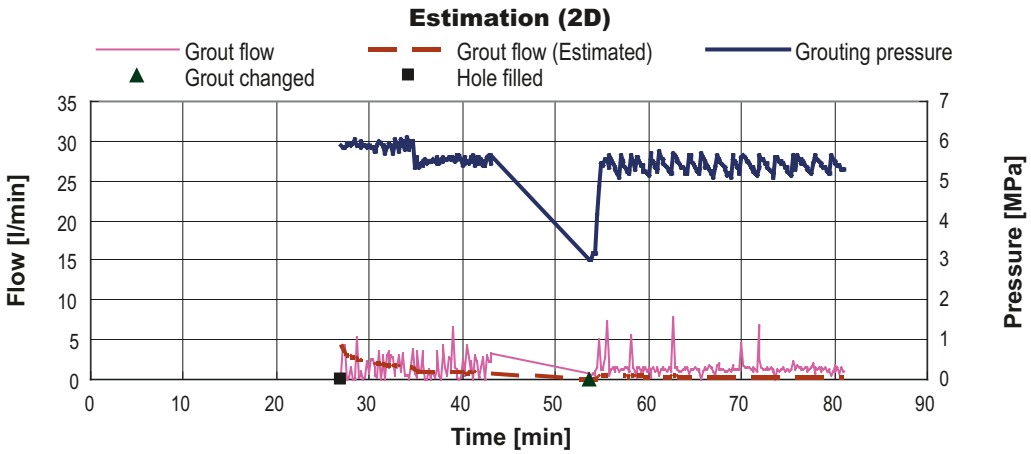

Figure E-50. *Estimated grout flow of borehole H18 in Fan1:2 (time-dependent grout properties).*

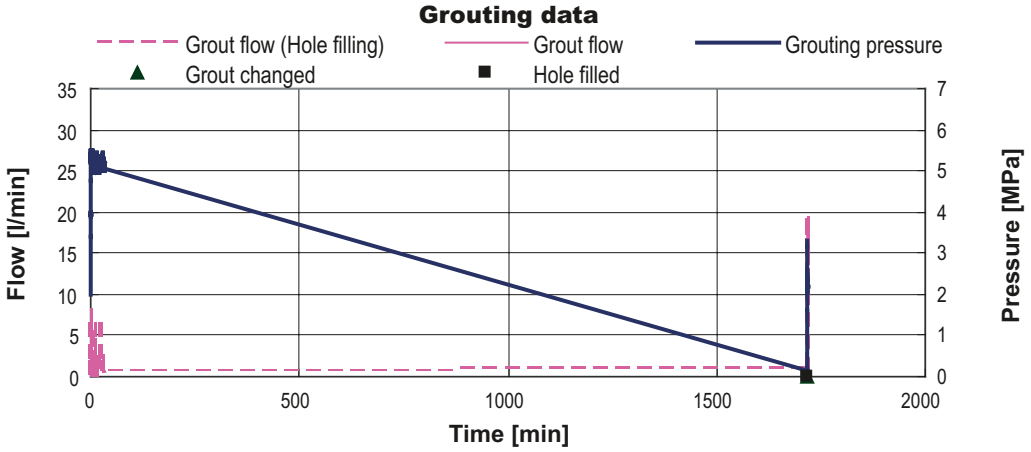

Figure E-51. *Grouting data on borehole I19 in Fan 1:2.*

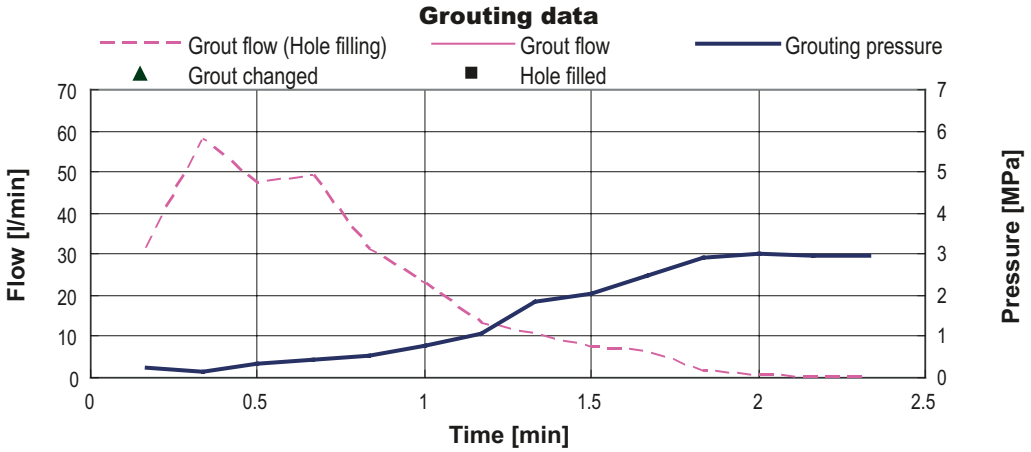

Figure E-52. *Grouting data on borehole I20 in Fan 1:2.*

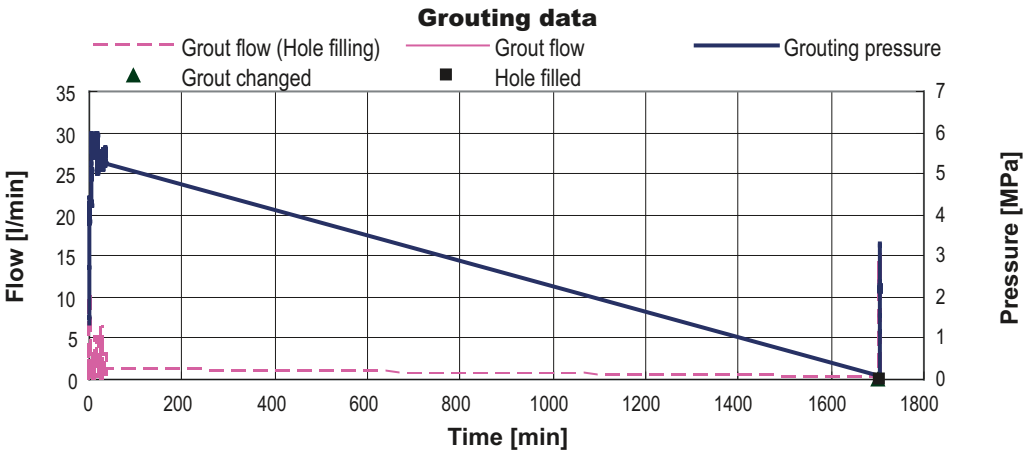

Figure E-53. *Grouting data on borehole D21 in Fan 1:2.*

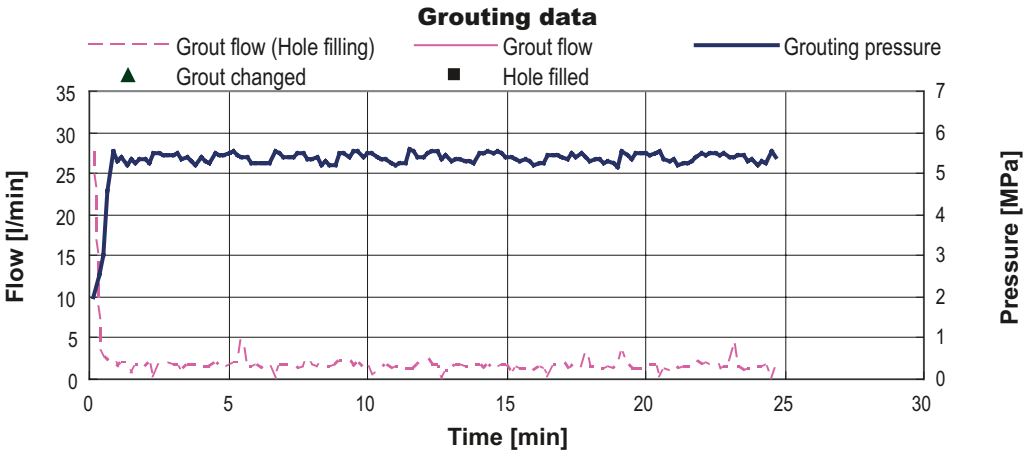

Figure E-54. *Grouting data on borehole D22 in Fan 1:2.*

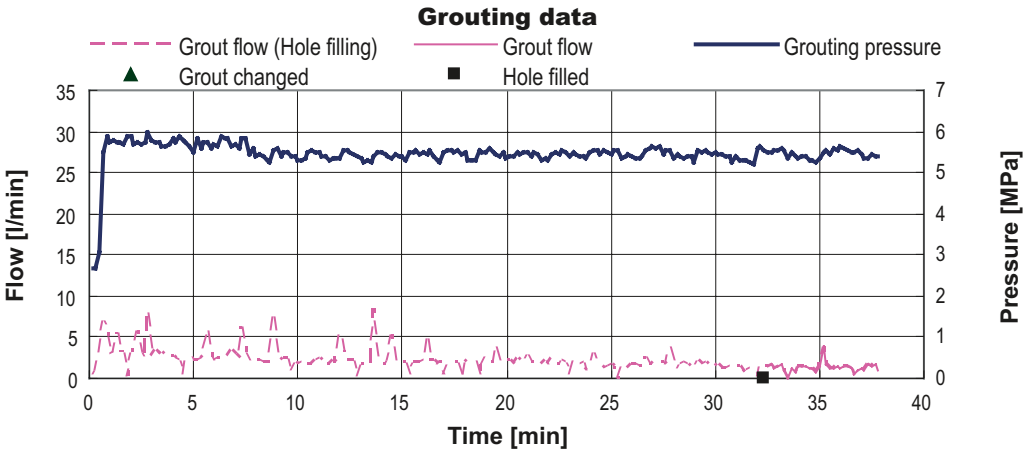

Figure E-55. *Grouting data on borehole B23 in Fan 1:2.*

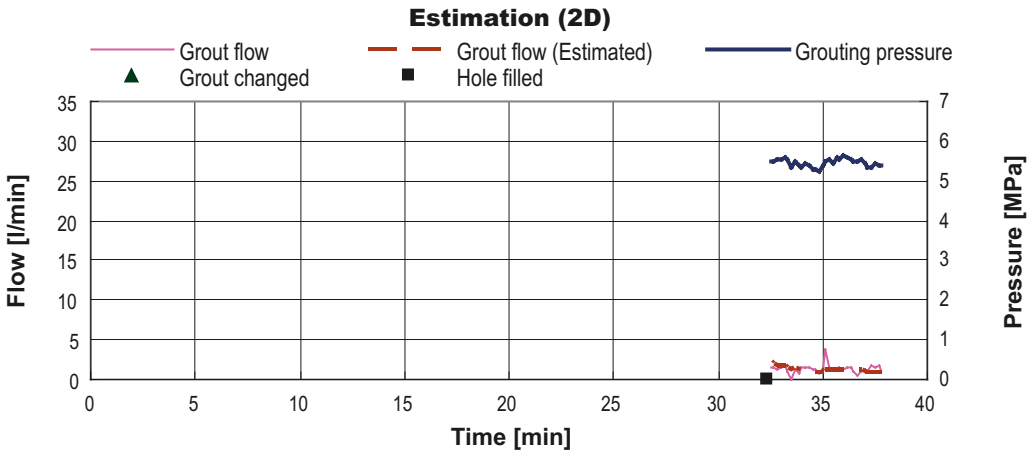

Figure E-56. *Estimated grout flow of borehole B23 in Fan 1:2 (time-independent grout properties).*

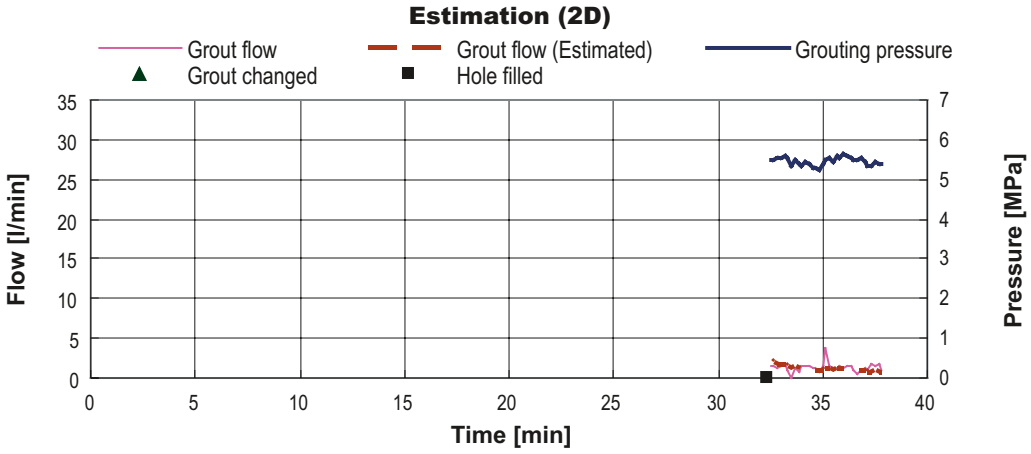

Figure E-57. *Estimated grout flow of borehole B23 in Fan1:2 (time-dependent grout properties).*

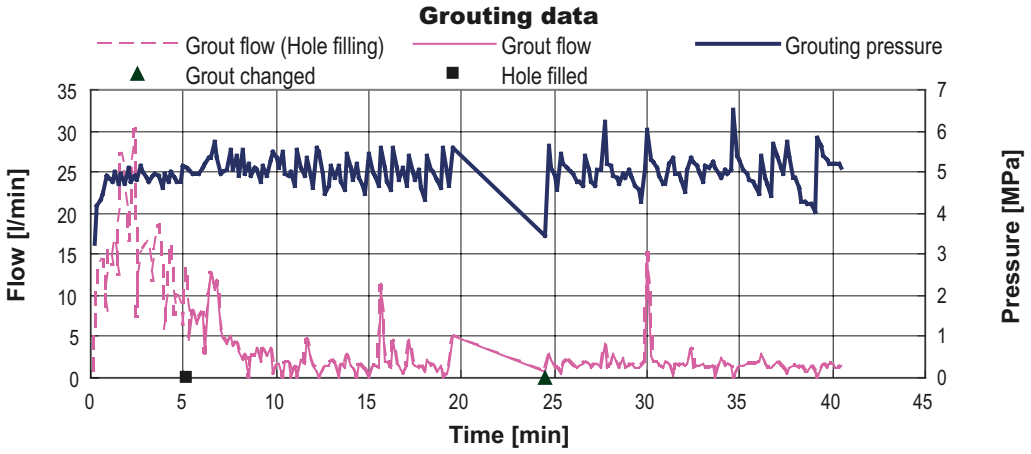

Figure E-58. *Grouting data on borehole B24 in Fan 1:2.*

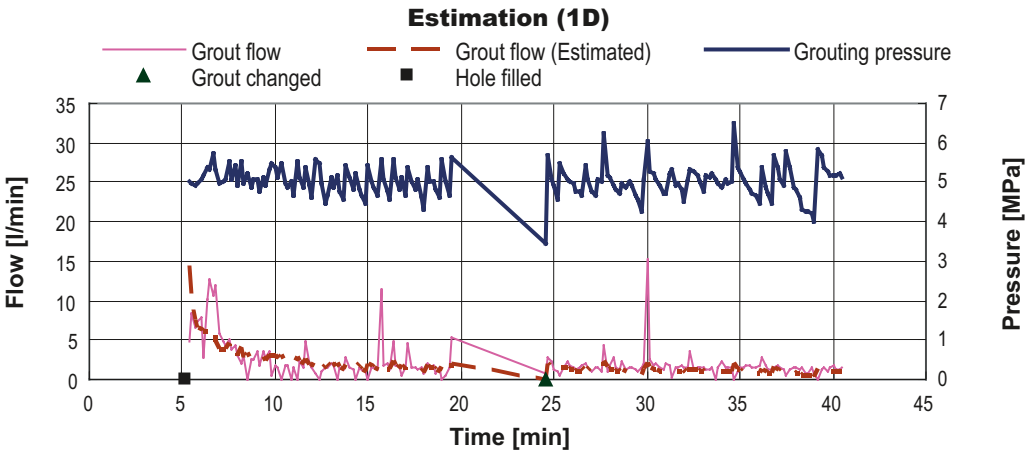

Figure E-59. *Estimated grout flow of borehole B24 in Fan 1:2 (time-independent grout properties).*

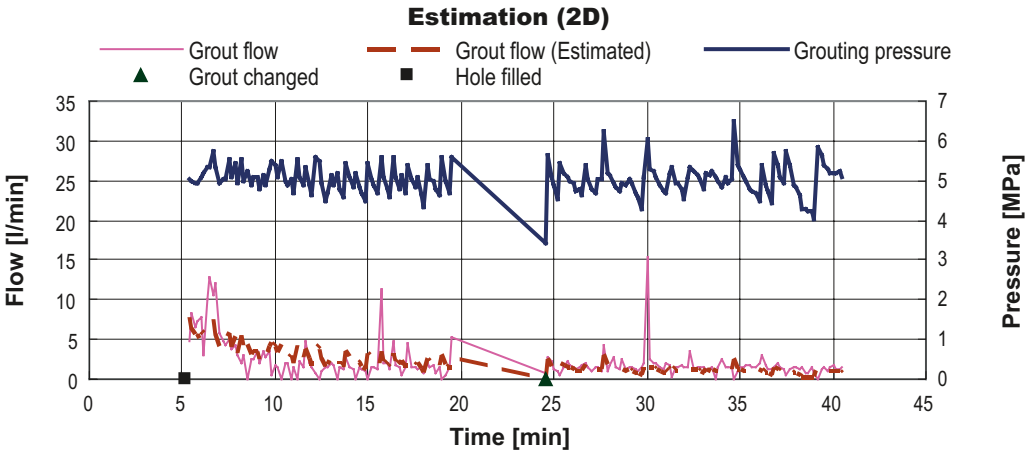

Figure E-60. *Estimated grout flow of borehole B24 in Fan1:2 (time-dependent grout properties).*

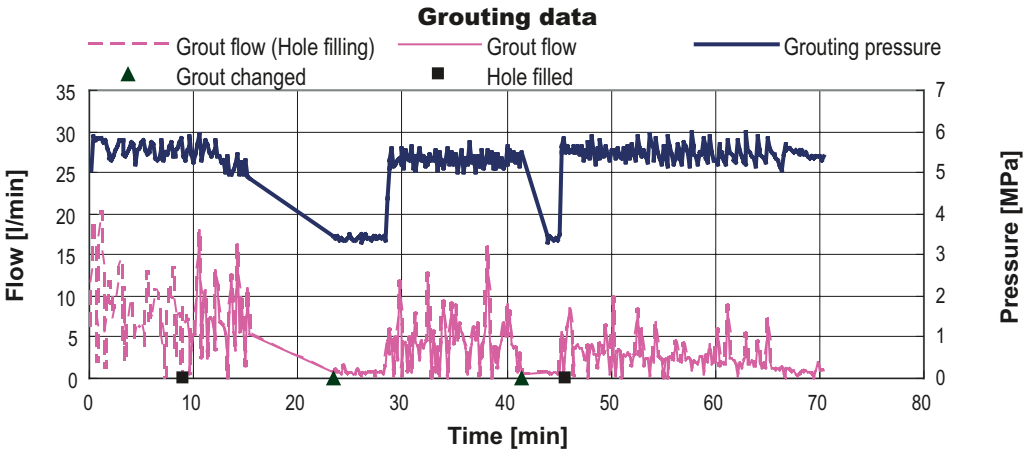

Figure E-61. *Grouting data on borehole B25 in Fan 1:2.*

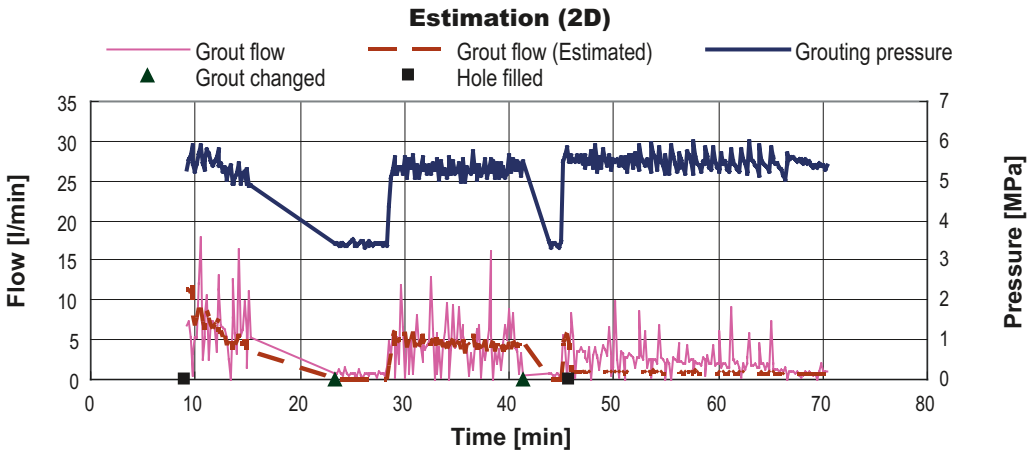

Figure E-62. *Estimated grout flow of borehole B25 in Fan 1:2 (time-independent grout properties).*

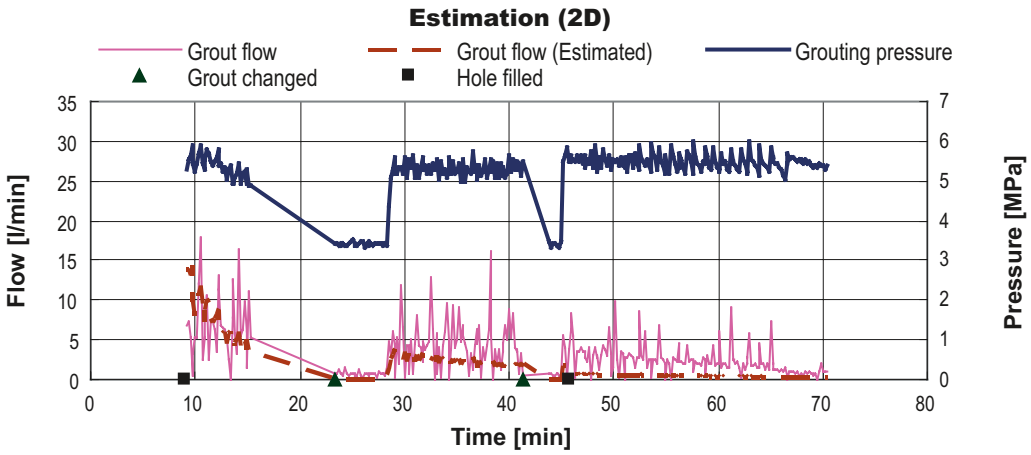

Figure E-63. *Estimated grout flow of borehole B25 in Fan1:2 (time-dependent grout properties).*

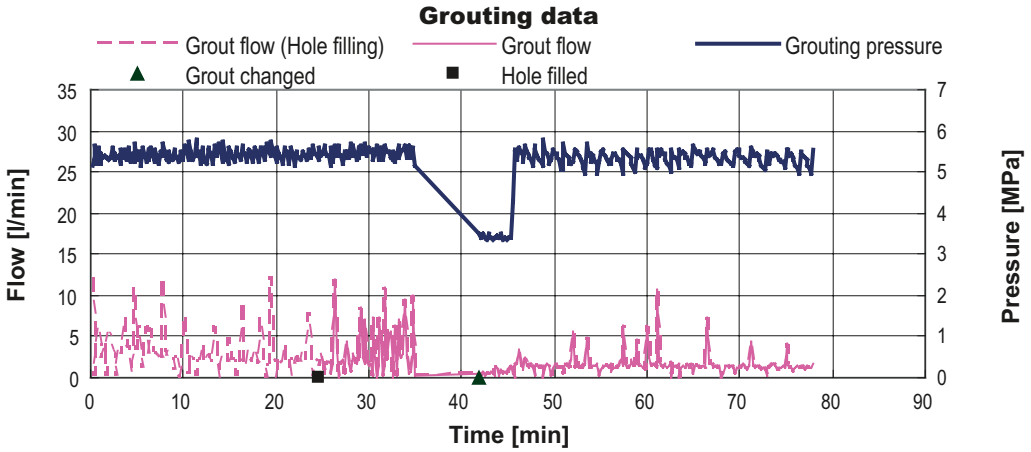

Figure E-64. *Grouting data on borehole G26 in Fan 1:2.*

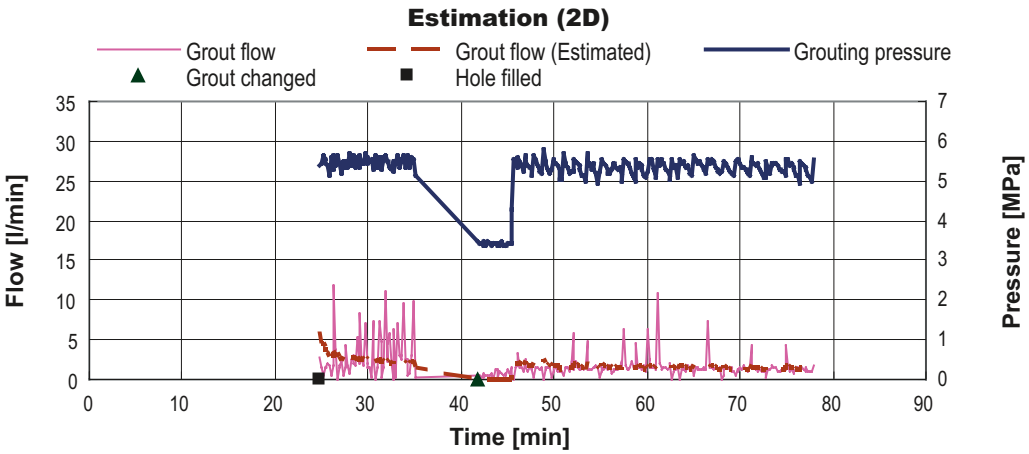

Figure E-65. *Estimated grout flow of borehole G26 in Fan 1:2 (time-independent grout properties).*

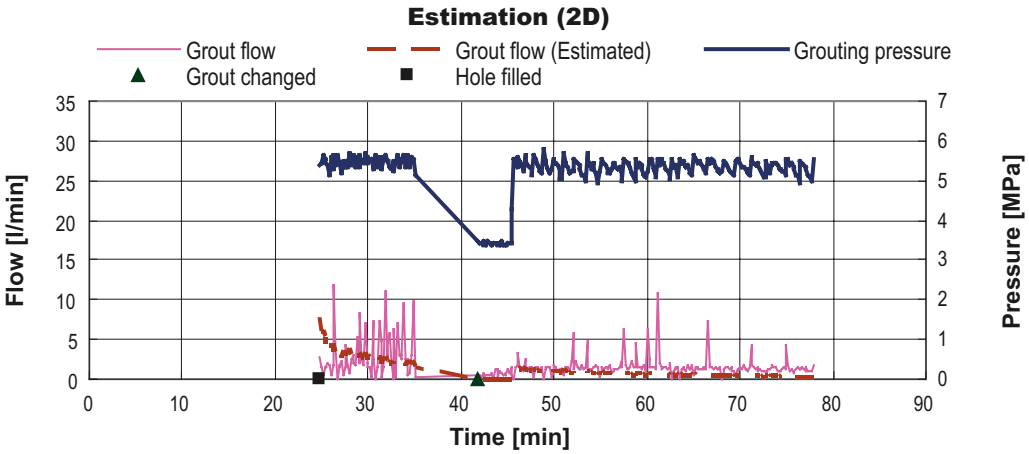

Figure E-66. *Estimated grout flow of borehole G26 in Fan1:2 (time-dependent grout properties).*

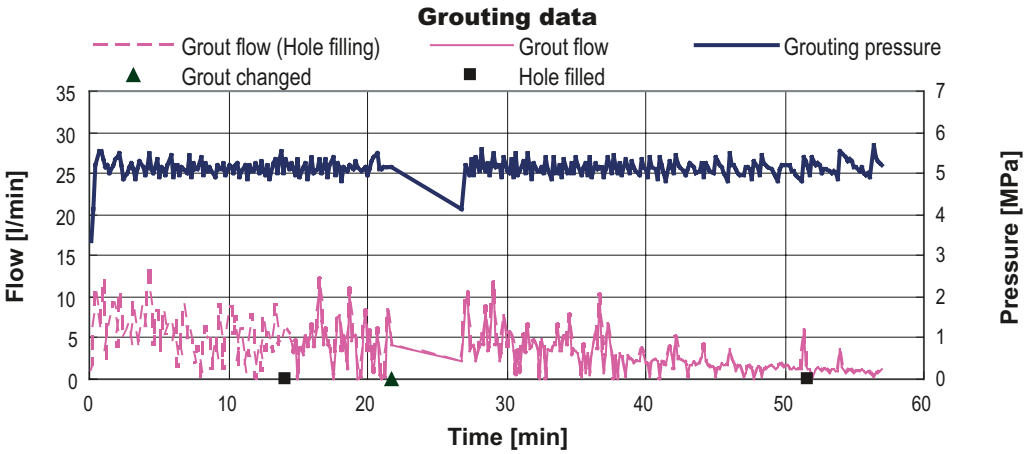

Figure E-67. *Grouting data on borehole G27 in Fan 1:2.*

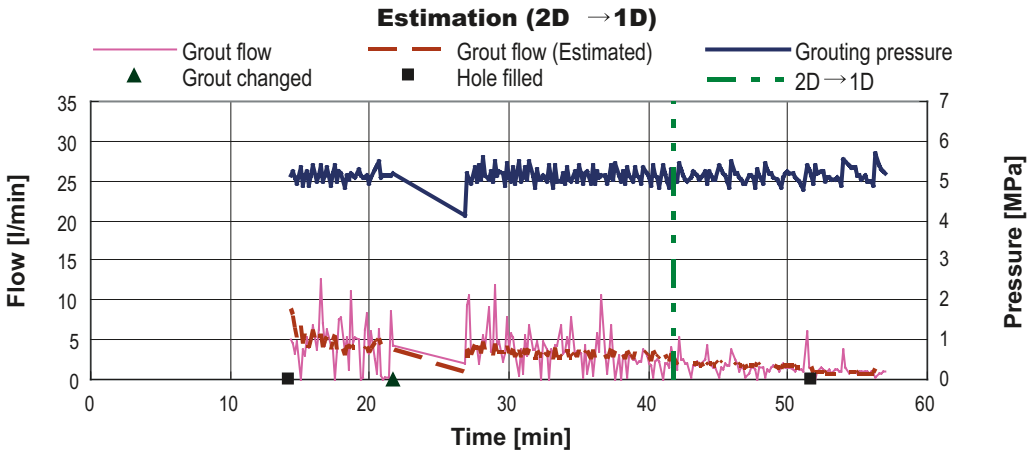

Figure E-68. *Estimated grout flow of borehole G27 in Fan 1:2 (time-independent grout properties).*

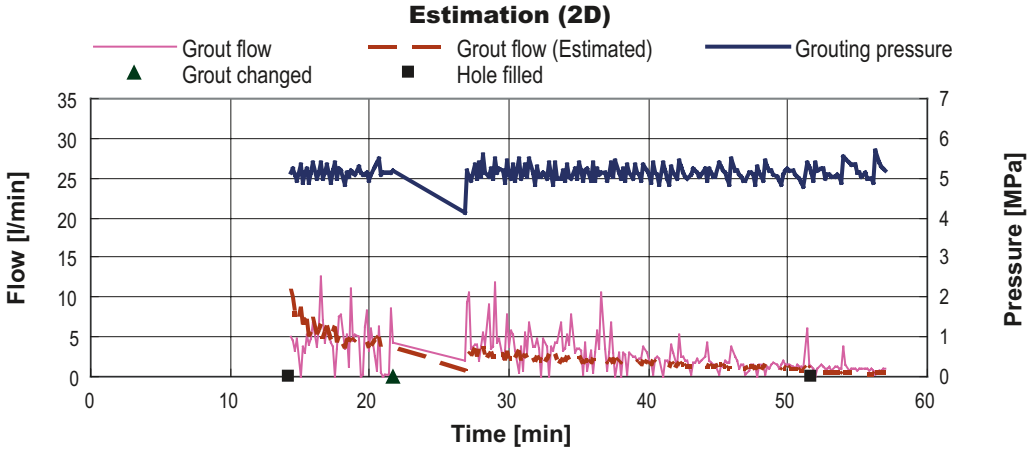

Figure E-69. *Estimated grout flow of borehole G27 in Fan1:2 (time-dependent grout properties).*

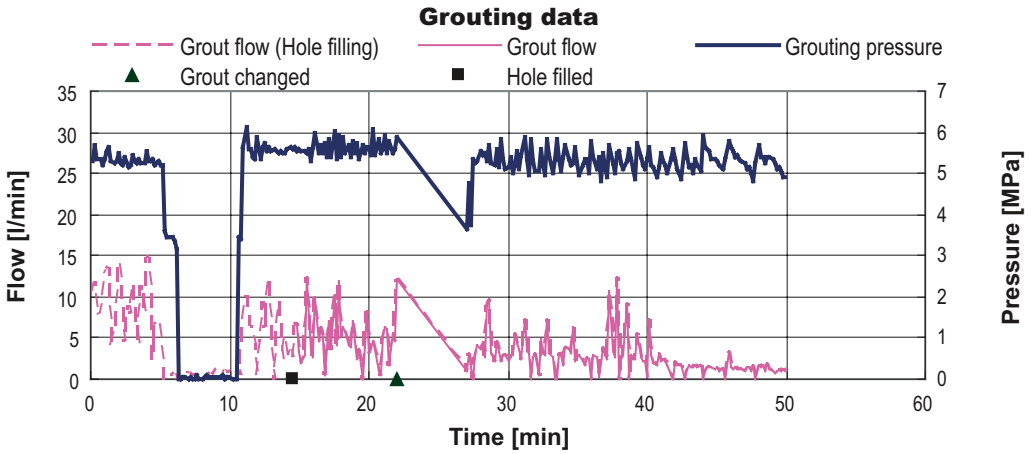

Figure E-70. *Grouting data on borehole G28 in Fan 1:2.*

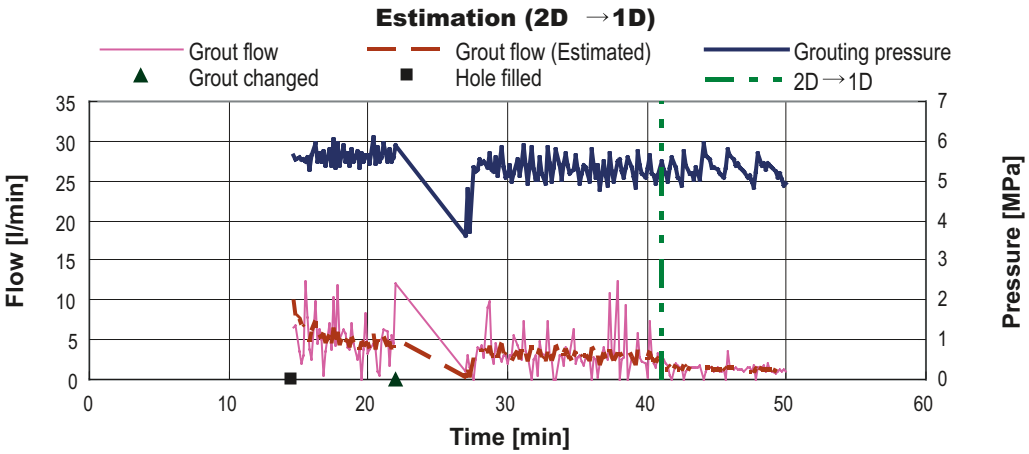

Figure E-71. *Estimated grout flow of borehole G28 in Fan 1:2 (time-independent grout properties).*

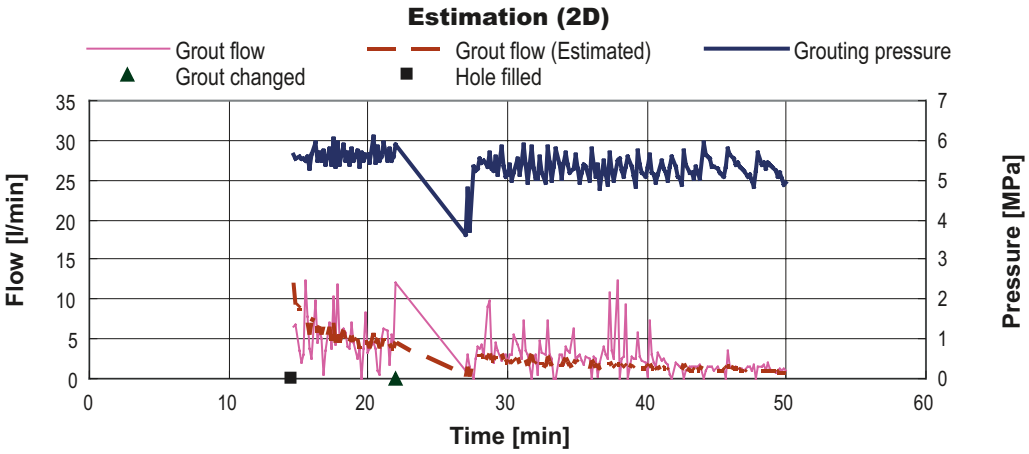

Figure E-72. *Estimated grout flow of borehole G28 in Fan1:2 (time-dependent grout properties).*

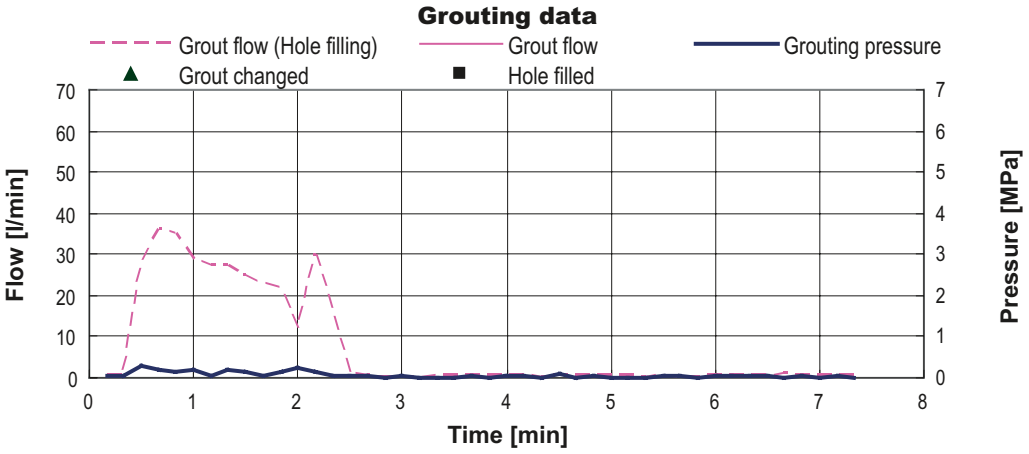

Figure E-73. *Grouting data on borehole G29 in Fan 1:2.*

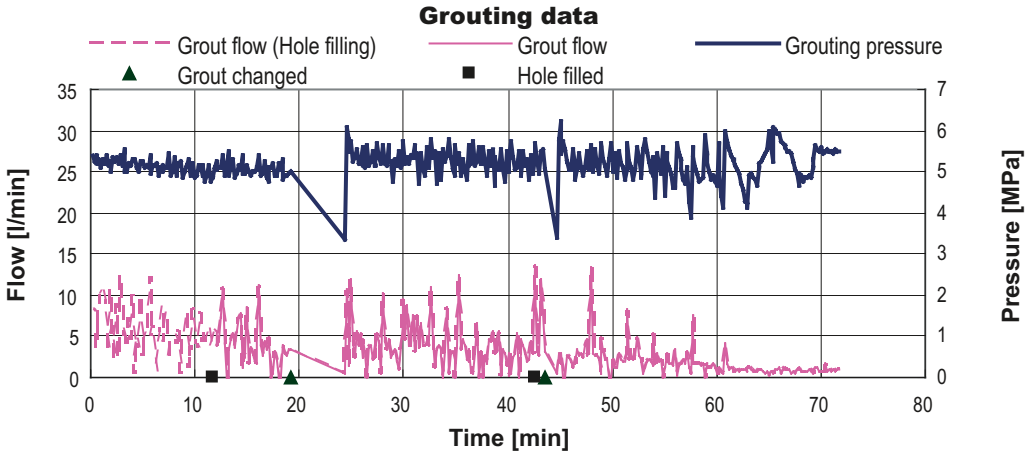

Figure E-74. *Grouting data on borehole G30 in Fan 1:2.*

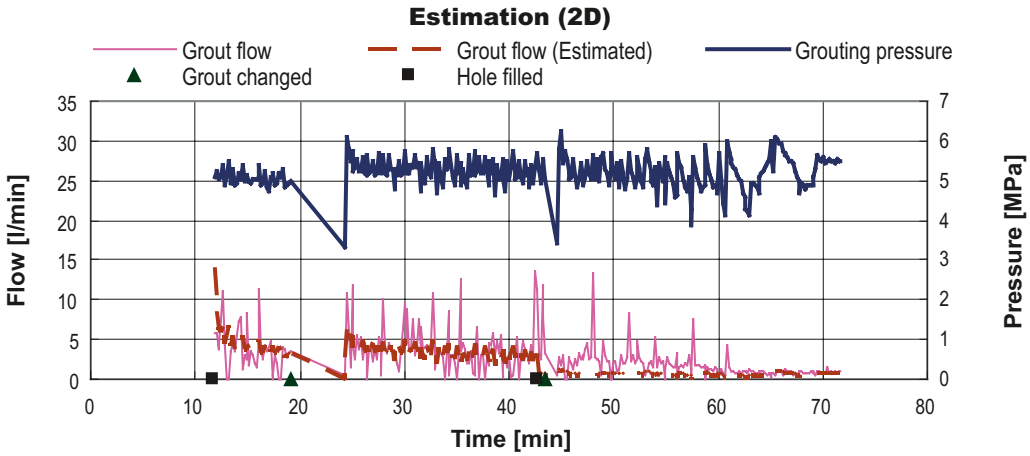

Figure E-75. *Estimated grout flow of borehole G30 in Fan 1:2 (time-independent grout properties).*

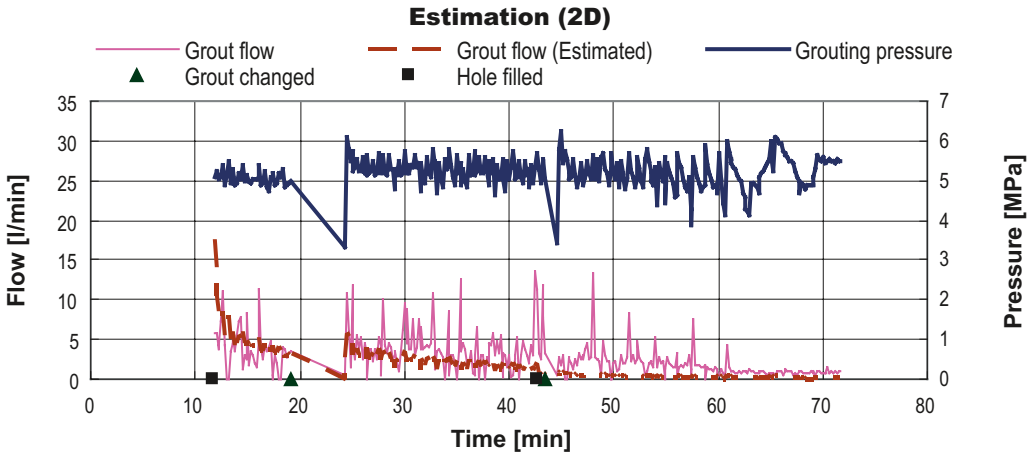

Figure E-76. *Estimated grout flow of borehole G30 in Fan1:2 (time-dependent grout properties).*

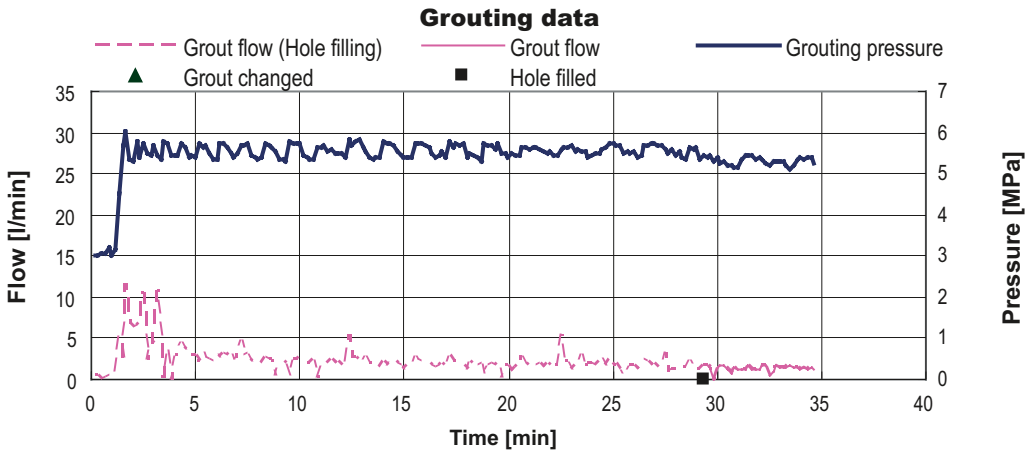

Figure E-77. *Grouting data on borehole G31 in Fan 1:2.*

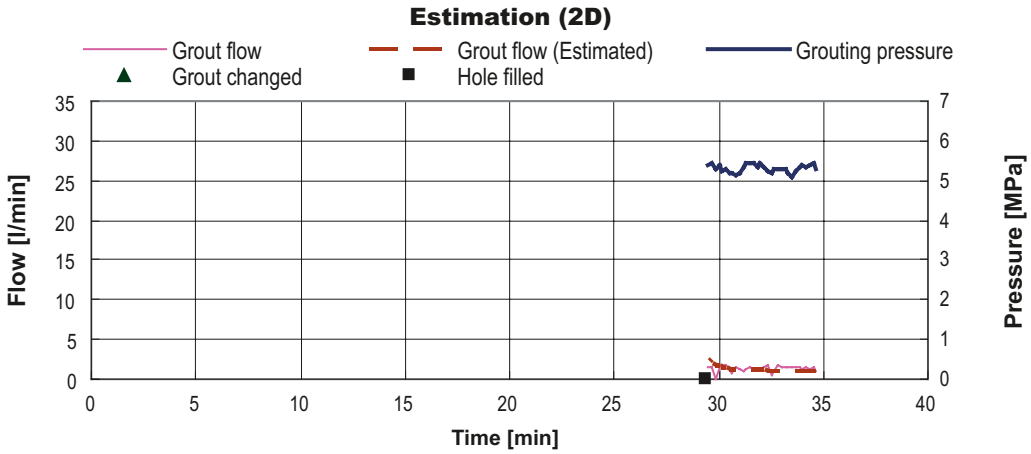

Figure E-78. *Estimated grout flow of borehole G31 in Fan 1:2 (time-independent grout properties).*

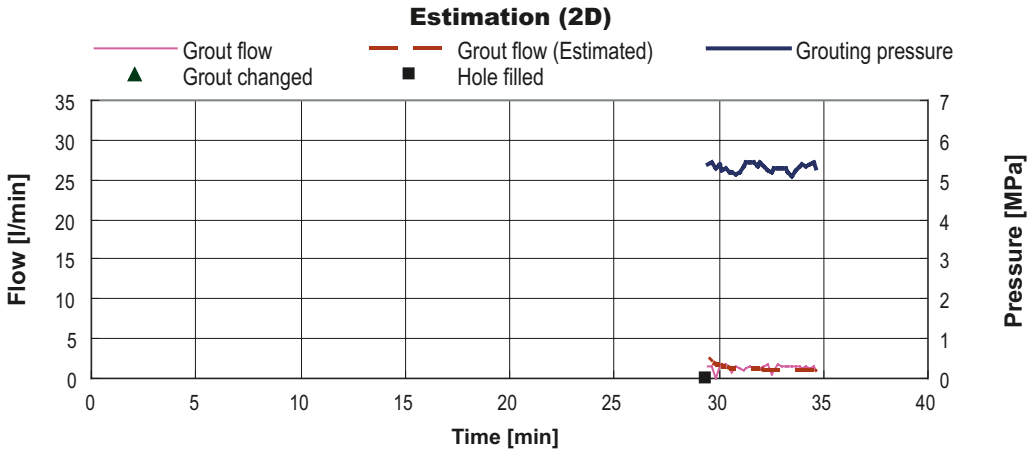

Figure E-79. *Estimated grout flow of borehole G31 in Fan1:2 (time-dependent grout properties).*

Appendix F

Inflow during drilling and estimated hydraulic apertures

Table F-1. Calculated penetration length in Fan1:1 (time-dependent grout properties).

Hole number/ Section	Penetration Length [m] 0–4.6 m	4.6–7.6 m	7.6–10.6 m	10.6–13.6 m	13.6–15.6 m
A1	0.0	0.0	5.1	9.6	7.0
A2	0.0	1.1	0.0	5.4	2.5
C3	0.0	0.0	9.8	9.2	0.0
H4	0.0	0.0	0.0	4.2	10.2
I5	0.0	0.0	7.8	0.0	0.0
D6	0.0	0.0	0.0	0.0	9.8
B7	0.0	0.0	4.1	3.9	8.9
B8	0.0	0.0	0.0	5.2	7.5
G9	0.0	0.0	3.0	3.0	6.2
G10	0.0	0.0	5.4	0.0	7.7
G11	0.0	0.0	0.0	0.0	0.0

Table F-2. Calculated penetration length in Fan1:1 (time-dependent grout properties).

Hole number/ Section	Penetration Length [m] 0–4.6 m	4.6–7.6 m	7.6–10.6 m	10.6–13.6 m	13.6–15.6 m
A12	0.0	0.0	0.0	0.0	13.6
A13	0.0	0.0	7.7	13.7	9.6
A14	0.0	0.0	0.0	0.0	0.0
C15	0.0	0.0	0.0	0.0	0.0
C16	0.0	0.0	0.0	19.2	0.0
H17	0.0	0.0	0.0	15.0	0.0
H18	0.0	0.0	0.0	11.9	13.1
I19	0.0	0.0	0.0	0.0	0.0
I20	0.0	0.0	0.0	0.0	0.0
D21	0.0	0.0	0.0	0.0	0.0
D22	0.0	0.0	0.0	0.0	0.0
B23	0.0	0.0	0.0	0.0	0.0
B24	0.0	7.2	0.0	0.0	14.2
B25	0.0	0.0	0.0	18.9	14.0
G26	0.0	0.0	0.0	10.9	13.7
G27	17.2	0.0	0.0	0.0	0.0
G28	16.4	0.0	0.0	0.0	0.0
G29	0.0	0.0	0.0	0.0	0.0
G30	20.7	0.0	0.0	0.0	0.0
G31	0.0	0.0	0.0	0.0	0.0

Table F-3. Calculated penetration length in Fan1:1 (time-dependent grout properties).

Hole number/ Section	Penetration Length [m] 0–4.6 m	4.6–7.6 m	7.6–10.6 m	10.6–13.6 m	13.6–15.6 m
A1	0.0	0.0	5.9	10.9	7.9
A2	0.0	1.2	0.0	5.7	2.7
C3	0.0	0.0	10.4	9.8	0.0
H4	0.0	0.0	0.0	4.4	10.8
I5	0.0	0.0	8.0	0.0	0.0
D6	0.0	0.0	0.0	0.0	10.8
B7	0.0	0.0	4.3	4.0	9.2
B8	0.0	0.0	0.0	5.4	7.8
G9	0.0	0.0	3.0	3.0	6.2
G10	0.0	0.0	5.6	0.0	8.1
G11	0.0	0.0	0.0	0.0	0.0

Table F-4. Calculated penetration length in Fan1:1 (time-dependent grout properties).

Hole number/ Section	Penetration Length [m] 0–4.6 m	4.6–7.6 m	7.6–10.6 m	10.6–13.6 m	13.6–15.6 m
A12	0.0	0.0	0.0	0.0	16.4
A13	0.0	0.0	8.5	15.2	10.7
A14	0.0	0.0	0.0	0.0	0.0
C15	0.0	0.0	0.0	0.0	0.0
C16	0.0	0.0	0.0	20.7	0.0
H17	0.0	0.0	0.0	16.4	0.0
H18	0.0	0.0	0.0	13.7	15.1
I19	0.0	0.0	0.0	0.0	0.0
I20	0.0	0.0	0.0	0.0	0.0
D21	0.0	0.0	0.0	0.0	0.0
D22	0.0	0.0	0.0	0.0	0.0
B23	0.0	0.0	0.0	0.0	0.0
B24	0.0	12.7	0.0	0.0	25.2
B25	0.0	0.0	0.0	20.5	15.1
G26	0.0	0.0	0.0	12.9	16.2
G27	28.4	0.0	0.0	0.0	0.0
G28	22.1	0.0	0.0	0.0	0.0
G29	0.0	0.0	0.0	0.0	0.0
G30	22.7	0.0	0.0	0.0	0.0
G31	0.0	0.0	0.0	0.0	0.0